ANALYTICAL ESTIMATION OF CO_2 STORAGE CAPACITY IN DEPLETED OIL AND GAS RESERVOIRS BASED ON THERMODYNAMIC STATE FUNCTIONS

A Thesis

by

ERNESTO VALBUENA OLIVARES

Submitted to the Office of Graduate Studies of
Texas A&M University
in partial fulfillment of the requirements for the degree of

MASTER OF SCIENCE

December 2011

Major Subject: Petroleum Engineering

Analytical Estimation of CO_2 Storage Capacity in Depleted Oil and Gas Reservoirs

Based on Thermodynamic State Functions

ANALYTICAL ESTIMATION OF CO_2 STORAGE CAPACITY IN DEPLETED OIL AND GAS RESERVOIRS BASED ON THERMODYNAMIC STATE FUNCTIONS

A Thesis

by

ERNESTO VALBUENA OLIVARES

Submitted to the Office of Graduate Studies of
Texas A&M University
in partial fulfillment of the requirements for the degree of

MASTER OF SCIENCE

Approved by:

Chair of Committee,	Maria Barrufet
Committee Members,	Gioia Falcone
	Thomas Blasingame
Head of Department,	Stephen Holditch

December 2011

Major Subject: Petroleum Engineering

ABSTRACT

Analytical Estimation of CO_2 Storage Capacity in Depleted Oil and Gas Reservoirs Based on Thermodynamic State Functions. (December 2011)

Ernesto Valbuena Olivares, B.S., La Universidad del Zulia

Chair of Advisory Committee: Dr. Maria Barrufet

Numerical simulation has been used, as common practice, to estimate the CO_2 storage capacity of depleted reservoirs. However, this method is time consuming, expensive and requires detailed input data. This investigation proposes an analytical method to estimate the ultimate CO_2 storage in depleted oil and gas reservoirs by implementing a volume constrained thermodynamic equation of state (EOS) using the reservoir's average pressure and fluid composition.

This method was implemented in an algorithm which allows fast and accurate estimations of final storage, which can be used to select target storage reservoirs, and design the injection scheme and surface facilities. Impurities such as nitrogen and carbon monoxide, usually contained in power plant flue gases, are considered in the injection stream and can be handled correctly in the proposed algorithm by using their thermodynamic properties in the EOS.

Results from analytical method presented excellent agreement with those from reservoir simulation. Ultimate CO_2 storage capacity was predicted with an average difference of 1.3%, molar basis, between analytical and numerical methods; average oil, gas, and water saturations were also matched. Additionally, the analytical algorithm performed several orders of magnitude faster than numerical simulation, with an average of 5 seconds per run.

ACKNOWLEDGEMENTS

To my **mother Elizabeth** and **father Eduardo**, for their unconditional support, advice, and love. For being my role models in life; walking on the excellence path would be very difficult without you.

To my **wife Karin**, you are a key stone is my life. Your support and love always drive me to be my best.

To **Dr. Maria Barrufet**, for her invaluable teachings, support, and friendship. Your dedication inspires me in the pursue of knowledge. There are no words to describe my appreciation to you.

To **Dr. Gioia Falcone** and **Dr. Thomas Blasingame**, for their guidance, suggestions, and support during my career at Texas A&M and as my committee members during the development of this research.

To the **professors and staff of the Petroleum Engineering Department of Texas A&M University** at College Station, for their lessons and academic integrity.

My appreciations to all of you.

NOMENCLATURE

Acronyms

BIC	binary interaction coefficient
B-O	black oil
CBM	coal-bed methane
CCS	carbon capture and sequestration
CO	carbon monoxide
CO_2	carbon dioxide
EOR	enhanced oil recovery
EOS	equation of state
G-C	gas condensate
GHG	greenhouse gas
N_2	nitrogen
OGIP	original gas in place
OOIP	original oil in place
PMV	partial molar volume
PR	Peng-Robinson
RHS	right-hand side
SRK	Soave-Redlich-Kwon
UCSC	ultimate CO_2 storage capacity
VLE	vapor/liquid equilibrium

V-O volatile oil

Variables

$(a\alpha)_m$ parameter of EOS for mixtures (See Appendix—Quadratic Mixing Rule)

b_m parameter of EOS for mixtures (See Appendix—Linear Mixing Rule)

c_{rock} rock compressibility, psi^{-1}

c_{water} water compressibility, psi^{-1}

f_v vapor fraction

HCPV hydrocarbon pore volume from rock-water compressibility, ft^3 or bbl

k_{ij} binary interaction coefficient between components *i* and *j*

k_{rg} gas relative permeability

k_{ro} oil relative permeability

k_{rw} water relative permeability

M_{w_l} molecular weight of liquid, lb/lb-mol

M_{w_v} molecular weight of vapor, lb/lb-mol

N_c number of components

n_{dep} number of moles at depletion, lb-mol

n_i number of moles of component *i*, lb-mol

Δn cumulative injected moles, lb-mol

p pressure, psia

Δp pressure differential, psi

P_c critical pressure, psia

p_c capillary pressure, psia

p_{cow} oil-water capillary pressure, psi

p_{cog} oil-gas capillary pressure, psi

p_{ref} reference pressure, psia

PV pore volume, ft^3 or bbl

R gas constant, 10.7316 ft^3-psi-°R^{-1}/lb-mol

R_{sb} CO_2 dissolved in brine, SCF-CO_2 / STB brine

R_{sw} CO_2 dissolved in water, SCF-CO_2 / STB water

S_g gas saturation

S_o oil saturation

S_w water saturation

T temperature, °F ([°F] = 32 + [°C] x 9/5)

T_c critical temperature, °R ([°R] = [°F] + 459.67)

V total volume, ft^3

υ molar volume, ft^3/lb-mol

$\bar{V}_i$ partial molar volume of component *i* (see derivation on Appendix A), ft^3/lb-mol

$\bar{V}_x$ generalized partial molar volume of pseudo component *x*; where *x* could be a mixture of components with constant composition (see derivation on Appendix A), ft^3/lb-mol

$V_{n_{dep}}$ fictitious volume occupied by n_{dep} moles of fluid at target p & T, ft^3

$V_{n_{dep}+\Delta n}$ final volume of fluid at p and T from equation of state, ft^3

x_i	liquid mole fraction of component i
y_i	vapor mole fraction of component i
z_i	total mole fraction of component i
ω	Pitzer acentric factor

Units

acres	area (1 acre = 43,560 ft^2 = 4,046.86 m^2)
bbl	barrel at p & T, volume (1 bbl = 42 gal = 158.99 Litres)
STB	stock tank barrel, standard conditions 14.7 psia and 60 °F, volume
MMSTB	million standard barrel, volume (1 MMSTB = 10^6 STB)
ft	feet, length (1 ft = 0.3048 m)
lb-mol	quantity of substance
mD	milli Darcy, permeability (1000 mD = 1 D = 9.869233×10^{-13} m^2)
MW	Megawatt, energy rate (1 MW = 10^6 W = 10^6 J/s = 10^6 kg-m^2/s^3)
ppm	parts per million
SCF	standard cubic feet, volume (5.615 SCF = 1 STB = 158.99 Litres)
BSCF	billion standard cubic feet, volume (1 BSCF = 10^9 SCF)
t or ton	tonne, mass (1 ton = 10^3 kg)
Gt	Gigatonne, mass (1 Gt = 10^9 ton = 10^{12} kg)
Mt	Megatonne, mass (1 Mt = 10^6 ton = 10^9 kg)

TABLE OF CONTENTS

CHAPTER Page

CHAPTER Page

LIST OF FIGURES

Page

Page

Page

LIST OF TABLES

Page

Page

Page

CHAPTER I

INTRODUCTION

Greenhouse gas (GHG) emissions have been continuously increasing in the past 3 decades. More than 70% of these emissions are composed of CO_2, which reached 30 Gt in 2009 (EIA 2011). Several environmental agencies and governments have shown concern about this statistic and its potential relation with global warming.

Several low- or nonemission alternative energy sources have been developed, but their high technological cost represents a major limitation for massive implementation. Therefore, current fossil fuel dependency will continue in the near future, increasing the need to develop economic and technologically feasible approaches to reduce and capture and dispose CO_2 emissions.

Geological storage of CO_2 in aquifers and depleted oil and gas reservoirs represents an attractive option, as it has been studied in the oil and gas industry for several years. Particularly, interest now exists in using depleted reservoirs, taking advantage of the higher storage density in comparison with aquifers; additionally, extensive knowledge of the reservoir's static and dynamic properties, acquired during the developing phase, are available to optimize the efficiency of the project and increase the final storage capacity and profits.

This thesis follows the style of *SPE Journal*.

In the past, numerical simulation has been used, as common practice, to estimate the CO_2 storage capacity of depleted reservoirs. However, this method is time consuming and requires detailed input data. This investigation proposes an analytical method to estimate the maximum CO_2 storage in depleted oil and gas reservoirs by implementing a volume-constrained thermodynamic equation of state (EOS) using the reservoir's average pressure and fluid composition.

Current analytical methods are mostly focused on applications for storage calculations in aquifers. The targets of the proposed analytical method are depleted oil and gas reservoirs, to benefit from the higher storage density, data availability, and already-in-place infrastructure including wells and facilities. The method is based on the partial molar volume (PMV) definition which relates the change in volume of a mixture with the change of the amount of one component holding constant pressure and temperature. Separation procedures to remove the impurities from the CO_2-based injection stream are expensive, consequently a considerable amount of impurities remain in the gas composition; hence, the PMV concept in this study has been generalized, to allow the change of the amount of more than one component.

The required input data for this model are initial pressure, pore volume and water saturation, reservoir temperature, depletion and target pressures, average fluid composition at depletion, rock and water compressibilities, and composition of injection gas. The water and pore volumes are estimated using their compressibilities, and the

volume of the hydrocarbon and injection fluid mixture is estimated with the PMV approach. The final outputs are the maximum amount of CO_2 injected at the target pressure, final average fluid composition, and saturations.

This method allows fast and accurate estimations of final storage that can help to design and schedule the injection scheme and surface facilities. Impurities such as nitrogen and carbon monoxide, usually contained in power plant flue gases, are considered in the injection stream and will be correctly handled in the proposed algorithm by using their thermodynamic properties into the EOS and the interaction of the hydrocarbons in the reservoir and the injected fluid.

1.1 Definition of the Problem

The success of a CO_2 capture and geological sequestration (CCS) project depends greatly on the correct selection of proper target reservoirs to store the injected gases. Such reservoirs must ensure large storage capability for long geologic periods to avoid fluid leakage to other subsurface formations or to the atmosphere. The accurate estimation of the maximum volume of the CO_2-based gas stream that can be injected in the reservoir is a key factor in the screening process to select good depleted oil and gas candidate formations for CCS processes.

Reservoir simulation is currently the most used tool to evaluate CO_2 storage projects. The results from this method are accurate; they can be used to understand the fluid

movement in the reservoir and plan the injection schedule and estimate the maximum amount of CO_2 that can be injected into the reservoir. Nonetheless, numerical simulation is time consuming and expensive and requires detailed input data to develop representative models.

This research is focused on developing an analytical algorithm to estimate the ultimate CO_2 storage capacity of depleted oil and gas reservoirs through the implementation of a volume-constrained thermodynamic equation of state (EOS) using the average reservoir pressure and fluid composition. The most important features of this algorithm are its accuracy, speed, and capability of properly handling impurities in the injection stream.

1.2 Relevance of the Study

Coal-fired electrical power generation produced nearly 45% of the CO_2 worldwide emissions in 2009 (EIA 2011). Several governments and environmental agencies, and in particular, the Department of Energy of the United States, have shown their concern regarding greenhouse gas (GHG) emissions and its potential relation with global warming.

Several pilot CCS projects have started operations or are planned to begin in the next few years (House et al. 2003; Koperna et al. 2009; Snow 2010; van der Meer and Ferhat 2009). Some of these projects may be intended to reinject the associated CO_2 produced from the oil and gas reservoirs; however, they also offer the opportunity to evaluate the

feasibility of the process to store the flue gases from coal-fired power plants into subsurface formations. This target would help to reduce part of the emissions from electric power generation.

CO_2 storage in depleted oil and gas reservoirs has significant advantages over the storage in aquifers; water contained in the aquifers may be considered as water reserves to be used in the future (depleted oil and gas reservoirs do not present this inconvenience), the wells are already drilled (decreasing capital expenditures), reservoir static and dynamic data are available and enhanced oil recovery (EOR) can be applied (Gallo et al. 2002). Additionally, depleted oil and gas reservoirs offer a larger pressure differential for injection, which translates into a much higher storage density than in aquifers.

Future development of CCS projects creates the need to develop fast and accurate techniques to estimate the storage potential of the reservoirs; this will allow the correct selection of the best target formations to achieve a successful injection process. Numerical simulation is the preferred tool to perform rigorous estimations of CO_2 storage potential in depleted reservoirs. Nonetheless, it requires long computational time, powerful processors and detailed input data, and it is expensive, becoming an inconvenient method, especially at the first stages of project planning.

Analytical methods offer more speed, less computer power, and less input information without compromising the accuracy and reliability of the ultimate CO_2 storage capacity

in depleted oil and gas reservoirs. Previous analytical methods have been developed to model CO_2 injection into aquifers, allowing estimation of gas solubility in brine, injectivity through relative permeability models, plume shape, and size and storage capacity (Burton et al. 2009; Okwen et al. 2010). These models cannot be directly applied to depleted oil and gas reservoirs, because they do not consider the interaction of CO_2 and impurities with the hydrocarbons in the reservoir.

The EOS allows modeling the interaction between the hydrocarbons in place and the injected gas. This is a rigorous approach, which can be implemented in an analytic algorithm, to estimate the ultimate storage capacity of CO_2 and impurities into depleted reservoirs. The analytic algorithm can perform fast and accurate calculations under different scenarios and reservoirs to create helpful information to select proper target reservoirs, design compression facilities, propose different schemes for separation of impurities in the CO_2 stream, and plan the possible duration of the project.

1.3 Objectives

The principal objectives of this research are to:

- Develop a fast and accurate analytical method to estimate the ultimate CO_2 storage capacity in depleted oil and gas reservoirs.
- Develop an algorithm to implement the analytical method and validate the results through numerical simulation.

To accomplish the principal objectives will involve the development of specific tasks:

- Derive an equivalent equation for the partial molar volume definition which involves the variation of more than one component in the mixture.
- Gather and validate two fluid models, representing a condensate gas and a black oil, both treated with a composition approach.
- Develop different reservoir models to analyze the behavior of the storage capacity under a wide range of pressures, temperatures, and injected gas composition.
- Validate the proposed analytical method against numerical reservoir simulation.

1.4 Deliverables

The results from this investigation will generate the following products:

- A fast and accurate algorithm based on a new analytical method to estimate the ultimate CO_2 storage in depleted oil and gas reservoirs, which handles correctly impurities in the injection stream. The algorithm is programmed in Visual Basic Applications (VBA) for Excel.

CHAPTER II

BACKGROUND RESEARCH

The increasing interest in carbon capture and storage (CCS) projects is reflected in the amount of recent publications on this topic. While most of the studies are focused in CO_2 storage into aquifers due to the large available volume for injection, various projects focus their attention on depleted oil and gas reservoirs due to several advantages that will be described later. This chapter presents a summary of the current knowledge on CSS projects and the fundamental thermodynamic bases necessary to develop this project.

2.1 Literature Review

The basis of this investigation relies on the carbon capture and geologic storage concept. Metz et al. (2005), Dooley et al. (2006), and EPA (2011) defined the carbon capture as a process consisting first of removing the impurities from a CO_2-based stream to increase the CO_2 concentration and improve the efficiency of the final storage process, and secondly, compressing the gas stream to transport it to a storage location, which can be geologic formations, such as aquifers and depleted oil and gas reservoirs, to achieve a long-term isolation from the atmosphere.

Coal consumption accounted for the release of nearly 14 Gt of CO_2 during 2009, almost 45% of the worldwide carbon dioxide emissions (EIA 2011). Given that coal is mainly

used in power plants to generate electricity, these locations are large sources of CO_2 and become the most important target for CCS processes. A large coal-fired power plant, generating 500 MW, emits approximately 2.9 Mt-CO_2 per year or 55.2 BSCF of CO_2 per year.

Several pilot projects have been proposed in different locations of the world and many have started operations already. Snow (2010) described a pilot test in the Citronelle field in Alabama. The purpose of this project is to inject CO_2 in a depleted formation for both, enhanced oil recovery (EOR) and geologic storage. This project is partially funded by the US Department of Energy (DOE).

Koperna et al. (2009) described the ongoing CSS project in Pump Cayon, New Mexico. This study is focused on the characterization of coalbed methane (CBM) reservoirs to ensure the success of the enhanced gas recovery and CO_2 storage process. They highlighted that monitoring the CO_2 plume growth is key to properly assess a larger CCS project. Additionally, they stressed that injectivity decrease may be expected in CBM reservoirs as the coal swells after CO_2 injection, reducing the permeability of the rock.

The interest in CO_2 storage projects creates the need to better understand the mechanisms involved to assess the key elements of successful operations. Sifuentes et al. (2009) developed an extensive effort to identify the key contributors in CO_2 storage processes in aquifers. Using the base model of the Stuttgart formation in Germany,

currently developing a pilot test, they evaluated the effect of temperature, salinity, permeability, dip angle, pressure, injection strategy, well location, among other parameters, on the process efficiency. They found that horizontal permeability is the most important parameter, since injectivity and lateral extent of the CO_2 plume depends highly on it. Well location, injection scheme and hysteresis enhance the residual trapping mechanism and CO_2 dissolution in the brine. However, CO_2 dissolution in brine during the injection process is negligible; only after a few hundred years will dissolution play an important role for low salinity brines. This indicates that interaction between CO_2 and brine may be neglected during the injection period of the storage process.

Rowe and Chou (1970) presented correlations to estimate CO_2 solubility in brine and brine physical properties at a wide range of pressures, temperatures and brine salinities. Chang et al. (1998) developed a compositional numerical model including CO_2 solubility in water, where the vapor/liquid equilibrium (VLE) in the hydrocarbon and CO_2 phases is calculated with a cubic EOS and the equilibrium between the CO_2 and water phases is calculated using a CO_2 fugacity table, which considers the solubility as a function of reservoir pressure and temperature. This approach uses two different equilibrium methods which may not be consistent; instead, a full three-phase VLE should be preferred to represent the thermodynamic consistently.

Nevertheless, the relationship between CO_2 solubility in brine, pressure, temperature, and salinity can be well described through correlations (Chang et al. 1998; Rowe and

Chou 1970). Solubility increases with pressure and it decreases as salinity and temperature increase. **Fig. 2.1 and Fig. 2.2** present these relationships for pressure ranging from 0 to 10,000 psia, temperature from 104 to 212 °F and salinity from 0 to 250,000 ppm. This model can be used to estimate the maximum CO_2 solubility in brine. Correlations from these references are presented in Appendix D.

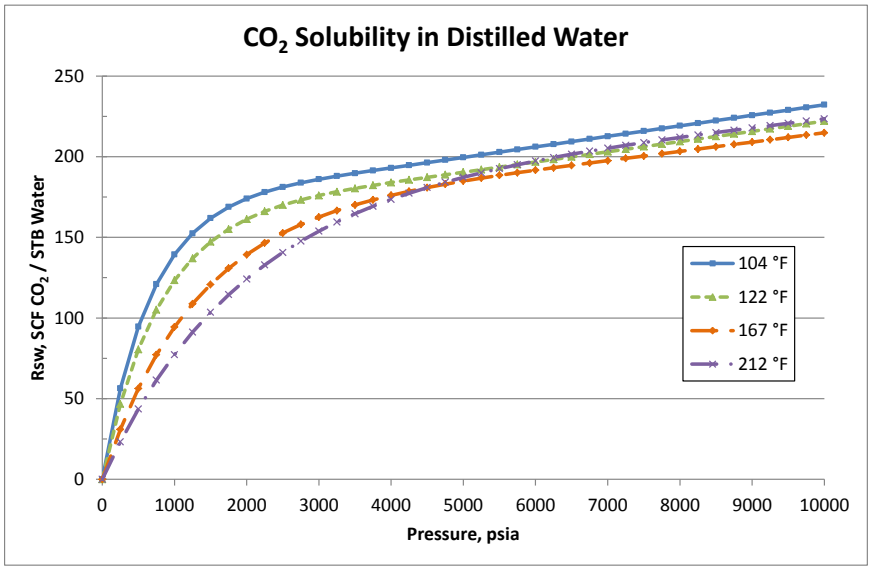

Fig. 2.1—Effect of pressure and temperature on CO_2 solubility in distilled water. CO_2 solubility is proportional to pressure and inversely proportional to temperature.

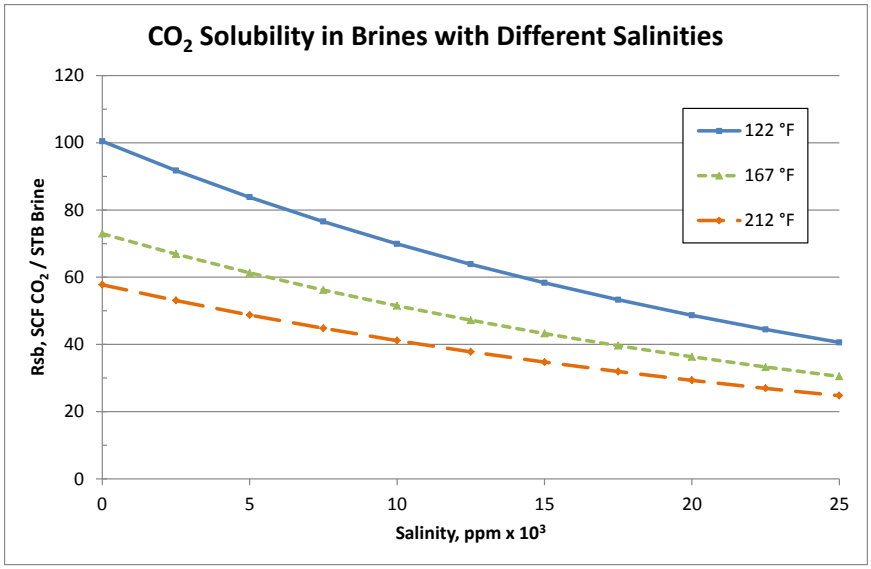

Fig. 2.2—Effect of salinity and temperature on CO_2 solubility in brine. CO_2 solubility decreases with salinity and temperature, and increases with pressure. Pressure in the graph is kept constant at 695.5 psia for reference.

Reservoir characterization is one of the most important aspects in the design of a CCS project. House et al. (2003) demonstrated that geologic complexities, such as fractures and faults, can provide a high permeability path for the CO_2 to migrate to other formations, reducing the storage capacity of the reservoir and possibly leading to final release of gases to the atmosphere; showing the significance of proper reservoir description in CCS projects.

Li et al. (2006) also suggested that caprock characterization plays an important role in the storage capacity of CO_2 in depleted oil and gas reservoirs. They established that if CO_2 is injected in the reservoir to restore the initial pressure, the caprock may allow gas

leaks since the interfacial tension of the fluids changes after injecting a fluid that was not originally in place.

Aquifers are very appealing targets for CCS. Aquifers have large volume and they can be easily found in many areas near CO_2 sources. Many numerical and analytical models have been developed to evaluate this type of projects. Burton et al. (2009) showed that relative permeability and thermodynamic interaction between the CO_2 and the brine in the near-wellbore region are important in the injection schedule and the compression requirements in surface. Additionally, Oruganti (2009) indicated that boundary effects may cause different pressure behaviors, such as linear pressure propagation when great number of faults are present, in CO_2 injection processes during the life of the project, according to the characteristics of the boundary.

However, aquifers are pressurized and the available pressure differential to inject CO_2, without compromising the integrity of the rock, is small. This leads to low storage density, which can be defined as the mass of CO_2 that is stored per unit of pore volume at reservoir pressure and temperature.

Injectivity plays an important role in the success of a CCS project. Assessing the injection capability is necessary to meet the requirements of the CO_2 source for the scheduled injection period. Van der Meer and Ferhat (2009) corroborated the importance of injectivity to estimate costs and plan the operations. Conversely, they mentioned that

the ultimate storage capacity is independent from the number of wells, spacing or stimulation techniques used. This fact suggests that the number of wells and the injectivity affect the duration of the injection process; nevertheless, the maximum amount of CO_2 stored in the reservoir depends on the pressure differential achieved, fluid compositions and characteristics, temperature, and saturations. CO_2 storage amount independency from injection rates and well constrains was also presented by Barrufet et al. (2010).

Okwen et al. (2010) presented an analytical model to estimate the storage efficiency in aquifers. Buoyancy effect and mobility ratio between the CO_2 and brine proved to be key parameters in the storage process. The results also showed that the storage efficiency in aquifers is low, below 5%. The storage efficiency can be defined as the ratio between the amount of CO_2 stored in an aquifer and the maximum amount of CO_2 that could theoretically be stored in the same aquifer volume (van der Meer 1995). This definition may be misleading since the CO_2 stored is highly dependent on the pressure differential available for injection and the final target pressure.

These observations drive this investigation to look into the advantages of developing CCS projects in depleted oil and gas reservoirs over aquifers; Gallo et al. (2002) presented some of these benefits. The reservoir contains hydrocarbons and it will not be considered as water reserves. Reservoir data is available, often with a good characterization. The wells are already drilled, decreasing the capital expenditure needs

and the possibility of developing EOR methods is available. Additional to the mentioned advantages, depleted reservoirs allow a large pressure differential between initial and final target pressure, leading to large CO_2 storage densities.

Furthermore, Gallo et al. (2002) cited the potential profitability of CCS projects. STATOIL has developed a CO_2 injection process, handling 1 Mt-CO_2 per year in the Sleipner field, in the North Sea section of Norway. Reinjecting the produced CO_2 into an aquifer, emission tax savings reach about 35 USD/ton of CO_2.

The concentration of CO_2, in typical flue gas from coal-fired power plants, is 14% (dry volume) (Metz et al. 2005). Other sources, such as gas turbines, natural gas power plants and cement production, can generate flue gases with CO_2 concentration between 3% and 20% (dry volume). The rest of the flue gas is normally composed by nitrogen, oxygen and carbon monoxide, among other components is smaller proportions.

GHG emissions are usually expressed in base of metric tonnes (unit symbol t). This is a mass unit, which represents the mass of water contained in a cubic meter at 4°C, and it is equal to 1,000 kg or 2,204.62 lb. The mass of any substance can also be expressed in moles, defined as the mass of a molecule or atom of the substance; that is, 1 lb-mol of CO_2 has approximately 44.01 lb. Additionally, the volume of 1 lb-mol of an ideal gas (at 14.7 psia and 60 °F) is 379.56 ft^3. **Table 2.1** summarizes these relationships for 1 mol of

pure CO_2 and for 2.9 Mt of CO_2, the average emission of a large coal-powered plant (Metz et al. 2005).

Table 2.1—CONVERSION FACTORS FOR CO_2. THE AMOUNT OF SUBSTANCE IS REPRESENTED BY THE UNIT MOL, POUNDS AND TON EXPRESS MASS AND SCF EXPRESS VOLUME AT STANDARD CONDITIONS

CO_2 Mass and Volume conversions			
mol	**lb**	**ton**	**SCF**
1	44.01	0.01993	379.56
$1.46x10^8$	$6.40x10^9$	$2.90x10^6$	$5.52x10^{10}$

Removing the impurities to increase the CO_2 concentration in the gas stream is an expensive process. The estimated cost for CO_2 capture and compression can range from USD 12 to USD 60 per ton of CO_2 (Dooley et al. 2006). However, this is an important procedure to maximize the ultimate storage capacity in the target formation.

Laboratory experimental results indicate that the storage capacity and displacement efficiency are severely reduced in dry gas coreflood experiments, when the injected gas is a typical flue gas, containing 14% CO_2, instead of a high-CO_2-concentration gas (Nogueira and Mamora 2005). This observation suggests that there must be a balance between separation cost and desired efficiency of the storage process. For this reason, understanding the effect of impurities in the ultimate CO_2 storage capacity represents a key factor in the design of any CCS project.

2.2 The Cubic Equation of State

The equation of state (EOS) is a simple, yet robust method, applied to calculate the thermodynamic properties of multicomponent mixtures. Since 1873, when J.D. van der Waals proposed his EOS consisting of a repulsion and an attraction term, many EOS have been developed for different applications.

The Peng-Robinson equation of state (PR-EOS), presented in Eq. (2.1) (Peng and Robinson 1976), has proven to be one of the most effective EOS for hydrocarbon mixtures. Although its performance is similar to the Soave-Redlich-Kwon (SRK) equation, the volumetric properties calculations are more accurate using the PR-EOS (Michelsen and Mollerup 2004).

$$p = \frac{RT}{\upsilon - b} - \frac{a\alpha}{\upsilon^2 + 2b\upsilon - b^2} \quad \text{..... (2.1)}$$

Eq. (2.1) presents the relation between pressure, volume and temperature, according to PR; pressure is expressed in psia, the temperature in absolute units °R, the molar volume υ in ft^3/lb-mol, the gas constant R is 10.7316 ft^3-psi-$°R^{-1}$/lb-mol for the units used in this work (The gas constant R may have different units depending on the system used). The parameters $a\alpha$ and b depend on the critical properties of the fluid, which are presented in the following subsections.

2.2.1 Parameters *a, b* and *α*

The parameters a and b, in the EOS, depend on the critical properties of the fluid. For pure substances, the first and second derivative of the pressure with respect to the molar volume are zero (van der Waals 1873), see Eq. (2.2). From these equations a and b are calculated for the PR-EOS as shown on Eq. (2.3).

$$\left(\frac{\partial p}{\partial v}\right)_{Tc} = 0 \text{ and } \left(\frac{\partial^2 p}{\partial v^2}\right)_{Tc} = 0 \quad \text{..... (2.2)}$$

$$a = 0.45724\frac{R^2 {T_c}^2}{P_c} \quad \text{and} \quad b = 0.07780\frac{RT_c}{P_c} \quad \text{..... (2.3)}$$

The term α was introduced, by Soave (1972), as a temperature-dependent dimensionless parameter which value is 1 at the critical temperature. The term was originally developed for the Redlich-Kwong EOS, and it was implemented in the PR-EOS as well. Eq. (2.4) presents the definition for α, where m is a parameter which depends on the Pitzer acentric factor ω and T_r is the reduced temperature of the pure component.

$$\alpha = \left[1 + m\left(1 - \sqrt{T_r}\right)\right]^2 = \left[1 + m\left(1 - \sqrt{\frac{T}{T_c}}\right)\right]^2 \quad \text{..... (2.4)}$$

with:

$$m = 0.37464 + 1.54226\,\omega - 0.2699\,\omega^2 \quad \text{for} \quad \omega < 0.49 \quad \text{..... (2.5)}$$

A correction for heavy components may be used to calculate m when the acentric factor is greater than 0.49 as follows:

$$m = 0.379642 + 1.48503\,\omega - 0.164423\,\omega^2 + 0.01667\,\omega^3 \text{ for } \omega > 0.49 \quad .. (2.6)$$

2.2.2 Mixing Rules

The description of the PR-EOS presented until now is applicable to define the behavior of pure components. Nevertheless, hydrocarbon fluids are multi-component mixtures, and in order to describe their behavior the a and b parameters of the EOS have to be calculated with mixing rules.

The mixing rule for the parameter $a\alpha$ is treated as a combined term to calculate the quadratic mixture parameter $(a\alpha)_m$. Eq. (2.6) shows the mixing rule procedure for a liquid with N_c components, where x_i is the mole fraction of component "i" in the liquid, a_i and α_i are the parameters for the pure component "i", and k_{ij} represents the binary interaction coefficient (BIC) between components "i" and "j".

$$(a\alpha)_m = \sum_{i=1}^{N_c}\sum_{j=1}^{N_c} x_i x_j \sqrt{a_i \alpha_i a_j \alpha_j}\left(1 - k_{ij}\right) \quad \text{..... (2.7)}$$

The mixing rule for the parameter b is linear. Eq. (2.7) presents the calculation of b_m for a liquid mixture of N_c components, where x_i and b_i are the liquid mole fraction and the b-parameter from the pure component "i".

$$b_m = \sum_{i=1}^{N_c} x_i b_i \quad \text{..... (2.8)}$$

The mixing rules presented in Eqs. (2.6) and (2.7) are also applied for the vapor phase, replacing the liquid mole fractions x_i by the vapor mole fractions y_i.

The final form of the PR-EOS for a multi-component fluid with the implementation of the mixing rule is presented in Eq. (2.8).

$$p = \frac{RT}{v - b_m} - \frac{(a\alpha)_m}{v^2 + 2b_m v - {b_m}^2} \quad \text{..... (2.9)}$$

2.3 The Partial Molar Volume

The partial molar property of a function F is defined its derivative with respect to n_i at constant pressure, temperature and the rest of the components in the mixture. This definition can be applied to the total volume V of a mixture by Eq. (2.10) (Michelsen and Mollerup 2004). The derivation of this equation is shown on Appendix A.

$$\bar{V}_i = \left(\frac{\partial V}{\partial n_i}\right)_{p,T,n_j} = -\frac{\left(\frac{\partial p}{\partial n_i}\right)_{V,T,n_j}}{\left(\frac{\partial p}{\partial V}\right)_{T,n}} \quad \text{..... (2.10)}$$

The partial molar volume represents the change of total volume of a mixture with respect to the change of moles of the component "i" at constant pressure and temperature. This property will allow the evaluation of the volume of the reservoir fluid as CO_2 is injected

and mixes with the original fluid in place. However, this definition can be directly applied when only one component is changing. This investigation will develop an alternative procedure to consider the injection of impurities in the CO_2-based stream.

2.4 Vapor-Liquid Equilibrium

The vapor-liquid equilibrium (VLE) refers to the calculation of the thermodynamic properties of the phases present in a fluid at certain specific conditions. The two-phase equilibrium calculations of an n-component mixture of overall composition z is detailed in Chapter 7 of "Thermodynamic Models: Fundamentals & Computational Aspects" (Michelsen and Mollerup 2004).

VLE is achieved when the liquid and vapor fugacities of each component are equal, Eq. (2.11). In relation with the chemical potential concept, this implies that for each component "i", the amount of molecules that pass from the liquid phase to the vapor phase is the same amount that passes from the vapor phase to the liquid phase, reaching equilibrium.

$$\hat{f}_i^l = \hat{f}_i^v \quad \text{for } i = 1, 2, \dots, N_c \qquad (2.11)$$

The liquid and vapor mole fractions, x_i and y_i, and the overall vapor fraction f_v must honor the material balance relationship for each component given in Eq.(2.12).

$$z_i = f_v y_i + (1 - f_v) x_i \quad \text{for } i = 1,2, \dots, N_c \qquad (2.12)$$

Finally, the liquid and vapor mole fractions must at to unity. This relationship can be written as shown on Eq. (2.13).

$$\sum_{i=1}^{N_c} x_i - \sum_{i=1}^{N_c} y_i = 0 \quad \text{.....} \quad (2.13)$$

The set of equations (2.10) to (2.13) present a general method to calculate the VLE of a multicomponent system. Alternative formulations for this general method exist, and can be applied to improve the speed and accuracy of the results.

The VLE calculations in this investigation will be performed using pressure, temperature and overall fluid composition as inputs. The key properties obtained from this calculation are fluid molar volume, vapor fraction, vapor and liquid phase densities ρ_v and ρ_l, and vapor and liquid molecular weights M_{w_v} and M_{w_l} respectively. The relationship between these variables is presented in Eq. (2.14).

$$\upsilon = f_l \upsilon_l + f_v \upsilon_v = (1 - f_v)\frac{M_{w_l}}{\rho_l} + f_v \frac{M_{w_v}}{\rho_v} \quad \text{.....} \quad (2.14)$$

2.5 Singular Value Decomposition

Singular value decomposition (SVD) is a factorization of a real or complex matrix, based on linear algebra principles with applications in statistics, engineering, and signal processing, among others. The SVD factorization form of matrix A is given by:

$$A = U\Sigma V^* \quad \text{(2.15)}$$

where A is an $m \times n$ matrix, U is an $m \times m$ orthogonal matrix, Σ is an $m \times n$ diagonal matrix formed with the singular values (positive square root of eigenvalues) of A, and V^* an $n \times m$ orthogonal matrix.

SVD is used to compute the pseudo-inverse of a singular matrix, which allows to solve least squares minimization problems, such as best fit straight line. The pseudo-inverse of the singular matrix A is calculated as follows:

$$A^\dagger = V\Sigma^\dagger U^T \quad \text{(2.16)}$$

The minimization of the 2-norm of a straight line equation is given by:

$$min\|Ax - b\|^2 \quad \text{(2.17)}$$

The solution of such system applying the pseudo-inverse concept is presented as:

$$x = A^\dagger b \quad \text{(2.18)}$$

where x is the unknown 2-dimensional vector with slope and intercept as variables; $A^\dagger$ is the pseudo-inverse of matrix A that is formed by 2 columns, the first with the known x-axis values and the second with unit value representing the coefficient of the intercept; and b is a vector formed by the known y-axis values. Solving this system outputs the slope and intercept that defines the best fit straight line through data points.

2.6 Excel Visual Basic for Applications

BASIC, an acronym for Beginner's All-purpose Symbolic Instruction Code, was first developed in the early 1,960's. This programming language gained for status in 1,991 when Microsoft introduced Visual Basic for Windows. Excel 5, in 1,993, was the first application on the market presenting Visual Basic for Application (VBA) (Walkenbach 2010).

Excel VBA allows to create algorithms and manipulate worksheets, charts, tables, functions, etc. The flexibility and ease of access to this language through Excel motivate its use for projects in diverse areas, such as mathematics, engineering, finance, business and more.

2.7 Reservoir Numerical Simulation

Reservoir numerical simulators allow to model fluid behavior and flow in reservoirs while production and injection processes are taking place. Numerical simulators are based on mass and energy conservation laws, fluid transport in porous media principles, and additional relationships between variables such as saturations, capillary pressures, and relative permeability. A typical simulator suite integrates several modules that include, among others, fluid characterization package, grid design, well design, uncertainty assessment, optimization, visualization of results, and the numerical simulator itself.

For this research several software packages were used in regards of numerical simulation, among most used are: PVTi™ 2010.1 (Schlumberger 2010c) was used for fluid characterization, pressure-volume-temperature, and fluid phase behavior and description; Eclipse300™ 2010.1 (Schlumberger 2010a) was used for numerical simulation processing; and Petrel™ 2010.1 (Schlumberger 2010b) as data pre- and post-processor.

CHAPTER III

DESCRIPTION OF SOLUTION

The main purpose of this study is to develop an analytical model to estimate the ultimate CO_2 storage capacity (UCSC) of depleted oil and gas reservoirs at a certain target reservoir pressure. An essential step to achieve this goal is to demonstrate that the UCSC can be estimated using average reservoir pressure and fluid compositions at the depletion stage, setting a final target pressure and applying thermodynamic principles. This chapter presents a semi-analytical method to prove the functionality of the concept and the final analytical solution to estimate the storage capacity.

3.1 Field Operations

The prime targets to apply the results of this research are depleted oil and gas reservoirs, which can be subject to CO_2 injection for geological storage. The life cycle of these types of reservoirs is well known in the oil industry; however, a brief description will clarify the source of the necessary information to apply the proposed methodology and will help to understand the overall process of a carbon capture and storage (CCS) project.

The production stage of a reservoir begins after the first discovery well is drilled. Once the well's potential is evaluated, the development of the field starts by building surface

facilities, planning and drilling additional wells, transportation pipelines, and endless crucial decision for the future exploitation resources.

During the production stage, part of the development consists on characterizing the fluid in place by taking samples for laboratory analysis, and estimating oil, gas and water saturations through core sampling and well logging. Moreover, the reservoir pressure is frequently measured in the wells and estimated for the entire reservoir through different methods, such as downhole pressure sampling, well testing and reservoir simulation models. Also of high importance, the original oil and gas in place can be estimated from seismic, material balance analysis and reservoir simulation. These three particular properties (fluids characterization, reservoir pressure, and fluids in place) are the most important input vectors for the proposed method in this investigation.

Fluid extraction from the reservoir causes a pressure decline; unless an enhanced oil recovery (EOR) process, such as waterflooding or gas injection, has been implemented. Once the reservoir cannot be economically produced, the wells are abandoned and the operations finish, it is at this stage that the CCS process may begin. The average reservoir pressure at the time production has finished will be defined, in this work, as depleted pressure.

CO_2 injection starts at the average depleted reservoir pressure and as more fluid is injected (without production), the average pressure increases until reaching a designed

target pressure. This target pressure can be limited by the initial reservoir pressure or by operational constraints. Initial reservoir pressure should not be exceeded to avoid sealing losses and to prevent CO_2 migration outside the reservoir boundaries. Operational constraints, such as compression power or pipeline capacity, can also limit the final target pressure to a specific value. In either case, the final reservoir average pressure is predetermined and operations can be designed to achieve that target.

The composition of the CO_2-based injection stream is also known in advance. The gas composition from the source, e.g. power plant, is characterized and a separation process can be designed to provide the desired composition of the fluid. Separation costs highly increase as the purity of the outlet stream increases (concentrated CO_2); the economic success of the project may be subject to the balance between fluid purity and the ultimate amount of CO_2 that can be stored. For this reason, performing fast sensitivities to understand the storage capacity for different injection fluid compositions becomes a strategic activity.

Supplementary properties such as water and rock compressibility are estimated with correlations depending on water salinity and rock type, or can be measured in the laboratory using reservoir samples, if they are available.

The proposed model assumes a closed boundary reservoir subject to pressure changes during the production and injection stages. The fluids are extracted from the reservoir by

depletion through production wells until reaching economic limit; water or gas injection processes can also be developed in the field in this stage. Subsequently, CO_2 injection operations start and no more fluids are produced from the reservoir.

The average reservoir fluid composition at the end of the production stage can be estimated if a good fluid characterization is available. Laboratory tests, such as constant volume depletion and differential liberation, support the understanding of the fluid phase behavior and composition during depletion of the reservoir. Additionally, reservoir simulation and compositional material balance may be used to validate laboratory analysis.

3.2 Solution Approach

The field operations described in the previous section validate a volume constrained solution approach using an EOS to estimate the properties of the hydrocarbon and injected fluid mixture at the estimated target pressure.

Total pore volume, before starting the injection, is filled with water and hydrocarbon at depleted conditions. Since the rock and water compressibility are known, final water and pore volumes can be estimated at the final target pressure, allowing to estimate the final hydrocarbon pore volume (HCPV). The fluid filling the HCPV at final target conditions is composed by a mixture of the hydrocarbons in place before the start of the injection

and the injected fluid. This mixture can be in single- or two-phase at any moment between the start and the end of the injection process.

The total volume V occupied by the fluid mixture at target pressure, at the end of the injection, is a function of pressure, temperature, and the total number of moles of fluid; that is:

$$V = f(p, T, n) \quad \text{..... (3.1)}$$

The total number of moles of fluid is given by the summation of the moles of hydrocarbons in place before the start of the injection (at depletion stage) and the injected fluid, as Eq. (3.2) shows.

$$n = n_{dep} + \Delta n \quad \text{..... (3.2)}$$

The change of the total volume, as the injection fluid mixes with the hydrocarbon evaluated at final target pressure and reservoir temperature, can be expressed by Eq. (3.3).

$$dV = \left(\frac{\partial V}{\partial p}\right)_{T,n} dp + \left(\frac{\partial V}{\partial T}\right)_{p,n} dT + \sum_{n_x} \left(\frac{\partial V}{\partial n_x}\right)_{p,T,n_j} dn_x \quad \text{..... (3.3)}$$

Notice that reservoir temperature is considered constant, which allows to drop the second term on the RHS. Additionally, taking advantage of the State Function, the path between depletion and target conditions was divided in two steps. In the first step, the pressure is increased at constant number of moles, which only causes fluid compression.

The second step is developed at constant target pressure and increasing the number of moles. For the second step, integrating Eq. (3.3) with respect to the number of moles injected at target pressure gives:

$$\int_{n_{dep}}^{n_{dep}+\Delta n} dV = \int_{n_{dep}}^{n_{dep}+\Delta n} \left(\frac{\partial V}{\partial n_x}\right)_{p,T,n_j} dn_x \quad \text{..... (3.4)}$$

where, n_{dep} is the number of moles of the reservoir fluid before injection and Δn is the cumulative number of injected moles at the end of the process. The solution of the left-hand side (LHS) integral of Eq. (3.4), and the application of $\bar{V}_x$, the definition for the generalized partial molar volume (PMV) developed in Appendix A, provides the form of Eq. (3.5)

$$V_{n_{dep}+\Delta n} = V_{n_{dep}} + \int_{n_{dep}}^{n_{dep}+\Delta n} \bar{V}_x \, dn_x \quad \text{..... (3.5)}$$

The LHS of Eq. (3.5) represent the total volume occupied by the fluid, hydrocarbons at depletion and injected fluid, at final target pressure and temperature. $V_{n_{dep}}$ is a fictional volume representing the volume that would be occupied by n_{dep} moles of hydrocarbons at target pressure and temperature; and is directly obtained by calculating the molar volume of the fluid composition at the depletion stage, using the target pressure and temperature. The final volume available for hydrocarbons and injected fluid $V_{n_{dep}+\Delta n}$

can be estimated by using the rock and water compressibilities, described in the following section. The only unknown is the added moles of injection fluid Δn in the upper limit of the integral.

Fig. 3.1 displays the relationship between fluid volume, pressure, and fluid total number of moles during injection. The process starts at depletion conditions, where the fluid volume occupies the HCPV at depletion $HCPV_{dep}$, the reservoir is at average depleted pressure p_{dep}, and total fluid moles n_{dep}. Reaching target conditions requires increasing the average reservoir pressure to p_{target} by injecting an unknown amount of fluid moles Δn; the pressure increase causes a HCPV increase due to rock and water compression, leading to a final $HCPV_{target}$ available for the hydrocarbon and injected gas mixture volume $V_{n_{dep}+\Delta n}$.

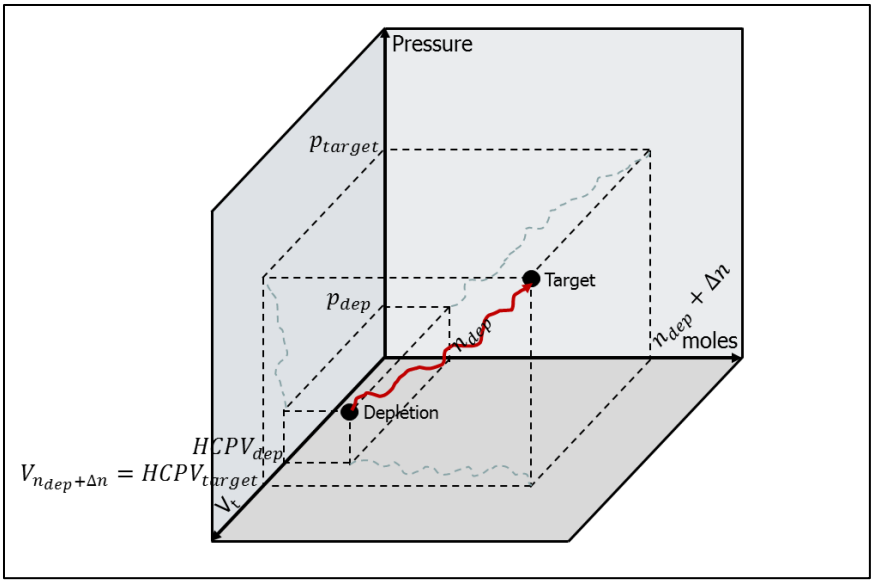

Fig. 3.1—Thermodynamic relationships between fluid volume, pressure, and moles during injection. Following a direct path from depletion to target conditions is complex to solve; instead, use the State Function.

Nevertheless, this path involves several variables changing at the same time and it is complex to solve. In its place, the new proposed analytical method takes advantage of the State Function, which indicates that fluid properties at the end of the process are independent from the path followed to reach final target conditions. **Fig. 3.2** shows two paths to reach target conditions. The first path starts at depletion conditions and ends at a fictitious condition by increasing the pressure to p_{target} without adding fluid moles; the pressure increase causes fluid compression to the fictitious volume $V_{n_{dep}}$. The second path starts at the fictitious condition and ends at target conditions; this path is performed at constant pressure by adding Δn moles of fluid until the hydrocarbon and injected gas mixture volume, $V_{n_{dep}+\Delta n}$, equals $HCPV_{target}$.

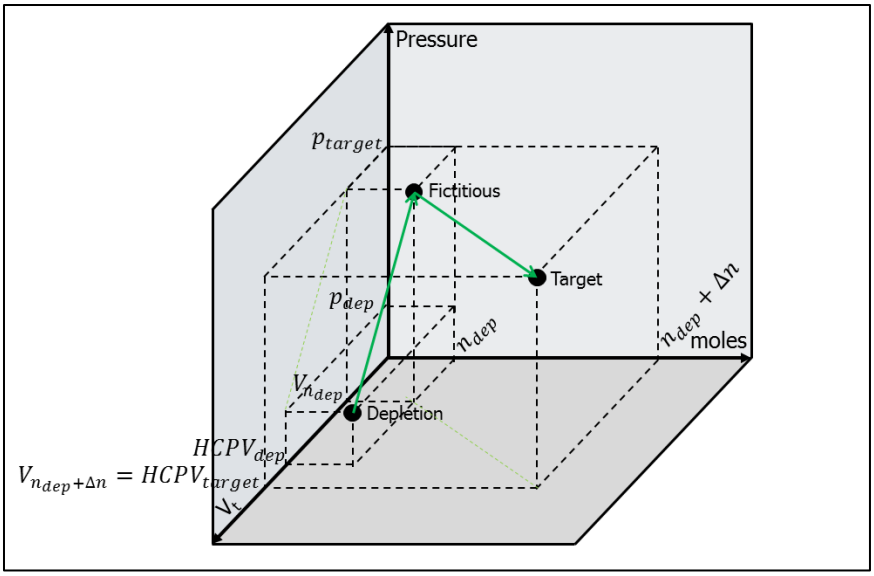

Fig. 3.2— Thermodynamic relationships between fluid volume, pressure, and moles during injection. Applying the State Function allows an easier estimation of added moles by creating a fictitious condition in the path between depletion and target states.

Recall that the only unknown in Eq. (3.5) is the added moles Δn of injection fluid. Two methods are proposed in this study, to find the solution of the integral in the RHS and the value of Δn that satisfies Eq. (3.5). The first method is semi-analytical, which considers the PMV, $\bar{V}_x$, to be constant; thus the change in total fluid volume with respect to the added moles can be approximated with a straight line. The second method is fully analytical and applies rigorously the concept of PMV and thermodynamic laws.

3.3 Semi-analytical Method

The semi-analytical method applied in this study uses a cubic equation of state (EOS) to estimate the fluid properties at reservoir conditions to estimate the UCSC; this method

should not be confused with reservoir numerical simulation which performs finite difference calculations to describe the fluid movement in the reservoir.

The general procedure for this method is presented in **Fig. 3.3**. The required input data are reservoir temperature, initial pressure, depleted pressure at the end of the production stage, average reservoir fluid composition at the end of the production stage, initial pore volume, initial water saturation and rock and water compressibility. The controls of the process are the target pressure at the end of the injection, desired EOS and the composition of the injection gas.

To explain in detail the calculations performed in each step, the method is divided in four stages. The first stage is the calculation of the pore volume and water saturation at depletion and at target conditions. The second stage estimates the fluid thermodynamic properties and saturations at depletion using the composition of the hydrocarbon fluid at these conditions. The third stage allows the estimation of the total volume occupied by the reservoir fluid after adding different quantities of injected fluid. Finally, the fourth stage characterizes the relationship between the total fluid volume and the added moles of injected gas with a straight line, which can be used to estimate the UCSC at the target pressure.

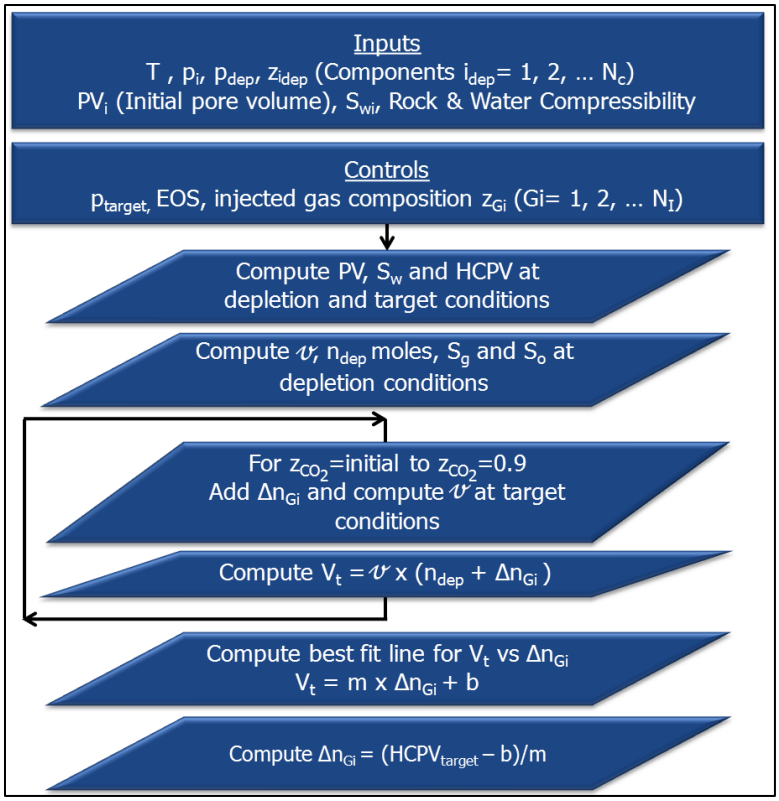

Fig. 3.3—Semi-analytical method flow chart to estimate CO_2 storage capacity. This method is based on the straight line approximation of the total volume vs. added moles behavior.

3.3.1 Pore Volume and Water Saturations at Depletion and Target Conditions

This stage performs volumetric calculations that will become the basis for the more accurate final estimation of CO_2 storage. The input data for this stage are initial, depletion and target pressures, initial pore volume and water saturation, rock and water compressibility at a reference pressure.

The rock matrix compresses when the fluid pressure increases in the pore volume PV, in other words, the pore volume expands as the pressure increase. Conversely, when

pressure decreases, the pore volume reduces. Both effects can be described with isothermal compressibility (Dake 1978), as shown in Eq. (3.6).

$$PV|_p = PV|_{ref} \times e^{-c_{rock}(p_{ref}-p)} \quad \text{(3.6)}$$

Correspondingly, the change in water volume can be estimated with the same approach. Water is nearly incompressible and Eq. (3.7) presents and accurate method to calculate isothermal water volume at different pressures.

$$V_{water}|_p = V_{water}|_{ref} \times e^{-c_{water}(p_{ref}-p)} \quad \text{(3.7)}$$

Both, Eqs. (3.6) and (3.7), result from the integration of the isothermal compressibility, presented in Eq. (3.8) (Dake 1978). Note that the direct solution of this integral assumes constant compressibility for the range of pressures used.

$$c = -\frac{1}{V}\frac{\partial V}{\partial p}\Big|_T \quad \text{(3.8)}$$

The initial water volume is computed from the initial pore volume and water saturation. The water and pore volumes at depletion conditions can be estimated using Eq. (3.6) and (3.7). If water is produced before the CO_2 injection process, it must be accounted for to properly estimate the remaining water volume in the reservoir at depletion conditions. The pore volume calculation is direct since it depends only on pressure and not on the fluids contained in it.

Water is assumed to be inert during production and injection; meaning that there is no mutual solubility between water and other fluids, and no chemical reactions take place. Mineralization rates in the reservoir volume base are very slow and current level of understanding in the long term chemical reactions does not allow to characterize this phenomena. Depending on reservoir rock and water properties, mineralization may occur during the CO_2 injection process reducing injectivity (Gallo et al. 2002).

The gas volume dissolved in water, during production stage, is negligible in comparison with the free gas volume in a gas condensate reservoir or the dissolved gas in the oil phase in a black oil reservoir. During the injection stage, CO_2 dissolution in water is also negligible (Sifuentes et al. 2009). This dissolution effect becomes noticeable only after a few hundred years of storage.

The results obtained from this stage are the pore volume and water saturation at depletion and at target conditions. The pore volume available for the hydrocarbon and CO_2 mixture at depletion and final conditions is also calculated as shown on Eq. (3.9). For the next stages, this volume will be denoted hydrocarbon pore volume (HCPV), which represents the total available space for the mixture between the original hydrocarbons in place and the injected CO_2-based stream, composed by CO_2 and impurities such as nitrogen and carbon monoxide (Metz et al. 2005).

$$HCPV = PV(1 - S_w) \quad \text{..... (3.9)}$$

3.3.2 Fluid Properties at Depletion Conditions

Fluid properties at depletion conditions are calculated using vapor-liquid equilibrium (VLE) calculations briefly described in Section 2.4. The input information are reservoir temperature, depletion pressure and reservoir fluid average composition at depletion.

VLE computations provide phase fractions and molar volume of the reservoir fluid before the injection starts. The total number of moles at this stage is estimated using the HCPV at depletion, calculated in the previous Section 3.3.1, and the molar volume of the fluid, solving Eq. (3.10).

$$n_{dep} = \frac{HCPV_{depleted}}{\vartheta_{depleted}} \quad \text{.....(3.10)}$$

Average oil and gas saturations at depletion are estimated through the liquid and vapor molar volumes and fractions, and pore volume showed in the previous Sections 2.4 and 3.3.1 respectively.

$$S_o = \frac{(1 - f_v)\vartheta_l n_{dep}}{PV} \quad \text{..... (3.11)}$$

$$S_g = \frac{f_v \vartheta_v n_{dep}}{PV} \quad \text{..... (3.12)}$$

The results obtained from this stage describe the fluid and reservoir characteristics before starting the injection for storage purposes. The main parameters calculated at this

stage are the total number of moles of fluid in the reservoir, pore volume and HCPV, and average oil, gas and water saturation.

3.3.3 Fluid Properties at Target Conditions

This stage consumes most of the computational time. The calculations consist on a loop to estimate the molar volume and total volume of different fluid mixtures at final average reservoir pressure and temperature. The different fluid mixtures are obtained by successively adding moles of CO_2, pure or with impurities, to the reservoir fluid after depletion, and therefore increasing its composition. The inputs for this step are the target pressure, injection fluid composition, and reservoir fluid composition at the end of the depletion process. Reservoir fluid composition may not be directly obtained from a fluid sample if the reservoir pressure dropped below saturation point. Fluid composition can be estimated from reservoir simulation or laboratory data from a representative fluid sample.

The first cycle of the loop starts with the original fluid composition at depletion. The molar volume of the fluid is obtained through VLE calculations at final target pressure and reservoir temperature, recall Eq. 2.13.

$$\upsilon = f_l \upsilon_l + f_v \upsilon_v = (1 - f_v)\frac{M_{w_l}}{\rho_l} + f_v \frac{M_{w_v}}{\rho_v} \quad \text{..... (2.13)}$$

Successively, the total volume occupied by the fluid at the specific conditions is calculated based on the molar volume, the total number of moles of the fluid at depletion stage, and the quantity of added moles from the injected fluid, see Eq. (3.13).

$$V_t = \left(n_{dep} + \Delta n\right) \times \vartheta \quad \text{..... (3.13)}$$

The following cycles of the loop involve successive additions of CO_2 to the original fluid mixture. The maximum CO_2 composition allowed 0.90, which in real cases would be difficult to achieve. After performing a sensitivity analysis, the addition of moles was finally set to 12 steps, increasing the number of moles exponentially to ensure high density of points in the low end of addition to increase the accuracy. **Table 3.1** presents a sample calculation of the methodology presented above. A fluid quantity of 100 moles at depletion stage, with 3% CO_2 content, is selected as base. The injected fluid contains 94% CO_2, 5% nitrogen and 1% carbon monoxide. This procedure can be used for any reservoir size and quantity of fluid, as expressed in Eq. (3.10).

Table 3.1—CO_2 COMPOSITION CALCULATION SAMPLE FOR 100 MOLES OF FLUID AT DEPLETION STAGE CONTAINING 3% CO_2. INJECTION FLUID COMPOSITION IS 94% CO_2, 5% N_2 AND 1% CO.

Loop Cycle	Δn, mol	Δn_{CO_2}, mol	CO_2 composition, %
0	0	0.0	3.00
1	1	0.9	3.90
2	2	1.9	4.78
3	4	3.8	6.50
4	8	7.5	9.74
5	16	15.0	15.55
6	32	30.1	25.06
7	64	60.2	38.51
8	128	120.3	54.09
9	256	240.6	68.44
10	512	481.3	79.13
11	1024	962.6	85.90
12	2048	1925.1	89.76

The calculations in each cycle begin with the determination of the number of CO_2 moles to be added. Knowing the composition of the injected fluid, the added moles of the rest of the components is also calculated. The new mixture, composed by original fluid and injection fluid, is re-normalized to obtain its overall composition and perform the VLE calculations. Additionally, the total volume of the new mixture is calculated at final conditions through Eq. (3.13).

At the end of the 12 cycles, the result is a list of total fluid volumes and corresponding added moles ratios, all at final target pressure and reservoir temperature.

3.3.4 Ultimate CO_2 Storage Capacity

This is the final stage of the semi-analytical method. The UCSC at the specified target pressure is calculated by defining a best fit line for the total volume vs. added moles points obtained in the previous stage.

Recall the partial molar volume definition, presented in the Chapter II, as the variation of the total fluid volume with respect to added moles of the component "i". The validation of the results show that this change in volume can be approximated with a straight line, that defines its behavior for the given target pressure, reservoir temperature, initial fluid composition and injected fluid composition; meaning that the argument of the integral in Eq. (3.5) is constant for some particular cases. The slope of the straight line is by definition the partial molar volume.

The best fit line is obtained through the singular value decomposition (SVD) pseudo-inverse method showed in Chapter II. Eq. (3.14) displays the final form of the straight line. The target total fluid volume V_t corresponds to the HCPV at final conditions, calculated in the first Section 3.3.1. Knowing the slope and the intercept, the added moles can be calculated solving Eq. (3.14).

$$V_t = m \times \Delta n + b \quad \text{..... (3.14)}$$

3.3.5 Limitations of the Semi-analytical Method

The proposed semi-analytical method is based on the partial molar volume concept. Simulation results show that the relationship between the total volume occupied by the hydrocarbon and injected fluid mixture can be approximated by a straight line, for practical purposes. However, there is no thermodynamic explanation to corroborate this phenomenon.

Fig. 3.4 shows Sample Case 1 results of the semi-analytical method. The symbols are the total fluid mixture volume with respect to the added moles of injected fluid, calculated at final target reservoir pressure and temperature, using the 4 steps showed previously in Sections 3.3.1 to 3.3.4. The straight line presents an excellent fit for the data points and the estimation of the UCSC was accurate within less than 0.1% difference with respect to the reservoir simulation results. Note that the intercept is forced to match $V_{n_{dep}}$ defined in Eq. (3.5). **Table 3.2** presents the properties for this case.

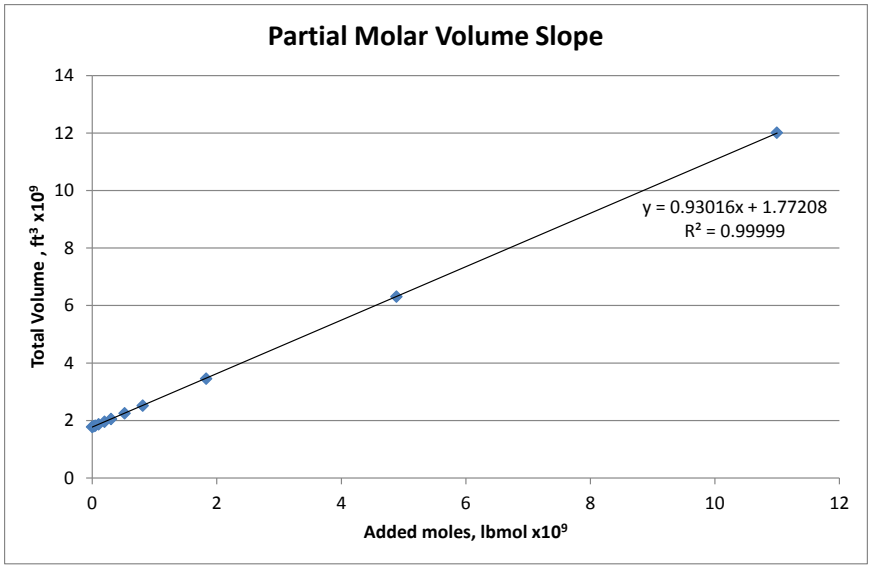

Fig. 3.4—Semi-analytical method Case 1 results. Volumes are computed from molar volume and total number of moles in the mixture with different mixing ratios. Straight line is fitted through the points.

Table 3.2—SAMPLE CASE 1 PROPERTIES. PRESENTS LARGE PRESSURE DIFFERENTIAL BETWEEN DEPLETION AND TARGET PRESSURE, INJECTED FLUID IS A MIXTURE OF CO_2 AND N_2.

Model Properties	
Pressure at depletion, psia	3,030
Final pressure, psia	6,995
Pressure differential, psi	3,965
Reservoir temperature, °F	200
Injected fluid	80% CO_2 20% N_2

Fig. 3.5 shows a zoom in the left section of Fig. 3.4, where the quantities of CO_2 injected in the reservoir are small; initial CO_2 composition is 4.5% and after injecting 3.06×10^8 lb-mol of fluid CO_2 composition only reaches 20%. For this case scenario, with a particular reservoir fluid, depletion and target pressures, and composition of the injection fluid, the match of the straight line with the calculated points in excellent.

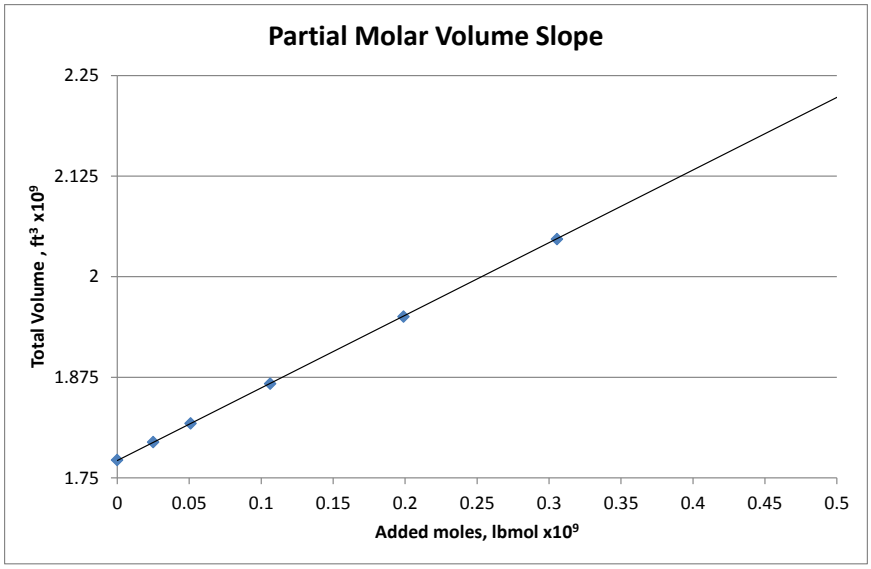

Fig. 3.5—Semi-analytical method Case 1 results. Zoom from Fig. 3.4 shows excellent match for small quantities of CO_2 injected.

On the other hand, **Fig. 3.6** presents the same semi-analytical method for a different reservoir fluid and similar depletion and target pressures (Sample Case 2). Although this sample was accurate within 1% error with respect to reservoir simulation, and the straight line fit seems reasonable, the early data points are not well matched. **Table 3.3** presents the properties for this case.

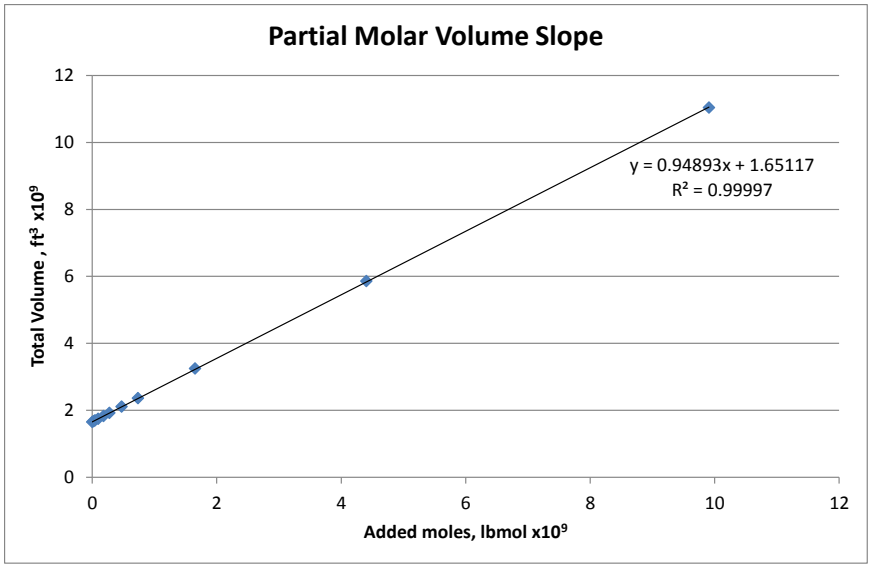

Fig. 3.6—Semi-analytical method Case 2 results. Volumes are computed from molar volume and total number of moles in the mixture with different mixing ratios. Straight line is fitted through the points.

Table 3.3—SAMPLE CASE 2 PROPERTIES. PRESENTS LARGE PRESSURE DIFFERENTIAL BETWEEN DEPLETION AND TARGET PRESSURE, INJECTED FLUID IS A MIXTURE OF CO_2 AND N_2.

Model Properties	
Pressure at depletion, psia	2,945
Final pressure, psia	7,000
Pressure differential, psi	4,056
Reservoir temperature, °F	200
Injected fluid	80% CO_2 20% N_2

Fig. 3.7 shows a poor match in the section that represents small quantities of CO_2 injected in the reservoir, the straight line starts to deviate from the matching trend when CO_2 composition ranges between 10 and 25%. This indicates that the argument of the integral in Eq. (3.5) is not constant and it cannot be described with a straight line behavior for every case.

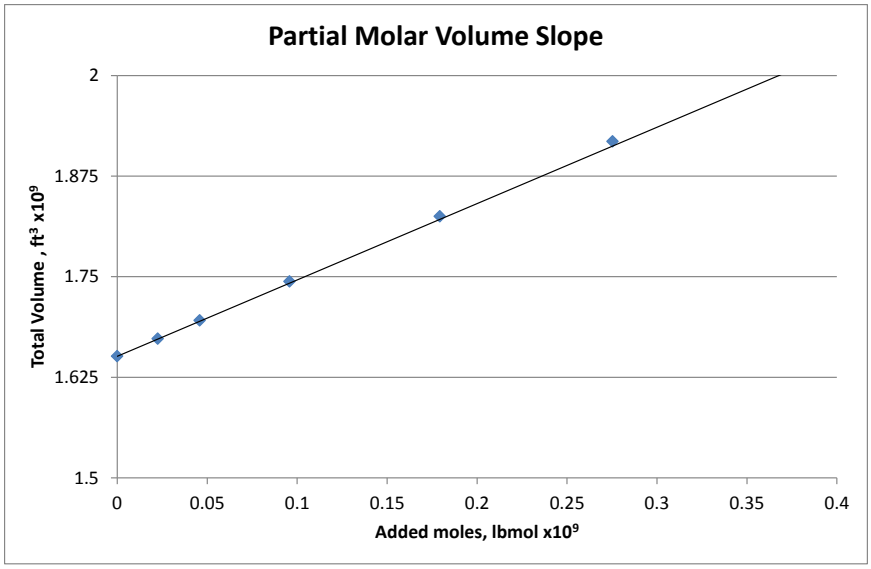

Fig. 3.7—Semi-analytical method Case 2 results. Zoom from Fig. 3.6 shows poor match for small quantities of CO_2 injected.

This method provides very accurate results for practical purposes, especially when the pressure differential between depletion and target pressures is large, and the calculation procedure is easy and fast. The confirmation of the excellent capabilities of this approach represents the first step in the development of a more rigorous method. The analytical, and more rigorous method, requires the application of thermodynamic concepts and definition intrinsically, to consider the variability of partial molar volume. This need drives the research for a fully analytical method to estimate the UCSC in depleted oil and gas reservoirs, presented in the following section.

3.4 Analytical Method

The analytical method is a more rigorous application of the semi-analytical method presented in the Section 3.3. The semi-analytical results indicated that the UCSC of a

depleted oil or gas reservoir, at a defined target pressure, can be estimated using an analytical approach. The previous method considered constant PMV, $\bar{V}_x$, at final reservoirs conditions while injecting the CO_2-based stream. This consideration is valid only in some cases, and a more rigorous solution for the integral of the PMV must be developed.

The general procedure for the analytical method is presented in **Fig. 3.8**. The required input data are the same as the semi-analytical method, which include reservoir temperature, initial pressure, depleted pressure at the end of the production stage, average reservoir fluid composition at the end of the production stage, initial pore volume, initial water saturation and rock and water compressibility. The controls of the process are also the target pressure at the end of the injection, desired EOS and the composition of the injection gas.

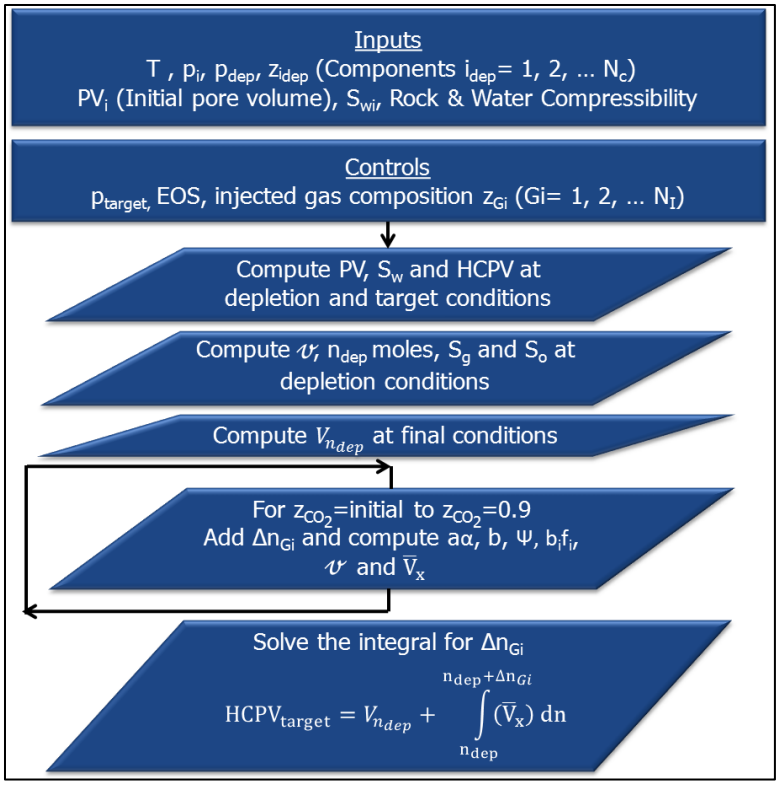

Fig. 3.8—Analytical method flow chart to estimate CO_2 storage capacity. This method is based on the generalization of the partial molar volume definition considering a mole fraction change in more than one component.

To explain in detail the calculations performed in each step, similarly to the semi-analytical method, the method will be divided in three stages. The first and second stages are the same as presented in the semi-analytical method, Sections 3.3.1 and 3.3.2. The third stage presents the solution of the integral of the PMV in Eq. (3.5), where the upper limit provides the UCSC at the selected target pressure.

3.4.1 Analytical Solution

The PV, HCPV and fluid properties at depletion conditions are calculated, as mentioned previously, following the same procedure presented for the semi-analytical method in Sections 3.3.1 and 3.3.2.

The third stage comprises the rigorous solution of the integral of the PMV. Recall Eq. (3.5):

$$V_{n_{dep}+\Delta n} = V_{n_{dep}} + \int_{n_{dep}}^{n_{dep}+\Delta n} \bar{V}_x \, dn_x \quad \text{..... (3.5)}$$

where all the terms are evaluated at final average reservoir pressure and temperature. The term $V_{n_{dep}+\Delta n}$ represents fluid volume at final target conditions and must match the HCPV at final target conditions to fill the pore space; although the amount of injected gas is unknown, using the target pressure and isothermal compressibility of rock and water, the HCPV at final average reservoir pressure can be estimated. The term $V_{n_{dep}}$ represents a fictitious volume occupied by the fluid with depletion stage composition, at final average reservoir pressure. Conversely, it can be expressed as compressing the depletion stage fluid from depletion pressure to final target pressure, with no change in composition.

All the terms in Eq. (3.5) are known, except Δn which is the objective of this study. The generalized PMV $\bar{V}_x$, derived in Appendix A, is defined by Eq. (3.15).

$$\bar{V}_x = -\frac{R_1 + A_1}{D_1} \quad \text{..... (3.15)}$$

where:

$$R_1 = \frac{RT}{\mathcal{v} - b_m} + \frac{RT\sum_{i=1}^{N_c} f_i b_i}{(\mathcal{v} - b_m)^2} \quad \text{..... (3.16)}$$

$$A_1 = -\frac{2\Psi}{(D_{\mathcal{v}})} + \frac{2(a\alpha)_m \mathcal{v}\sum_{i=1}^{N_c} f_i b_i}{(D_{\mathcal{v}})^2} - \frac{2(a\alpha)_m b\sum_{i=1}^{N_c} f_i b_i}{(D_{\mathcal{v}})^2} \quad \text{..... (3.17)}$$

$$D_1 = -\frac{RT}{(\mathcal{v} - b_m)^2} + \frac{2(a\alpha)_m(\mathcal{v} + b_m)}{(D_{\mathcal{v}})^2} \quad \text{..... (3.18)}$$

and

$$\Psi = \sum_{i=1}^{N_c}\sum_{j\neq i=1}^{N_c}\left[f_i x_j\left(a\alpha_{ij}\right)\right] + \sum_{i=1}^{N_c}[f_i x_i a_i \alpha_i] \quad \text{..... (3.19)}$$

$$D_{\mathcal{v}} = \mathcal{v}^2 + 2b_m\mathcal{v} - {b_m}^2 \quad \text{..... (3.20)}$$

Given the complex dependence of this Eq. (3.15) with respect to the number of moles n, no direct analytical solution was found feasible. Instead, the integral in Eq. (3.5) will be solved numerically, ensuring an accurate result and honoring the thermodynamic principles used in the derivation of the equations. The objective is then, finding the upper limit Δn value that satisfies Eq. (3.5).

This task is performed iteratively, adding small quantities of injection fluid to the reservoir fluid and evaluating the properties of the resulting mixture at final target conditions. The methodology of injected fluid addition is based on CO_2 composition rather than total amounts. The CO_2 composition of the fluid at depletion stage is selected as base, and starting from that reference, quantities of injection fluid are added in small steps until the CO_2 mole fraction composition is 0.9. Performed sensitivities suggested that 200 steps are sufficient to provide accurate results for the numerical integration procedure.

For each step, the number of moles added Δn is recorded, and the properties $(a\alpha)_m$, b, Ψ, $\sum f_i b_i$, $\mathcal{v}$, and $\bar{V}_x$ are computed to evaluate the integral numerically. At the end of the procedure, the UCSC at the average target pressure is given by the unique Δn value that satisfies Eq. (3.5). Subsequently, the final fluid composition in the reservoir is calculated and a flash allows to estimate the phase saturations at the end of the injection process.

This method allows to estimate the UCSC of a reservoir by selecting a depletion pressure where the injection starts and designing different scenarios for target pressure and CO_2 concentration in the injection stream.

CHAPTER IV

RESERVOIR SIMULATION MODELS

Reservoir simulation is the current common practice to understand CO_2 injection processes and estimate the ultimate CO_2 storage capacity (UCSC) of depleted oil and gas reservoirs. This chapter presents two numerical models developed in a commercial software package (Schlumberger 2010a) for this study, to validate the results of the proposed analytical method. The first model is a gas condensate reservoir, while the second is a compositionally simulated black-oil-type fluid. Both models have heterogeneous and anisotropic petrophysical properties distribution, and the fluid models have been constructed by calibration of the Peng-Robinson equation of state with experimental PVT data.

4.1 Reservoir Description

The reservoir model is representative of the Cupiagua field in Colombia. The selected section of the stratigraphic column is formed by layered sandstone sections, which display sheet-like packages of shoreface bodies (Ramon and Fajardo 2006).

Fig. 4.1 shows the dimensions of the reservoir model. The thickness of the reservoir is 270 ft and its areal extension is 8,000 ft x 8,000 ft, nearly 1,470 acres. The vertical discretization of the grid is 10 ft for the 21st layers in the top, and 50 ft and 100 ft for the

bottom layers correspondingly to improve modeling of aquifer influx. The horizontal length and width of the cells is 320 ft. **Table 4.1** further displays grid dimensions.

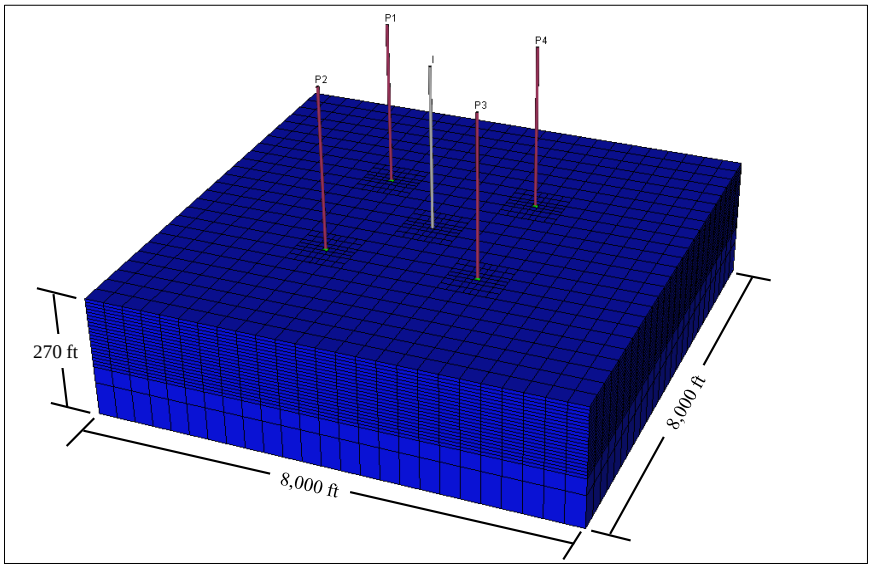

Fig. 4.1—Reservoir model dimensions. Areal extension of the reservoir is 1,470 acres and the thickness is 270 ft.

Table 4.1—RESERVOIR MODEL DIMENSIONS. VERTICAL DISCRETIZATION OF GRID SIZE ALLOWS TO IMPROVE AQUIFER INFLUX MODELING

Reservoir Model Dimensions		
Length, ft		8,000
Width, ft		8,000
Thickness, ft		270
Grid size x-direction, ft		320
Grid size y-direction, ft		320
Grid size z-direction, ft	Layers 1-21	10
	Layer 22	50
	Layer 23	100
Gridblocks in *x* direction		25
Gridblocks in *y* direction		25
Gridblocks in *z* direction		23
Total number of gridblocks		14,375

Additional grid refinements were performed in the near-wellbore to attain a better description of the fluid movement and components interaction in that region. Local grid refinement details are discussed in the well design section.

Fig. 4.2 presents the porosity distribution of the reservoir model. The vertical variation of porosity ranges from 1.54% to 18.22%, with an average value of 13%, and 4.2% of standard deviation.

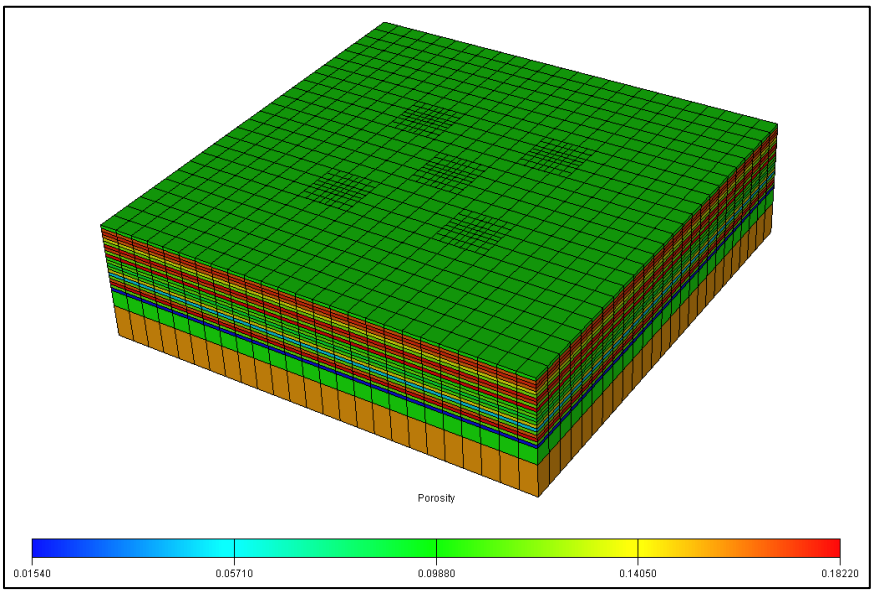

Fig. 4.2—Reservoir model porosity distribution. The reservoir is formed by sandstone layers with an average porosity of 13%.

Fig. 4.3 presents the permeability distribution of the reservoir model. The horizontal permeability in the reservoir ranges from 0.21 to 85.4 mD, with an average value of 28.5 mD, and 28.7 mD of standard deviation. Dykstra-Parsons coefficient for this model is

0.79, indicating high heterogeneity. The anisotropy is given by vertical to horizontal ratio of 0.1.

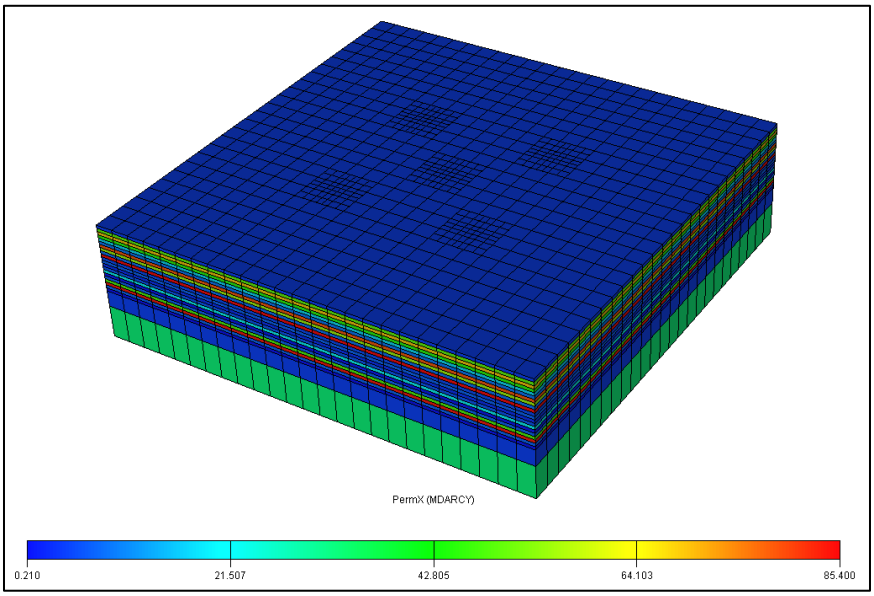

Fig. 4.3—Reservoir model horizontal permeability distribution. The reservoir is formed by sandstone layers with an average horizontal permeability of 28.5 mD.

The heterogeneity and anisotropy in the reservoir properties, among other characteristics, will influence the lateral and vertical advance of the CO_2 plume. The formation of the plume creates pressure and compositional gradients in the reservoir, thus, the pressure and fluid composition is different in each part of the reservoir.

The proposed analytical method is a zero dimensional model, which does not consider vertical and horizontal variations of pressure nor composition. Instead, the analytical

method uses average pressure and compositions to calculate average fluid properties in the reservoir and from that information estimate average phase saturations.

Table 4.2 offers further information about the reservoir. The specified reservoir initial pressure and temperature correspond to the base case. The reservoir temperature is a sensitivity factor in this study, to assess its influence on the UCSC, phase saturations, and the validity of the proposed analytical method over a wide range of conditions. The initial reservoir pressure is recalculated for each temperature to ensure the thermodynamic equilibrium during the simulation. The sensitivities to reservoir temperature were performed at 100, 150, 200, 250, 270, and 285 °F.

Table 4.2—RESERVOIR MODEL PROPERTIES.

Reservoir Model Properties	
Porosity, % (min, mean, max)	1.54, 13.00, 18.22
Permeability, mD (min, mean, max)	0.2, 28.5, 85.4
Dykstra-Parsons coefficient	0.79
k_v/k_h, fraction	0.10
Rock compressibility, psi^{-1}	$4x10^{-6}$
Water compressibility, psi^{-1}	$3x10^{-6}$
Reference pressure, psia	5,868
Reservoir top, ft	12,540
Initial pressure*, psia	5,852
Reservoir temperature*, °F	285

*Reservoir temperature is varied in the sensitivities. Initial reservoir pressure is recalculated accordingly to new conditions, maintaining the thermodynamic equilibrium.

Fluid contacts, water-oil and water-gas, are also recalculated according to temperature changes. Thermodynamic equilibrium must be ensured at initial conditions in each reservoir model. Cases were water production is required, for validation of the analytical

algorithm, water contact is set within the reservoir thickness and equilibration is recomputed.

4.2 Fluid Models Description

This subsection presents the fluid models used in this study. Two different fluids, a gas condensate and a black oil, were used to demonstrate the robustness of the analytical algorithm regardless of the reservoir fluid. Both fluids are modeled compositionally, with the Peng-Robinson equation of state (PR-EOS), to properly represent and describe the interactions between the components in the reservoir fluid and the injected fluid.

4.2.1 Gas Condensate Model

The gas condensate fluid model has 7 components. Carbon dioxide, nitrogen and methane are modeled as pure components to properly describe fluid behavior under injection of CO_2-based streams, the rest of the components are lumped in pseudocomponents. Fluid composition and component properties, molecular weight, critical temperature and pressure, and acentric factor are shown in **Table 4.3**.

Table 4.3—GAS CONDENSATE FLUID MODEL PROPERTIES.

Component	Z_i, %	M_w, lb/lb-mol	T_c, °R	P_c, psia	ω
CO_2	4.596	44.010	548.46	1071.33	0.28686
N_2	0.000	28.013	227.16	492.31	0.04000
C_1	61.719	16.093	342.60	667.05	0.01672
C_2- C_3	14.418	34.940	590.00	676.20	0.14952
C_4- C_6	4.815	63.213	777.78	520.02	0.26301
C_7- C_{10}	7.507	105.660	1027.22	423.52	0.40695
C_{11+}	6.944	254.193	1367.80	231.55	0.86200

Binary interaction coefficients (BIC), presented in **Table 4.4**, were obtained through the EOS calibration to match fluid properties measured in the lab. EOS calibration was performed previously to this study (Barrufet et al. 2010).

Table 4.4—GAS CONDENSATE FLUID MODEL BIC.

Binary Interaction Coefficients							
BIC	**CO_2**	**N_2**	**C_1**	**C_2- C_3**	**C_4- C_6**	**C_7- C_{10}**	**C_{11+}**
CO_2	0						
N_2	-0.012	0					
C_1	0.100	0.100	0				
C_2- C_3	0.100	0.100	0.03672	0			
C_4- C_6	0.100	0.100	0.01348	0	0		
C_7- C_{10}	0.100	0.100	0.03700	0	0	0	
C_{11+}	0.100	0.100	0.05212	0	0	0	0

The initial fluid composition, showed in Table 4.3, corresponds to a typical gas condensate fluid at 285 °F. Calculated critical temperature of this fluid is 265 °F and reservoir temperature sensitivities range from 100 to 285 °F, which indicates that for temperatures lower than 265 °F, this fluid will behave as a volatile oil, while for temperatures greater than 265 °F will exhibit as gas condensate behavior. **Fig. 4.4** illustrates the computed phase envelope for this fluid.

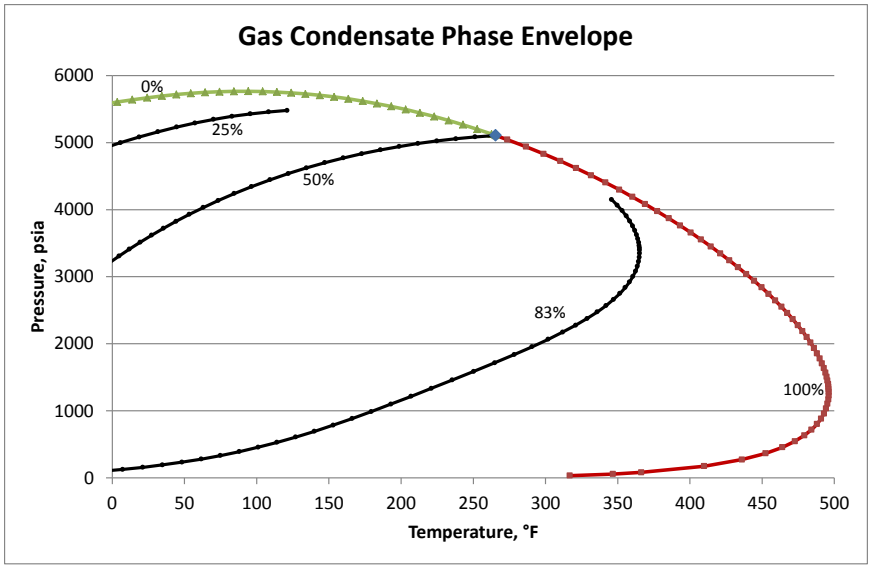

Fig. 4.4—Phase envelope for gas condensate sample. Critical temperature is 265°F and reservoir temperatures sensitivities range from 100 to 285°F. Sensitivities above critical temperature exhibit gas condensate behavior, while sensitivities below this value exhibit volatile oil behavior.

4.2.2 Black Oil Model

The black oil fluid model has 6 components. This fluid is named black oil for its properties and behavior; however, it is treated and simulated using a compositional description. Carbon dioxide, nitrogen, and methane are modeled as pure components, the rest are lumped in pseudocomponents. Fluid composition and component properties, molecular weight, critical temperature and pressure, and acentric factor are shown in **Table 4.5**.

Table 4.5—BLACK OIL FLUID MODEL PROPERTIES.

Component	Z_i, %	M_w, lb/lb-mol	T_c, °R	P_c, psia	ω
CO_2	0.06	44.010	548.46	1071.33	0.28686
N_2	0.00	28.013	227.16	492.31	0.04000
C_1	60.01	16.093	342.60	667.78	0.01300
C_2- C_4	6.55	43.369	592.35	578.51	0.02567
C_5- C_6	4.03	78.943	1065.10	510.15	0.19164
C_{7+}	29.35	265.350	1090.00	357.87	0.89134

Binary interaction coefficients (BIC), presented in **Table 4.6**, were obtained through an EOS calibration performed in a previous study (Nguyen 2009).

Table 4.6—BLACK OIL FLUID MODEL BIC.

Binary Interaction Coefficients						
BIC	CO_2	N_2	C_1	C_2- C_4	C_5- C_6	C_{7+}
CO_2	0					
N_2	0.100	0				
C_1	0.100	0	0			
C_2- C_4	0.100	0	0	0		
C_5- C_6	0.100	0	0	0	0	
C_{7+}	0.100	0	0	0	0	0

Fluid composition, showed in Table 4.5 corresponds to a black oil fluid at any temperature used in the sensitivity range, from 200 to 285°F. The computed critical temperature of this fluid is 403°F. **Fig. 4.5** illustrates the phase envelope for this fluid.

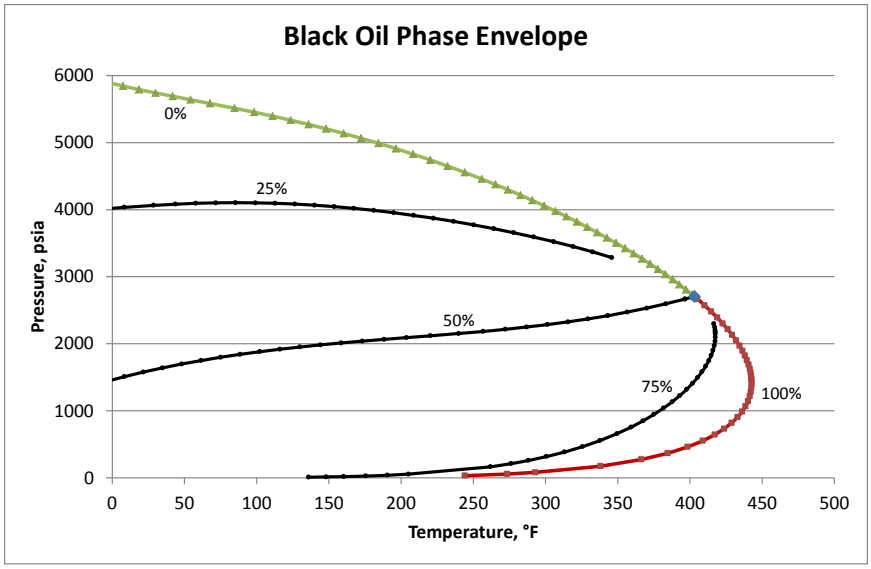

Fig. 4.5—Phase envelope for black oil fluid sample. Critical temperature is 403°F and reservoir temperatures sensitivities range from 200 to 285°F. Fluid behaves as black oil in all sensitivity range.

4.3 Rock-fluid Models Description

Rock-fluid models describe the interactions between the different phases (oil, gas, and water) flowing in the porous media. These interactions are defined by relative permeability curves provided in this section.

4.3.1 Gas Condensate Rock-Fluid Properties

A simple but effective three-phase oil relative permeability processing model allows to estimate phases flow in the porous media with numerical simulation. This model assumes gas and water complete segregation within each grid cell (Schlumberger 2010a). **Fig. 4.6** illustrates the oil-water and gas-liquid relative permeability curves for the gas condensate fluid system (Jaramillo and Barrufet 2001). **Table C.1**, in Appendix

C, shows specific data for the relative permeability curves displayed in Fig. 4.6 and the capillary pressure information for this fluid system.

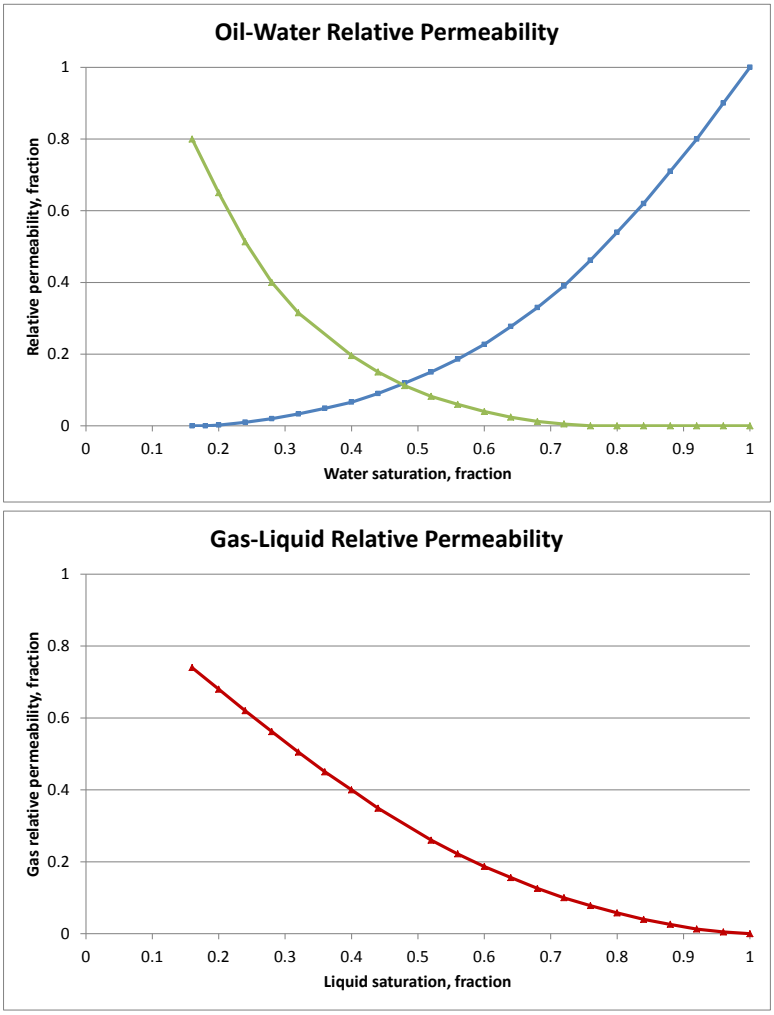

Fig. 4.6—Relative permeability curves for gas condensate fluid model. Three-phase oil relative permeability model assumes gas and water complete segregation.

4.3.2 Black Oil Rock-Fluid Properties

The three-phase relative permeability model used for the black oil fluid system in numerical simulations assumes gas and water complete segregation within each grid cell

(Schlumberger 2010a). **Fig. 4.7** illustrates the oil-water and gas-liquid relative permeability curves for the black oil fluid system (Nguyen 2009). **Table C.2**, in Appendix C, shows specific data for the relative permeability curves displayed in Fig. 4.7 and the capillary pressure information for this fluid system.

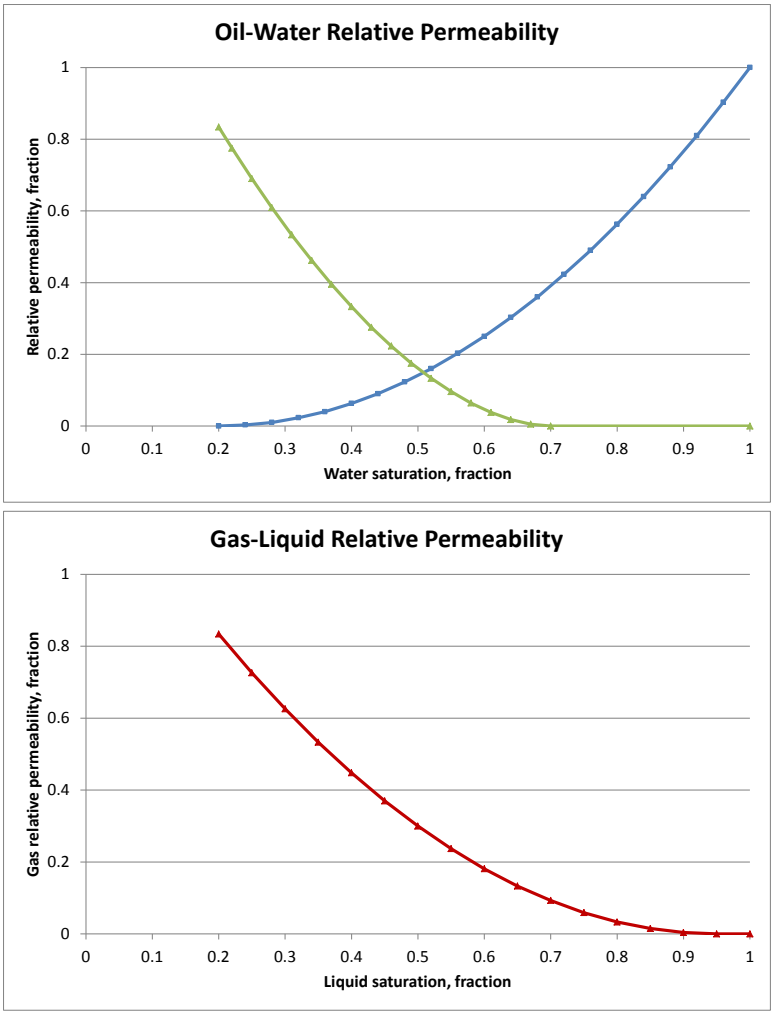

Fig. 4.7—Relative permeability curves for black oil fluid model. Three-phase oil relative permeability model assumes gas and water complete segregation.

4.4 Well Design

Wells were designed in a 5-spot pattern with vertical completion through the entire thickness of the reservoir. This type of configuration allows flexibility in the production/injection schedule under different scenarios.

Original grid cells had 320ft x 320ft dimensions. Central blocks for each well location were divided in three portions vertically and horizontally. The eight blocks adjacent to the central well position were divided in two or three portions (vertically or horizontally) depending on location. **Fig. 4.8** illustrates the local grid refinement performed for the models; wells are located in the center of each refinement.

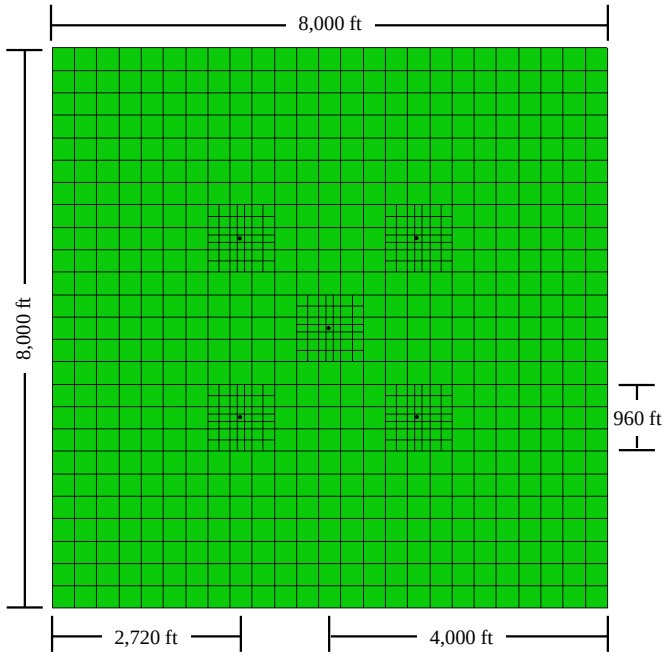

Fig. 4.8—Near-wellbore region grid refinement in 5-spot pattern. Local grid refinement improves the representation of pressure drop and fluid behavior near the wellbore.

Further detail of the local grid refinement near-wellbore is showed in **Fig. 4.9**.

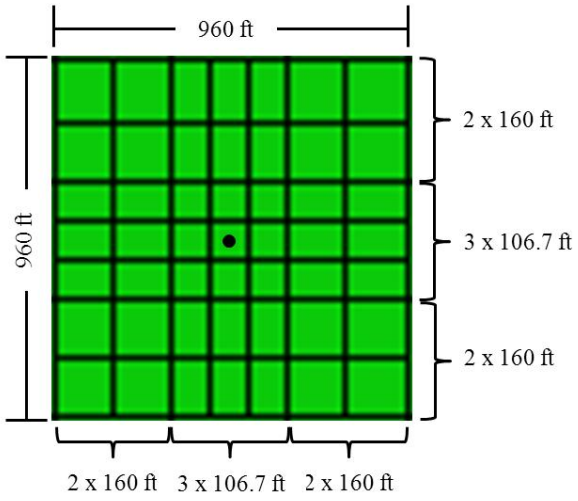

Fig. 4.9—Near-wellbore region grid refinement detailed description.

4.5 Injected Gas Composition

The composition of injected gas is rarely pure (100% CO_2). Due to high cost of separation procedures CO_2-based streams will have different levels of impurities. Nitrogen and carbon monoxide, for instance, are usually found in certain percentage, between 86% before separation and traces (< 1%) after a complete CO_2 separation.

Assessing a good economic balance in the process design is very important to select between two cases: injecting a highly concentrated CO_2-based gas at a high cost; or reducing the purity of the gas to lower the cost, causing a reduction in the final amount of stored CO_2. Performing sensitivities on the injection gas composition to determine separation and compression costs and final amount of CO_2 stored supports the project

design. Different injection gas compositions, presented in **Table 4.7**, were used in numerical simulation cases and analytical models to demonstrate the capability to handle multi-component injection streams with accurate and fast results in the proposed analytical method.

Table 4.7—CO_2-BASED STREAM GAS COMPOSITION. NITROGEN AND CARBON MONOXIDE ARE CONSIDERED IMPORTANT SINCE THEY ARE COMMONLY FOUND IN FLUE GAS AND SEPARATION COSTS TO OBTAIN PURE-CO_2 GAS ARE HIGH.

Injected Gas Compositions			
Case	CO_2%	N_2%	CO%
1	100	0	0
2	90	10	0
3	80	20	0
4	60	40	0
5	80	15	5
6	75	15	10

Carbon monoxide (CO) is not present in the original fluid composition of the gas condensate or black oil fluids. This component was only considered during injection stage.

CHAPTER V

DISCUSSION OF RESULTS

Validation of the proposed analytical method and algorithm was performed using numerical simulation as base of comparison. Numerical simulation has been the common practice to understand and design CO_2 injection process, and to estimate the ultimate CO_2 storage capacity (UCSC) of depleted oil and gas reservoirs at predefined target pressures. This chapter presents and compares the results from numerical simulation with the proposed analytical method to confirm the applicability of this new algorithm and validate the theoretical background on which it is based. Comprehensive analysis of simulation and analytical cases is presented in this chapter.

5.1 Reservoir Cases

The validation procedure was performed through 24 sensitivity cases, shown on **Table 5.1**. These cases were run in the commercial reservoir simulation package and in the proposed analytical algorithm to analyze and compare the results. Given the extensive amount of sensitivities and the detailed description required to evaluate each case, four general cases, namely A, B, C, and D, will be explained in detail in this section.

Table 5.1—SENSITIVITY CASES. 24 SCENARIOS COVER DIFFERENT RESERVOIR AND INJECTED FLUIDS, TEMPERATURES, SINGLE- AND TWO-PHASE CONDITIONS, AND WATER PRODUCTION.

Sensitivity Cases							
Case	Res. Fluid	Inj. Fluid	Inj. Fluid Comp.	T, °F	Depletion Condition**	Target Condition**	Water Prod.
1	V-O	1	CO_2	100	S	S	No
2	V-O	2	CO_2-N_2	100	T	S	No
3*	V-O	3	CO_2-N_2	150	T	S	No
4	V-O	4	CO_2-N_2	150	S	S	No
5	V-O	5	CO_2-N_2-CO	200	T	S	Yes
6	V-O	6	CO_2-N_2-CO	200	T	T	No
7	V-O	1	CO_2	250	S	S	No
8	V-O	2	CO_2-N_2	250	T	S	Yes
9	G-C	3	CO_2-N_2	270	T	T	No
10	G-C	4	CO_2-N_2	270	S	S	No
11	G-C	5	CO_2-N_2-CO	270	T	S	Yes
12*	G-C	6	CO_2-N_2-CO	285	T	T	No
13	G-C	1	CO_2	285	S	S	No
14	G-C	2	CO_2-N_2	285	T	S	Yes
15	G-C	3	CO_2-N_2	285	T	T	No
16	G-C	4	CO_2-N_2	285	S	S	Yes
17*	B-O	1	CO_2	250	S	S	No
18*	B-O	2	CO_2-N_2	200	T	S	Yes
19	B-O	3	CO_2-N_2	200	T	T	Yes
20	B-O	4	CO_2-N_2	250	S	S	No
21	B-O	5	CO_2-N_2-CO	250	T	S	No
22	B-O	6	CO_2-N_2-CO	250	T	T	Yes
23	B-O	1	CO_2	285	S	S	No
24	B-O	2	CO_2-N_2	285	T	S	Yes

* Denotes Cases A, B, C, and D, detailed in the following sections.
** (S) Single-phase hydrocarbon fluid. (T) Two-phase hydrocarbon fluid.

Case A represents a simplified scenario where the reservoir fluid remains in single-phase during depletion and injection. Case B exemplifies a more realistic scenario, in which the reservoir fluid falls in the two-phase region during depletion and returns to single-phase during repressurization in the injection process. In Case C, the reservoir fluid falls

in the two-phase region and remains in two-phase during the injection process. Finally, Case D presents a water production scenario during depletion.

The four presented cases encompass three reservoir fluids (gas condensate, volatile oil, and black oil), different reservoir temperatures and injection fluids. Numerical simulation, semi-analytical, and analytical models results are compared against each other. A summary of results from the 24 sensitivities are presented at the end of this chapter.

5.1.1 Single-Phase Depletion and Single-Phase Target

Case A is represented by a black oil reservoir fluid at 250 °F temperature. The black oil composition was given in Section 4.2.2. Injected fluid was 100% CO_2 (Fluid 1 from Table 4.7). Initial reservoir pressure was 6,092 psia. The reservoir was produced until average pressure reached 5,821 psia and injection was performed to repressurize the reservoir to 6,090 psia average pressure. No water was produced during depletion stage. **Table 5.2** summarizes reservoir and fluid properties for Case A. Reservoir fluid remains in single-liquid-phase during depletion and injection.

Table 5.2—CASE A—SINGLE-PHASE DEPLETION AND SINGLE-PHASE TARGET. RESERVOIR AND FLUID PROPERTIES.

Case A—Reservoir and Fluid Properties	
Reservoir fluid	B-O
Injection fluid	1
Injection fluid components	CO_2
Temperature, °F	250
Initial pressure, psia	6,092
Depletion pressure, psia	5,821
Target pressure, psia	6,090
Δp, psi	269
Water production, MMSTB	0
OOIP, MMSTB	242
Initial pore volume, MMbbl	546
Initial water saturation, %	22.52

After depletion, reservoir pressure reached 5,821 psia. Cumulative oil production during depletion was 2 MMSTB, representing 0.8% recovery factor. Such small production and pressure differential between initial and depletion conditions were designed to ensure reservoir hydrocarbon fluid remained in single-phase during depletion. **Table 5.3** displays the fluid composition and moles at depletion conditions from the reservoir simulation model.

Table 5.3—CASE A—FLUID COMPOSITION AND MOLES AT DEPLETION CONDITIONS FROM NUMERICAL SIMULATION. FLUID IS IN SINGLE-LIQUID-PHASE

Case A—Depletion Fluid Composition		
Component	**Z_i,** %	**moles,** MMlb-mol
CO_2	0.06	0.91
N_2	0.00	0.00
C_1	60.01	910.47
C_2- C_4	6.55	99.38
C_5- C_6	4.03	61.14
C_{7+}	29.35	445.31

Subsequently, the CO_2 stream was injected to repressurize the reservoir to 6,090 psia average pressure, a 269 pressure differential, ensuring not to exceed initial reservoir pressure. Final amount of injected fluid was 19.77 MMlb-mol of CO_2. **Table 5.4** displays the fluid composition, amount of moles, and injected moles, at final conditions from the reservoir simulation model.

Table 5.4—CASE A—FLUID COMPOSITION AND MOLES AT FINAL CONDITIONS FROM NUMERICAL SIMULATION. FLUID IS IN SINGLE-LIQUID-PHASE

Case A—Final Fluid Composition			
Component	**Z_i,** %	**moles,** MMlb-mol	**Inj. Moles,** MMlb-mol
CO_2	1.35	20.68	19.77
N_2	0.00	0.00	0.00
C_1	59.24	910.47	0.00
C_2- C_4	6.47	99.38	0.00
C_5- C_6	3.98	61.14	0.00
C_{7+}	28.97	445.31	0.00

Fig. 5.1 illustrates the CO_2 molar density (moles per reservoir volume) distribution at the end of the injection stage. The CO_2 does not reach most of the reservoir extension; it flows through the most permeable layers creating zones with high CO_2 concentration near-wellbore and low CO_2 concentrations in the rest of the reservoir. High vertical and horizontal compositional gradients are handled in the analytical calculations by using average reservoir pressures and compositions. A different injection well-pattern can be used to achieve a more homogeneous distribution of the plume; however, the UCSC will remain constant regardless of the injection scheme (van der Meer and Ferhat 2009).

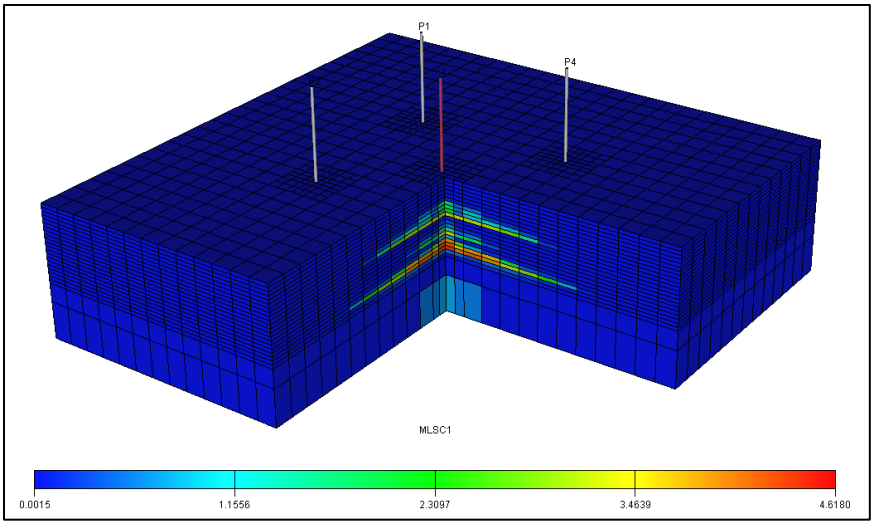

Fig. 5.1—Case A—CO_2 molar density distribution at the end of injection. The CO_2 flows through most permeable layers.

Fig. 5.2 shows fluid redistribution 100 years after injection ends. Fluid components move through the pore space to reach thermodynamic equilibrium; in this case, part of the injected fluid moved towards the top of the reservoir and the rest distributed more homogeneously in the near-wellbore area. This process can last long periods of time depending on diffusion. Total fluid composition in the reservoirs remains the same, since the quantity of each component is constant when no production or injection take place.

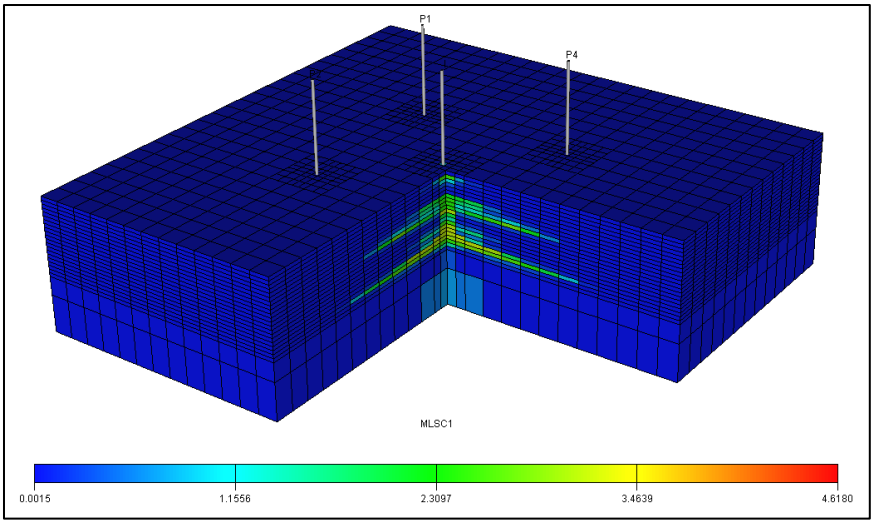

Fig. 5.2—Case A—CO_2 molar density distribution 100 years after the end of injection. Injected fluid redistributes to equilibrate. Reservoir average fluid composition remains constant.

The semi-analytical model, described in Section 3.3, predicted a total amount of injected fluid of 18.70 MMlb-mol of CO_2. The difference between the semi-analytical and numerical simulation results is 5.39% molar basis with respect to the total amount of fluid injected. **Fig. 5.3** shows the results for the straight line approximation; although the line presents a good overall match, in the small-injection range the match is poor and the prediction is not accurate. Slope estimation in the small-injection range is different than the one using all the data points, misleading the correct use of the straight line approximation.

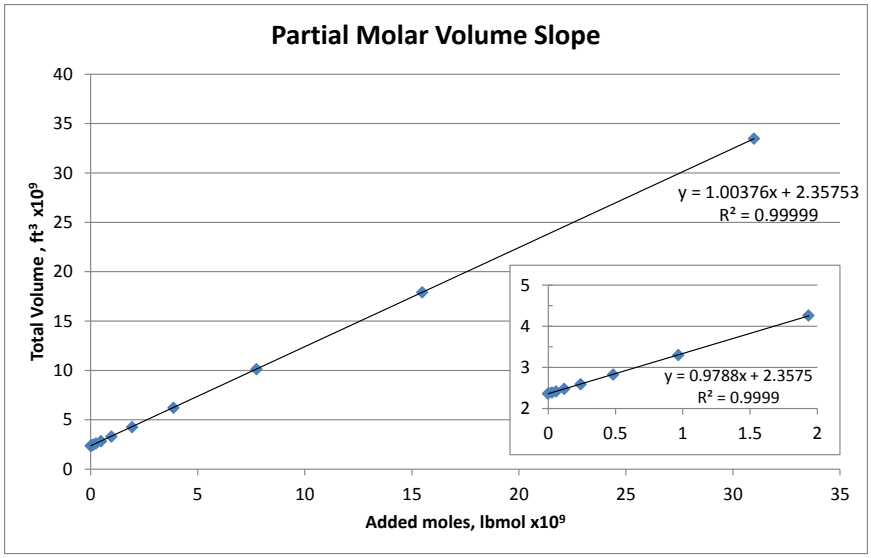

Fig. 5.3—Case A—Semi-analytical model results. Prediction of injected moles in the small-injection range is not accurate.

As mentioned previously, the semi-analytical model considers the partial molar volume to be constant as the fluid is injected at constant pressure and temperature, this limitation becomes more evident in scenarios with small injection quantities such as Case A.

The analytical model, described in Section 3.4, predicted a total amount of injected fluid of 19.82 MMlb-mol of CO_2. The difference between the analytical and numerical simulation results are 0.2%. The analytical method considers the variation of the partial molar volume as the fluid is injected at constant pressure and temperature, yielding more accurate and reliable results.

Table 5.5 shows the comparison of results between numerical simulation, semi-analytical, and analytical models. The semi-analytical model presents a discrepancy of

5.39% molar basis in the amount of injected fluid with respect to numerical simulation. Additionally, the calculation of saturations presents an error; saturations do not add to unit since the semi-analytical model underestimates the hydrocarbon volume for small amounts of injected fluid; injected amount of fluid is nearly one order of magnitude smaller, in molar basis, than the original amount of fluid in the reservoir at depletion stage.

On the other hand, results from the analytical model provide an excellent match with numerical simulation. Calculation of fluid saturations is consistent and the differences between calculated parameters with the analytical method and reservoir simulation are below 1%. Additionally, the analytical model performs nearly 125 times faster than numerical simulation, indicating the capacity to perform sensitivity analysis more rapidly.

Table 5.5—CASE A—COMPARISON OF RESULTS FROM NUMERICAL SIMULATION, SEMI-ANALYTICAL, AND ANALYTICAL MODELS. ANALYTICAL MODEL RESULTS MATCH THOSE FROM NUMERICAL SIMULATION AND PERFORMS 125 TIMES FASTER.

Case A—Comparison of Results					
Property	**Numerical Simulation**	**Semi-Analytical**	**Difference, %**	**Analytical**	**Difference, %**
Depletion PV, ft^3x10^9	3.06	3.06	0.00	3.06	0.00
Final PV, ft^3x10^9	3.07	3.07	0.00	3.07	0.00
$Moles_{dep}$, lb-mol x 10^9	1.5172	1.5127	0.29	1.5127	0.29
Mol $Volume_{dep}$, ft^3/lb-mol	1.5637	1.5683	0.29	1.5683	0.29
$S_{o,dep}$, %	77.44	77.44	0.01	77.44	0.01
$S_{g,dep}$, %	0.0	0.0	0.00	0.0	0.00
$S_{w,dep}$, %	22.56	22.56	0.01	22.56	0.01
$Moles_{injected}$, lb-mol x 10^9	0.0198	0.0187	5.39	0.0198	0.22
Mol $Volume_{final}$, ft^3/lb-mol	1.5461	1.5517	0.36	1.5505	0.29
$S_{o,final}$, %	77.45	77.48	0.03	77.48	0.03
$S_{g,final}$, %	0.01	0.0	0.01	0.0	0.01
$S_{w,final}$, %	22.54	22.52	0.02	22.52	0.02
CPU time, sec	376	1	376x	3	125x

Further analysis of the reservoir fluid behavior during the injection stage was performed with the analytical model and a PVT commercial software package (Schlumberger 2010c) to validate the results. The generalized partial molar volume (PMV), $\bar{V}_x$, presented in Eq. (3.15), was calculated at final target reservoir pressure and temperature, as the CO_2-based fluid is injected.

Validation of the generalized PMV concept was performed through a commercial PVT package by creating a wide range of fluid compositions. The process starts with the fluid

composition at depletion and manually adding moles of the injected fluid to create new fluid compositions in the desired range, CO_2 mole composition from initial 0.06% to 90% was divided into 32 samples. Successively, the software determines the molar volume of each sample at target conditions. The amount of added injection fluid moles and total volume occupied by the fluid are calculated in a spreadsheet corresponding to each fluid sample and molar volume. Finally, the numeric first derivative of the total volume with respect to added moles is calculated.

Fig. 5.4 shows the comparison of the PMV calculation between the analytical model and the calculations performed with the output of the PVT commercial package. Results show that the PMV, argument of the integral in Eq. (3.5), is not constant as the semi-analytical model incorrectly assumed. Data points calculated from the PVT commercial package present scattering due to limited significant digits in the molar volume calculation. The complex behavior of the PMV depends on reservoir fluid compositions, components characteristics, pressure, temperature, and injected fluid composition, and it is unique for each scenario. Notice that in this case the trend is not monotonic.

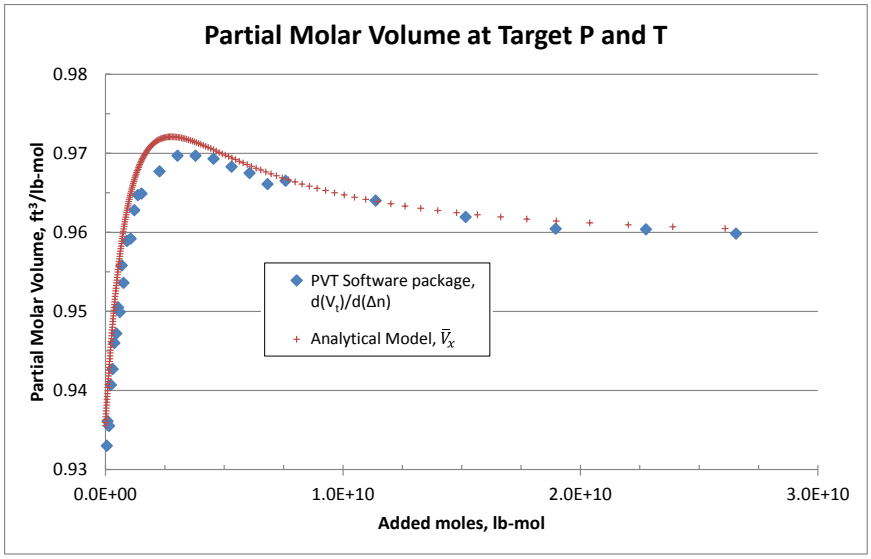

Fig. 5.4—Case A—Partial molar volume comparison from analytical model and calculations from commercial PVT software package. Results present excellent agreement. Limited significant digits in commercial software lead to scattered data.

Finally, the area under the curve in Fig. 5.4 provides the volume occupied by the fluid at target conditions; fluid volume must fill the hydrocarbon pore volume (HCPV) at target conditions. **Fig. 5.5** displays the results from the integration, analytical and PVT commercial package show good agreement. From this plot, having estimated the HCPV at target conditions and the fictitious volume $V_{n_{dep}}$ in Eq. (3.5) the amount of injected fluid can be determined. HCPV is calculated from the pore volume (PV) and water saturation at final conditions.

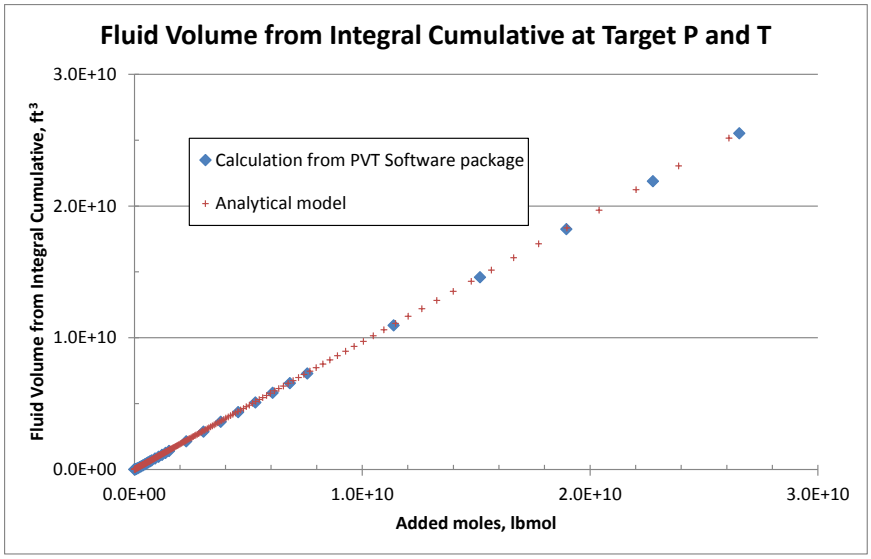

Fig. 5.5—Case A—Fluid volume comparison from analytical model and calculations from commercial PVT software package. Results present excellent agreement.

Table 5.6 presents the final fluid composition comparison between numerical simulation, semi-analytical, and analytical models. The analytical model offers an excellent match with numerical simulation.

Table 5.6—CASE A—FLUID COMPOSITION AT FINAL CONDITIONS COMPARISON BETWEEN NUMERICAL SIMULATION, SEMI-ANALYTICAL, AND ANALYTICAL MODELS. ANALYTICAL MODEL PRESENTS BETTER AGREEMENT WITH NUMERICAL SIMULATION.

Case A—Final Fluid Composition Comparison			
Component	Numerical Simulation %	Semi-Analytical %	Analytical %
CO_2	1.346	1.279	1.366
N_2	0.000	0.000	0.000
C_1	59.238	59.277	59.225
C_2- C_4	6.466	6.470	6.464
C_5- C_6	3.978	3.981	3.977
C_{7+}	28.973	28.992	28.967

In summary, UCSC for given reservoir and injection fluids, reservoir properties, and designed pressures, predicted by the analytical model was 19.8 MMlb-mol. This is equivalent to 0.4 Mt of injected CO_2, given the injection fluid composition. This amount corresponds to 1.5 years of CO_2 emissions from a 50 MW coal-fired power plant. Recall that this case is unrealistic, pressure differential available for injection is small to ensure single-phase fluid during depletion; following cases present more realistic scenarios.

5.1.2 Two-Phase Depletion and Single-Phase Target

Case B is represented by a volatile oil reservoir at high initial pressure and 150 °F temperature. The volatile oil composition was given in Section 4.2.1 for the gas condensate sample; recall Fig. 4.4, this fluid behaves as a volatile oil in temperatures below 265 °F (critical temperature).

Injected fluid was 80% CO_2 and 20% N_2 (Fluid 3 from Table 4.7). Initial reservoir pressure was 8,847 psia. The reservoir was produced until average pressure reached 4,004 psia and injection was performed to repressurize the reservoir to 8,790 psia average pressure. No water was produced during depletion stage. **Table 5.7** summarizes reservoir and fluid properties for Case B.

Table 5.7—CASE B—TWO-PHASE DEPLETION AND SINGLE-PHASE TARGET. RESERVOIR AND FLUID PROPERTIES.

Case B—Reservoir and Fluid Properties	
Reservoir fluid	V-O
Injection fluid	3
Injection fluid components	CO_2-N_2
Temperature, °F	150
Initial pressure, psia	8,847
Depletion pressure, psia	4,004
Target pressure, psia	8,790
Δp, psi	4,786
Water production, MMSTB	0
OOIP, MMSTB	189
Initial pore volume, MMbbl	553
Initial water saturation, %	19.68

After depletion, reservoir pressure reached 8,790 psia. Cumulative oil production during depletion was 31 MMSTB, representing 16.4% recovery factor. The reservoir hydrocarbon fluid fell in two-phase during depletion, thus its composition was altered from its initial condition. **Table 5.8** displays the fluid composition and moles at depletion conditions from the reservoir simulation model.

Table 5.8—CASE B—FLUID COMPOSITION AND MOLES AT DEPLETION CONDITIONS FROM NUMERICAL SIMULATION. FLUID IS IN TWO-PHASE

Case B—Depletion Fluid Composition		
Component	**Z_i,** %	**moles,** MMlb-mol
CO_2	4.582	71.83
N_2	0.000	0.00
C_1	60.764	952.67
C_2- C_3	14.515	227.58
C_4- C_6	4.919	77.12
C_7- C_{10}	7.840	122.92
C_{11+}	7.381	115.72

Subsequently, the CO_2-based stream was injected to repressurize the reservoir to 8,790 psia average pressure, a 4,786 pressure differential. Final amount of injected fluid was 633.56 MMlb-mol, corresponding to 506.85 MMlb-mol of CO_2 and 126.71 MMlb-mol of N_2. **Table 5.9** displays the fluid composition, amount of moles, and injected moles, at final conditions from the reservoir simulation model.

Table 5.9—CASE B—FLUID COMPOSITION AND MOLES AT FINAL CONDITIONS FROM NUMERICAL SIMULATION. FLUID IS IN SINGLE-LIQUID-PHASE

Case B—Final Fluid Composition			
Component	**Z_i,** %	**moles,** MMlb-mol	**Inj. Moles,** MMlb-mol
CO_2	26.287	578.68	506.85
N_2	5.756	126.71	126.71
C_1	43.276	952.67	0.00
C_2- C_3	10.338	227.58	0.00
C_4- C_6	3.503	77.12	0.00
C_7- C_{10}	5.584	122.92	0.00
C_{11+}	5.257	115.72	0.00

Fig. 5.6 illustrates the CO_2 molar density (moles per reservoir volume) distribution at the end of the injection stage. The CO_2 plume is located in the near-wellbore region and the CO_2 does not reach most of the reservoir extension; it flows through the most permeable layers creating zones with high CO_2 concentration near-wellbore and low CO_2 concentrations in the rest of the reservoir. Reservoir numerical simulation, opposed to the semi-analytical and analytical models, shows the high vertical and horizontal compositional gradients at the end of the injection process. The objective of this evaluation is to ensure that the zero-dimensional analytical model accurately predicts average composition and saturations with respect to numerical simulation. A different

injection well-pattern can be used to achieve a more homogeneous distribution of the plume; however, the UCSC will remain constant regardless of the injection scheme (van der Meer and Ferhat 2009).

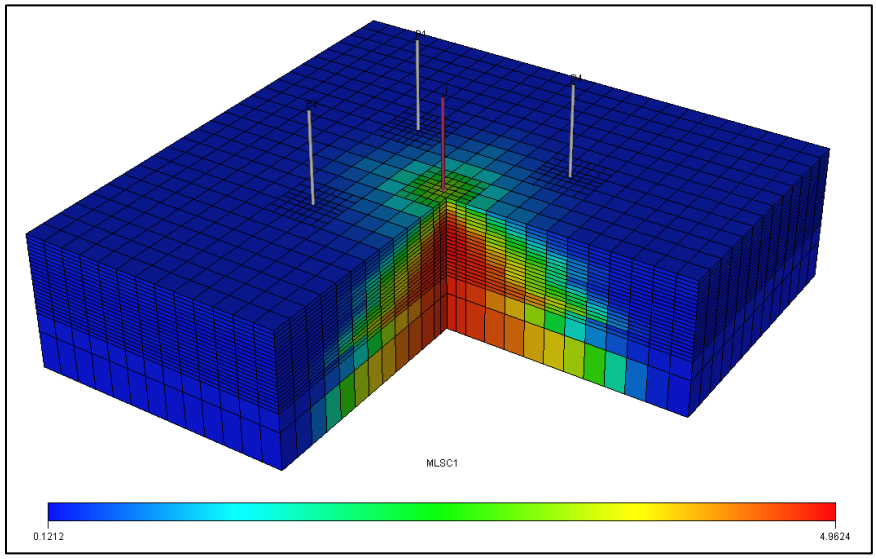

Fig. 5.6—Case B—CO_2 molar density distribution at the end of injection. The CO_2 is concentrated in the injection near-wellbore region.

The semi-analytical model, described in Section 3.3, predicted a total amount of injected fluid of 619.30 MMlb-mol, corresponding to 495.44 MMlb-mol of CO_2 and 123.86 MMlb-mol of N_2. The difference between the semi-analytical and numerical simulation results is 2.25%. This improvement, in comparison with the error obtained in Case A, is given by the relatively large amount of fluid injected, nearly half of the quantity of fluid moles in the reservoir at depletion stage.

Fig. 5.7 shows the results for the straight line approximation in the semi-analytical model; the line presents a good overall match except for the small injection range where the match is poor. Slope estimation in the small-injection range is different than the one using all the data points, misleading the correct use of the straight line approximation. However, the prediction is relatively accurate in the amount of fluid injected; final amount of injected fluid is nearly half of the quantity of fluid moles in the reservoir at depletion stage.

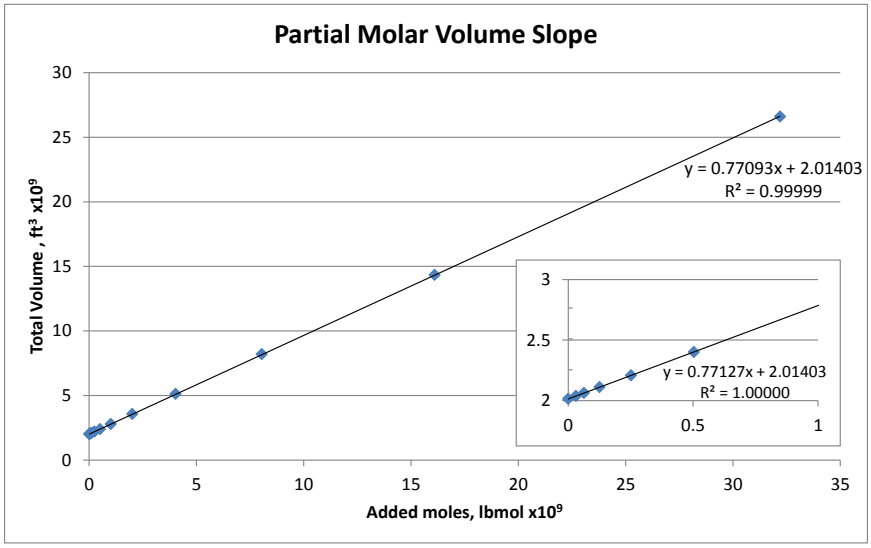

Fig. 5.7—Case B—Semi-analytical model results. Prediction of injected moles is accurate in the relatively large amount of fluid injected, nearly half of the quantity of fluid moles in the reservoir at depletion stage.

The analytical model, described in Section 3.4, predicted a total amount of injected fluid of 619.40 MMlb-mol, corresponding 495.52 MMlb-mol of CO_2 and 123.88 MMlb-mol of N_2. The difference between the analytical and numerical simulation results is 2.23%.

The analytical method considers the variation of the partial molar volume as the fluid is injected at constant pressure and temperature, yielding more accurate and reliable results.

Table 5.10 shows the comparison of results between numerical simulation, semi-analytical, and analytical models. The semi-analytical model presents a discrepancy of only 2.25% molar basis in the amount of injected fluid with respect to numerical simulation. Results from the analytical model provide an excellent match with numerical simulation as well. Calculation of water, oil, and gas saturations are consistent. On a different note, the analytical model performs 233 times faster than numerical simulation. Difference in oil and gas saturations between numerical simulation and analytical method could be attributed to different thresholds in phase-recognition logics in the models.

Table 5.10—CASE B—COMPARISON OF RESULTS FROM NUMERICAL SIMULATION, SEMI-ANALYTICAL, AND ANALYTICAL MODELS. ANALYTICAL MODEL RESULTS MATCH THOSE FROM NUMERICAL SIMULATION AND PERFORMS NEARLY 233 TIMES FASTER.

Case B—Comparison of Results					
Property	**Numerical Simulation**	**Semi-Analytical**	**Difference, %**	**Analytical**	**Difference, %**
Depletion PV, ft^3x10^9	3.04	3.04	0.00	3.04	0.00
Final PV, ft^3x10^9	3.10	3.10	0.00	3.10	0.00
$Moles_{dep}$, lb-mol x 10^9	1.5678	1.5719	0.26	1.5719	0.26
Mol $Volume_{dep}$, ft^3/lb-mol	1.5460	1.5419	0.26	1.5419	0.26
$S_{o,dep}$, %	49.42	50.74	1.32	50.74	1.32
$S_{g,dep}$, %	30.22	28.90	1.32	28.90	1.32
$S_{w,dep}$, %	20.36	20.36	0.00	20.36	0.00
$Moles_{injected}$, lb-mol x 10^9	0.6336	0.6193	2.25	0.6194	2.23
Mol $Volume_{final}$, ft^3/lb-mol	1.1318	1.1370	0.46	1.1370	0.46
$S_{o,final}$, %	80.31	80.31	0.00	80.31	0.00
$S_{g,final}$, %	0.0	0.0	0.00	0.0	0.00
$S_{w,final}$, %	19.69	19.69	0.00	19.69	0.00
CPU time, sec	932	1	932x	4	233x

Validation of the generalized PMV, $\bar{V}_x$, was performed through a commercial PVT package by creating a wide range of fluid compositions, as explained in Case A analysis. For the analysis, CO_2 mole composition from depletion stage 4.6% to 76% was divided into 32 samples.

Fig. 5.8 shows the comparison of the PMV calculation between the analytical model and the calculations performed with the output of the PVT commercial package. Results show that the PMV, argument of the integral in Eq. (3.5), is not constant as the semi-

analytical model incorrectly assumes. Data points calculated from the PVT commercial package present scattering due to limited significant digits in the molar volume calculation. The complex behavior of the PMV depends on reservoir fluid compositions, components characteristics, pressure, temperature, and injected fluid composition, and it is unique for each scenario. Notice that in this case the trend is not monotonic.

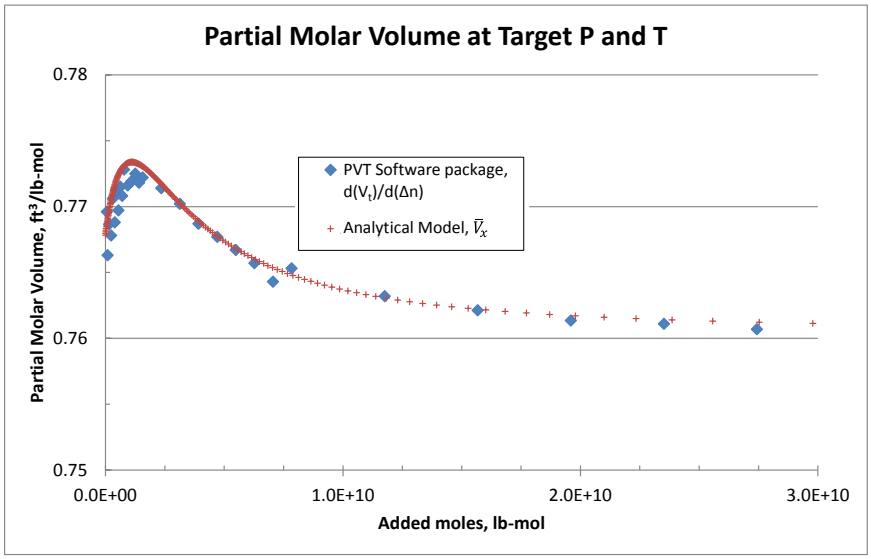

Fig. 5.8—Case B—Partial molar volume comparison from analytical model and calculations from commercial PVT software package. Results present excellent agreement. Limited significant digits in commercial software lead to scattered data.

Finally, the area under the curve in Fig. 5.8 provides the volume occupied by the fluid at target conditions; fluid volume must fill the HCPV at target conditions. **Fig. 5.9** displays the results from the integration, analytical and PVT commercial package show good agreement. From this plot, having estimated the HCPV at target conditions and the

fictitious volume $V_{n_{dep}}$ in Eq. (3.5) the amount of injected fluid can be determined. HCPV is calculated from the PV and water saturation at final conditions.

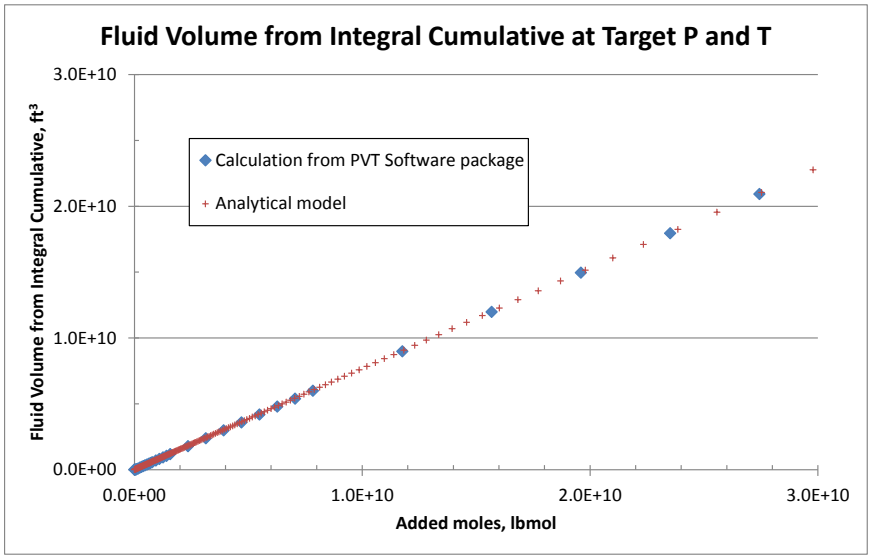

Fig. 5.9—Case B—Fluid volume comparison from analytical model and calculations from commercial PVT software package. Results present excellent agreement.

Table 5.11 presents the final fluid composition comparison between numerical simulation, semi-analytical, and analytical models. The analytical model offers an excellent with numerical simulation.

Table 5.11—CASE B—FLUID COMPOSITION AT FINAL CONDITIONS COMPARISON BETWEEN NUMERICAL SIMULATION, SEMI-ANALYTICAL, AND ANALYTICAL MODELS. ANALYTICAL MODEL PRESENTS BETTER AGREEMENT WITH NUMERICAL SIMULATION.

Case B—Final Fluid Composition Comparison			
Component	Numerical Simulation %	Semi-Analytical %	Analytical %
CO_2	26.287	25.897	25.900
N_2	5.756	5.653	5.653
C_1	43.276	43.590	43.588
C_2- C_3	10.338	10.413	10.412
C_4- C_6	3.503	3.529	3.528
C_7- C_{10}	5.584	5.624	5.624
C_{11+}	5.257	5.295	5.294

In summary, UCSC for given reservoir and injection fluids, reservoir properties, and designed pressures, predicted by the analytical model was 619.40 MMlb-mol of injected fluid, corresponding 495.52 MMlb-mol of CO_2 and 123.88 MMlb-mol of N_2. This is equivalent to 9.88 Mt of CO_2, given the injection fluid composition. This amount corresponds to 17 years of CO_2 emissions from a 100 MW coal-fired power plant.

5.1.3 Two-Phase Depletion and Two-Phase Target

Case C is represented by a gas condensate reservoir at high initial pressure and 285 °F temperature. The gas condensate composition was given in Section 4.2.1; recall Fig. 4.4, this fluid behaves as a gas condensate in temperatures above 265 °F (critical temperature).

Injected fluid was 75% CO_2, 15% N_2, and 10% CO (Fluid 6 from Table 4.7). Initial reservoir pressure was 8,849 psia. The reservoir was produced until average pressure reached 2,914 psia and injection was performed to repressurize the reservoir to 6,049 psia average pressure. No water was produced during depletion stage. **Table 5.12** summarizes reservoir and fluid properties for Case C.

Table 5.12—CASE C—TWO-PHASE DEPLETION AND TWO-PHASE TARGET. RESERVOIR AND FLUID PROPERTIES.

Case C—Reservoir and Fluid Properties	
Reservoir fluid	G-C
Injection fluid	6
Injection fluid components	CO_2-N_2-CO
Temperature, °F	285
Initial pressure, psia	8,849
Depletion pressure, psia	2,914
Target pressure, psia	6,049
Δp, psi	3,135
Water production, MMSTB	0
OGIP, BSCF	582
Initial pore volume, MMbbl	553
Initial water saturation, %	18.87

After depletion, reservoir pressure reached 2,914 psia. Cumulative gas production during depletion was 274.6 BSCF, representing 47.2% gas recovery factor. The reservoir hydrocarbon fluid fell in two-phase during depletion, thus its composition was altered from its initial condition. **Table 5.13** displays the fluid composition and moles at depletion conditions from the reservoir simulation model.

Table 5.13—CASE C—FLUID COMPOSITION AND MOLES AT DEPLETION CONDITIONS FROM NUMERICAL SIMULATION. FLUID IS IN TWO-PHASE

Case C—Depletion Fluid Composition		
Component	**Z_i,** %	**moles,** MMlb-mol
CO_2	4.405	44.43
N_2	0.000	0.00
CO	0.000	0.00
C_1	57.010	574.98
C_2- C_3	14.490	146.14
C_4- C_6	5.222	52.66
C_7- C_{10}	9.231	93.10
C_{11+}	9.642	97.25

Subsequently, the CO_2-based stream was injected to repressurize the reservoir to 6,049 psia average pressure, a 3,135 pressure differential. Final amount of injected fluid was 661.78 MMlb-mol, corresponding to 496.34 MMlb-mol of CO_2, 99.27 MMlb-mol of N_2, and 66.18 MMlb-mol of CO. **Table 5.14** displays the fluid composition, amount of moles, and injected moles, at final conditions from the reservoir simulation model.

Table 5.14—CASE C—FLUID COMPOSITION AND MOLES AT FINAL CONDITIONS FROM NUMERICAL SIMULATION. FLUID IS IN TWO-PHASE.

Case C—Final Fluid Composition			
Component	**Z_i,** %	**moles,** MMlb-mol	**Inj. Moles,** MMlb-mol
CO_2	32.374	540.76	496.34
N_2	5.943	99.27	99.27
CO	3.962	66.18	66.18
C_1	34.423	574.98	0.00
C_2- C_3	8.749	146.14	0.00
C_4- C_6	3.153	52.66	0.00
C_7- C_{10}	5.574	93.10	0.00
C_{11+}	5.822	97.25	0.00

Fig. 5.10 illustrates the CO_2 molar density (moles per reservoir volume) distribution at the end of the injection stage. The CO_2 plume is mostly located in the near-wellbore region and the CO_2 slightly reaches some reservoir zones far from the injector.

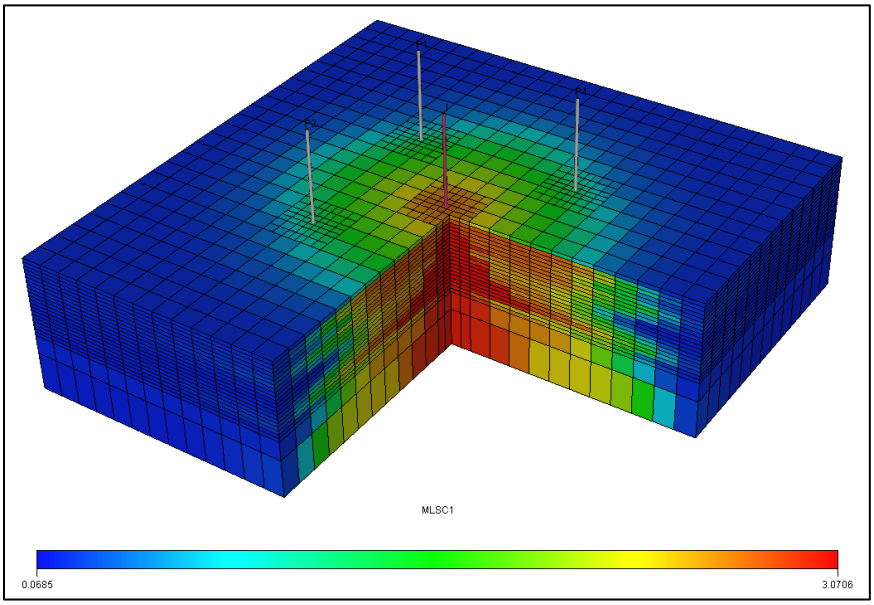

Fig. 5.10—Case C—CO_2 molar density distribution at the end of injection. The CO_2 is mostly concentrated in the injection near-wellbore region and slightly reaches some reservoir zones far from the injector.

The semi-analytical model, described in Section 3.3, predicted a total amount of injected fluid of 634.65 MMlb-mol, corresponding to 475.99 MMlb-mol of CO_2, 95.20 MMlb-mol of N_2, and 63.46 MMlb-mol of CO. The difference between the semi-analytical and numerical simulation results is 4.10%. This improvement, in comparison with the error obtained in Case A, is given by the relatively large amount of fluid injected, more than half of the quantity of fluid moles in the reservoir at depletion stage.

Fig. 5.11 shows the results for the straight line approximation in the semi-analytical model; the line presents a good overall match except for the small injection range where the match is poor. Slope estimation in the small-injection range is different than the one using all the data points, misleading the correct use of the straight line approximation. However, the prediction is relatively accurate in the amount of fluid injected; final amount of injected fluid is more than half of the quantity of fluid moles in the reservoir at depletion stage.

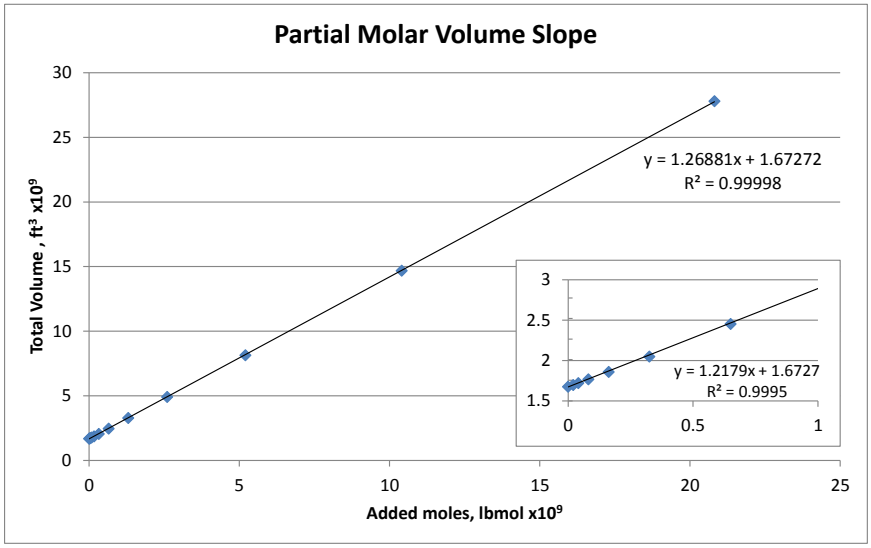

Fig. 5.11—Case C—Semi-analytical model results. Prediction of injected moles is accurate in the relatively large amount of fluid injected, more than half of the quantity of fluid moles in the reservoir at depletion stage.

The analytical model, described in Section 3.4, predicted a total amount of injected fluid of 685.65 MMlb-mol, corresponding 514.24 MMlb-mol of CO_2, 102.85 MMlb-mol of N_2, and 68.56 MMlb-mol of CO. The difference between the analytical and numerical simulation results is 3.61%. The analytical method considers the variation of the partial

molar volume as the fluid is injected at constant pressure and temperature, yielding more accurate and reliable results.

Table 5.15 shows the comparison of results between numerical simulation, semi-analytical, and analytical models. The semi-analytical model presents a discrepancy of only 4.10% molar basis in the amount of injected fluid with respect to numerical simulation. Results from the analytical model provide an excellent match with numerical simulation as well with 3.61% difference in the injected fluid moles. On a different note, the analytical model performs 104 times faster than numerical simulation. Difference in oil and gas saturations between numerical simulation and analytical method could be attributed to different thresholds in phase-recognition logics in the models.

Validation of the generalized PMV was performed through a commercial PVT package by creating a wide range of fluid compositions, as presented in Case A. For the analysis, CO_2 mole composition from depletion stage 4.4% to 74% was divided into 32 samples.

Table 5.15—CASE C—COMPARISON OF RESULTS FROM NUMERICAL SIMULATION, SEMI-ANALYTICAL, AND ANALYTICAL MODELS. ANALYTICAL MODEL RESULTS MATCH THOSE FROM NUMERICAL SIMULATION AND PERFORMS 104 TIMES FASTER.

Case C—Comparison of Results					
Property	**Numerical Simulation**	**Semi-Analytical**	**Difference, %**	**Analytical**	**Difference, %**
Depletion PV, ft^3x10^9	3.03	3.03	0.00	3.03	0.00
Final PV, ft^3x10^9	3.07	3.07	0.00	3.07	0.00
$Moles_{dep}$, lb-mol x 10^9	1.0086	1.0163	0.77	1.0163	0.77
Mol $Volume_{dep}$, ft^3/lb-mol	2.4135	2.3950	0.76	2.3950	0.76
$S_{o,dep}$, %	34.22	35.12	0.90	35.12	0.90
$S_{g,dep}$, %	46.11	45.21	0.90	45.21	0.90
$S_{w,dep}$, %	19.67	19.67	0.00	19.67	0.00
$Moles_{injected}$, lb-mol x 10^9	0.6618	0.6346	4.10	0.6856	3.61
Mol $Volume_{final}$, ft^3/lb-mol	1.4835	1.5009	1.17	1.4660	1.18
$S_{o,final}$, %	44.89	48.91	4.02	47.24	2.35
$S_{g,final}$, %	35.87	31.85	4.02	33.52	2.35
$S_{w,final}$, %	19.24	19.24	0.00	19.24	0.00
CPU time, sec	1044	1.5	696x	10	104x

Fig. 5.12 shows the comparison of the PMV calculation between the analytical model and the calculations performed with the output of the PVT commercial package. Results show that the PMV, argument of the integral in Eq. (3.5), is not constant as the semi-analytical model incorrectly assumes. Data points calculated from the PVT commercial package present scattering due to limited significant digits in the molar volume calculation. The complex behavior of the PMV depends on reservoir fluid compositions, components characteristics, pressure, temperature, and injected fluid composition, and it is unique for each scenario. Notice that in this case the trend is not monotonic.

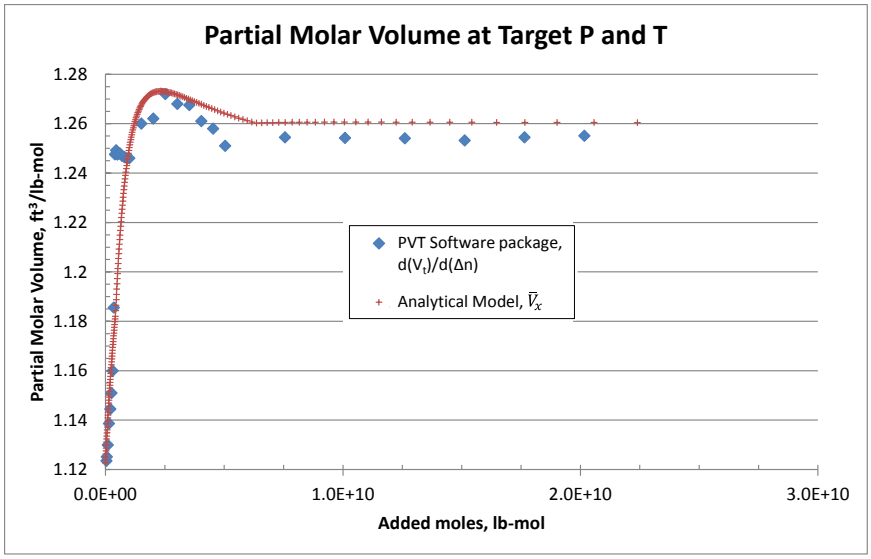

Fig. 5.12—Case C—Partial molar volume comparison from analytical model and calculations from commercial PVT software package. Results present excellent agreement. Limited significant digits in commercial software lead to scattered data.

Finally, the area under the curve in Fig. 5.12 provides the volume occupied by the fluid at target conditions; fluid volume must fill the HCPV at target conditions. **Fig. 5.13** displays the results from the integration, analytical and PVT commercial package show good agreement. From this plot, having estimated the HCPV at target conditions and the fictitious volume $V_{n_{dep}}$ in Eq. (3.5) the amount of injected fluid can be determined. HCPV is calculated from the PV and water saturation at final conditions.

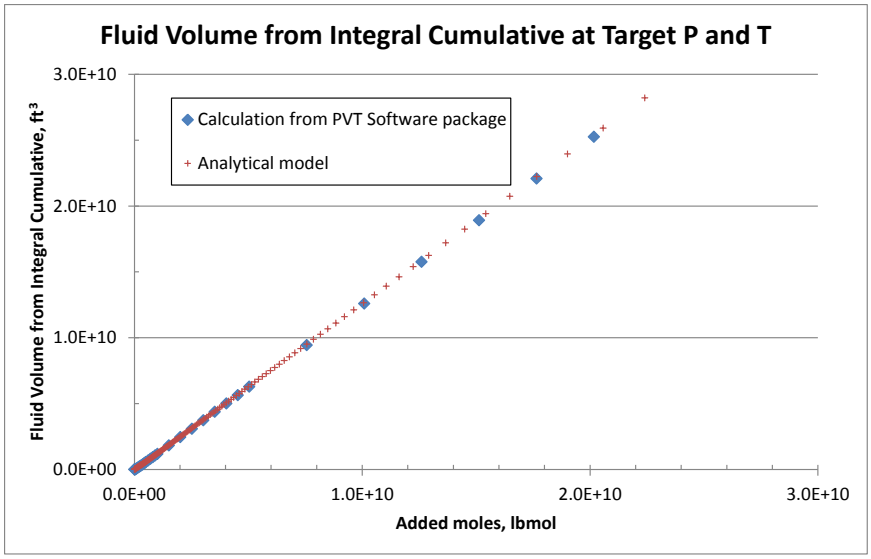

Fig. 5.13—Case C—Fluid volume comparison from analytical model and calculations from commercial PVT software package. Results present excellent agreement.

Table 5.16 presents the final fluid composition comparison between numerical simulation, semi-analytical, and analytical models. The analytical model offers an excellent with numerical simulation.

Table 5.16—CASE C—FLUID COMPOSITION AT FINAL CONDITIONS COMPARISON BETWEEN NUMERICAL SIMULATION, SEMI-ANALYTICAL, AND ANALYTICAL MODELS. ANALYTICAL MODEL PRESENTS BETTER AGREEMENT WITH NUMERICAL SIMULATION.

Case C—Final Fluid Composition Comparison			
Component	Numerical Simulation %	Semi-Analytical %	Analytical %
CO_2	32.374	31.542	32.844
N_2	5.943	5.766	6.043
CO	3.962	3.844	4.029
C_1	34.423	35.095	34.043
C_2- C_3	8.749	8.920	8.653
C_4- C_6	3.153	3.214	3.118
C_7- C_{10}	5.574	5.683	5.512
C_{11+}	5.822	5.936	5.758

In summary, UCSC for given reservoir and injection fluids, reservoir properties, and designed pressures, predicted by the analytical model was 685.65 MMlb-mol of injected fluid, corresponding 514.24 MMlb-mol of CO_2, 102.85 MMlb-mol of N_2, and 68.56 MMlb-mol of CO. This is equivalent to 10.25 Mt of CO_2, given the injection fluid composition. This amount corresponds to 18 years of CO_2 emissions from a 100 MW coal-fired power plant.

5.1.4 Water Production

Case D is represented by a black oil reservoir fluid at 200 °F temperature. The black oil composition was given in Section 4.2.2. Injected fluid was 90% CO_2 and 10% N_2 (Fluid 2 from Table 4.7). Initial reservoir pressure was 6,094 psia. The reservoir was produced until average pressure reached 978 psia and injection was performed to repressurize the reservoir to 6,038 psia average pressure. Water production during depletion stage was 80.9 MMSTB. **Table 5.17** summarizes reservoir and fluid properties for Case D. Reservoir fluid falls in two-phase during depletion and after injection the fluid returns to single-phase.

Table 5.17—CASE D—TWO-PHASE DEPLETION AND SINGLE-PHASE TARGET WITH WATER PRODUCTION. RESERVOIR AND FLUID PROPERTIES.

Case D—Reservoir and Fluid Properties	
Reservoir fluid	B-O
Injection fluid	2
Injection fluid components	CO_2-N_2
Temperature, °F	200
Initial pressure, psia	6,094
Depletion pressure, psia	978
Target pressure, psia	6,038
Δp, psi	5,059
Water production, MMSTB	80.9
OOIP, MMSTB	102.4
Initial pore volume, MMbbl	546
Initial water saturation, %	68.56

After depletion, reservoir pressure reached 978 psia. Cumulative oil production during depletion was 8 MMSTB, representing 7.8% recovery factor. Low recovery factor is caused by high initial water saturation and water production during depletion, nearly 81 MMSTB of water. **Table 5.18** displays the fluid composition and moles at depletion conditions from the reservoir simulation model.

Table 5.18—CASE D—FLUID COMPOSITION AND MOLES AT DEPLETION CONDITIONS FROM NUMERICAL SIMULATION. FLUID IS IN TWO-PHASE

Case D—Depletion Fluid Composition		
Component	**Z_i,** %	**moles,** MMlb-mol
CO_2	0.05	0.18
N_2	0.00	0.00
C_1	36.67	138.66
C_2- C_4	6.55	24.78
C_5- C_6	6.65	25.16
C_{7+}	50.08	189.38

Subsequently, the CO_2-based stream was injected to repressurize the reservoir to 6,038 psia average pressure, a 5,059 pressure differential, ensuring not to exceed initial reservoir pressure. Final amount of injected fluid was 809.96 MMlb-mol of fluid, corresponding to 728.96 MMlb-mol of CO_2 and 81.00 MMlb-mol of N_2. **Table 5.19** displays the fluid composition, amount of moles, and injected moles, at final conditions from the reservoir simulation model.

Table 5.19—CASE D—FLUID COMPOSITION AND MOLES AT FINAL CONDITIONS FROM NUMERICAL SIMULATION. FLUID IS IN SINGLE-PHASE

Case D—Final Fluid Composition			
Component	**Z_i,** %	**moles,** MMlb-mol	**Inj. Moles,** MMlb-mol
CO_2	61.37	729.14	728.96
N_2	6.82	81.00	81.00
C_1	11.67	138.66	0.00
C_2- C_4	2.09	24.78	0.00
C_5- C_6	2.12	25.16	0.00
C_{7+}	15.94	189.38	0.00

Fig. 5.14 illustrates the CO_2 molar density (moles per reservoir volume) distribution at the end of the injection stage. The CO_2 reaches great extension into the reservoir. High vertical and horizontal compositional gradients are imbedded in the analytical calculations by using average reservoir pressures and compositions.

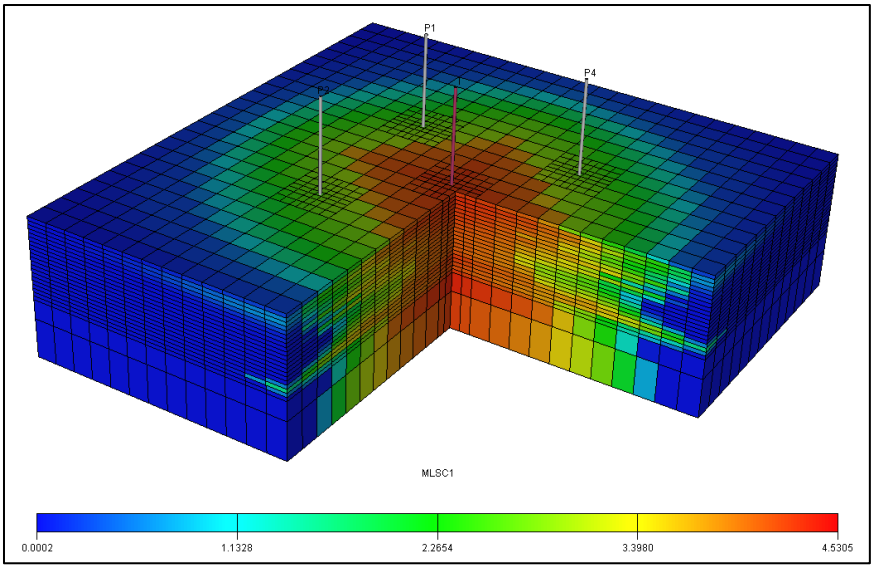

Fig. 5.14—Case D—CO_2 molar density distribution at the end of injection. The CO_2 reaches great extent of the reservoir.

The semi-analytical model, described in Section 3.3, predicted a total amount of injected fluid of 755.67 MMlb-mol, corresponding to 680.10 MMlb-mol of CO_2 and 75.57 MMlb-mol of N_2. The difference between the semi-analytical and numerical simulation results is 6.7%. **Fig. 5.15** shows the results for the straight line approximation.

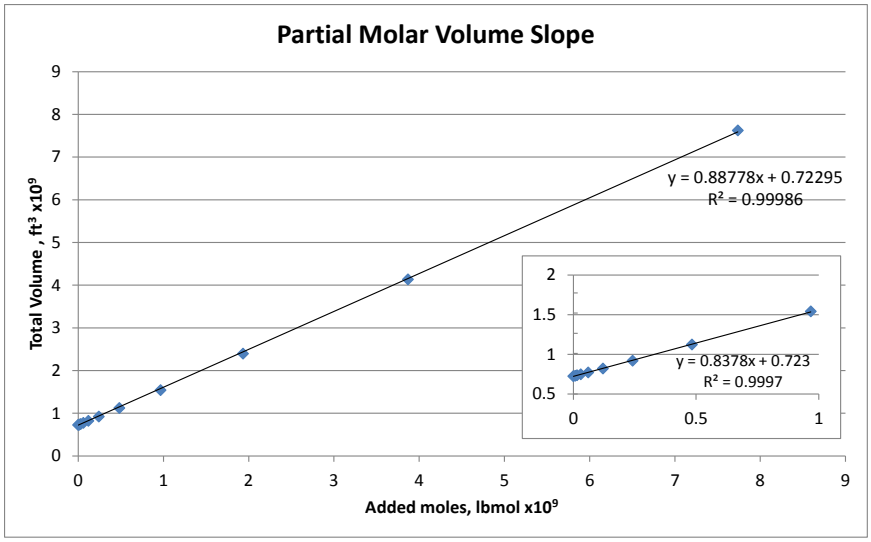

Fig. 5.15—Case D—Semi-analytical model results. Good overall match with straight-line.

The analytical model, described in Section 3.4, predicted a total amount of injected fluid of 808.91 MMlb-mol, corresponding to 728.02 MMlb-mol of CO_2 and 80.89 MMlb-mol of N_2. The difference between the analytical and numerical simulation results is 0.13%. The analytical method considers the variation of the partial molar volume as the fluid is injected at constant pressure and temperature, yielding more accurate and reliable results.

Table 5.20 shows the comparison of results between numerical simulation, semi-analytical, and analytical models. The semi-analytical model presents a discrepancy of 6.70% molar basis in the amount of injected fluid with respect to numerical simulation. Additionally, the calculation of saturations presents an error; saturations do not add to unit since this model underestimates the hydrocarbon volume for small amounts of

injected fluid; injected amount of fluid is nearly one order of magnitude smaller, in molar basis, than the original amount of fluid in the reservoir at depletion stage.

On the other hand, results from the analytical model provide an excellent match with numerical simulation. Calculation of saturations is consistent and the differences between calculated parameters and reservoir simulation are 0.13% in molar basis and largest difference in saturation estimations is 1.13%. In addition, the analytical model performs nearly 291 times faster than numerical simulation.

Table 5.20—CASE D—COMPARISON OF RESULTS FROM NUMERICAL SIMULATION, SEMI-ANALYTICAL, AND ANALYTICAL MODELS. ANALYTICAL MODEL RESULTS MATCH THOSE FROM NUMERICAL SIMULATION AND PERFORMS 291 TIMES FASTER.

Case D—Comparison of Results					
Property	**Numerical Simulation**	**Semi-Analytical**	**Difference, %**	**Analytical**	**Difference, %**
Depletion PV, ft^3x10^9	3.00	3.00	0.00	3.00	0.00
Final PV, ft^3x10^9	3.07	3.07	0.00	3.07	0.00
$Moles_{dep}$, lb-mol x 10^9	0.3782	0.3778	0.08	0.3778	0.08
Mol $Volume_{dep}$, ft^3/lb-mol	3.4974	3.5005	0.09	3.5005	0.09
$S_{o,dep}$, %	22.22	22.30	0.08	22.30	0.08
$S_{g,dep}$, %	22.05	21.71	0.34	21.71	0.34
$S_{w,dep}$, %	55.72	55.99	0.26	55.99	0.26
$Moles_{injected}$, lb-mol x 10^9	0.8099	0.7557	6.70	0.8089	0.13
Mol $Volume_{final}$, ft^3/lb-mol	1.1862	1.2434	4.82	1.1875	0.11
$S_{o,final}$, %	45.10	45.04	0.06	45.96	0.86
$S_{g,final}$, %	1.13	0.0	1.13	0.0	1.13
$S_{w,final}$, %	53.77	54.04	0.27	54.04	0.27
CPU time, sec	872	1	872x	3	291x

The validation of the generalized PMV was performed through a commercial PVT package by creating a wide range of fluid compositions; CO_2 mole composition from initial 0.05% to 85% was divided into 32 samples.

Fig. 5.16 shows the comparison of the PMV calculation between the analytical model and the calculations performed with the output of the PVT commercial package. Results show that the PMV, argument of the integral in Eq. (3.5), is not constant as the semi-analytical model incorrectly assumes. Notice that in this case the trend is monotonic, opposed to the behavior observed in the previous cases.

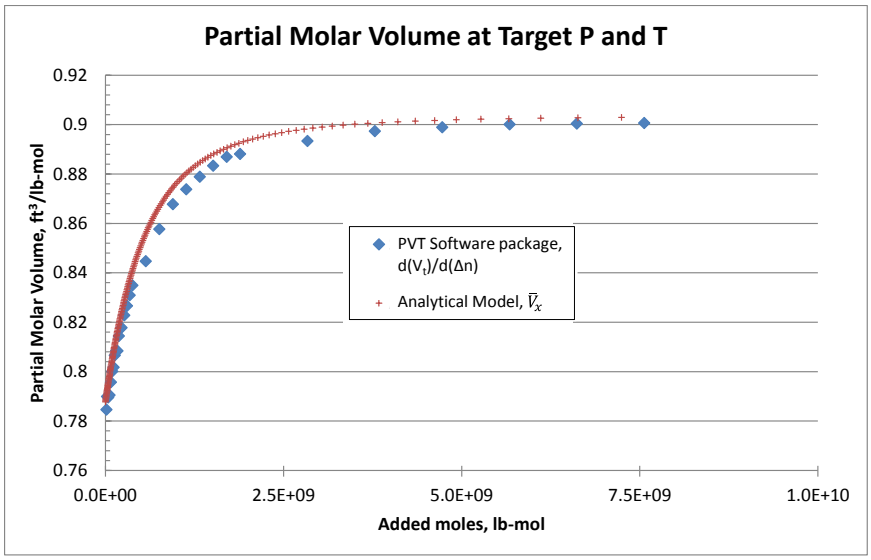

Fig. 5.16—Case D—Partial molar volume comparison from analytical model and calculations from commercial PVT software package. Results present excellent agreement.

Finally, the area under the curve in Fig. 5.16 provides the volume occupied by the fluid at target conditions; fluid volume must fill the hydrocarbon pore volume (HCPV) at

target conditions. **Fig. 5.17** displays the results from the integration, analytical and PVT commercial package show good agreement. From this plot, having estimated the HCPV at target conditions and the fictitious volume $V_{n_{dep}}$ in Eq. (3.5) the amount of injected fluid can be determined. HCPV is calculated from the pore volume (PV) and water saturation at final conditions.

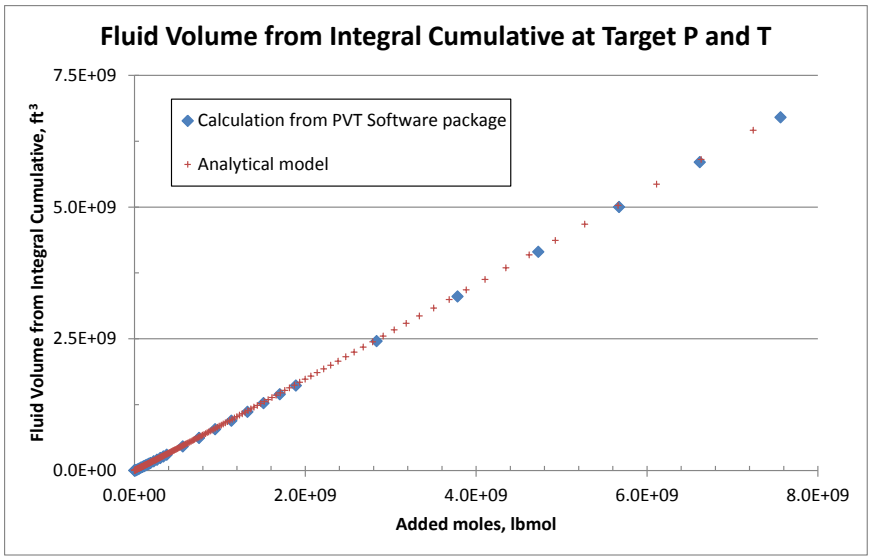

Fig. 5.17—Case D—Fluid volume comparison from analytical model and calculations from commercial PVT software package. Results present excellent agreement.

Table 5.21 presents the final fluid composition comparison between numerical simulation, semi-analytical, and analytical models. The analytical model offers an excellent with numerical simulation.

Table 5.21—CASE D—FLUID COMPOSITION AT FINAL CONDITIONS COMPARISON BETWEEN NUMERICAL SIMULATION, SEMI-ANALYTICAL, AND ANALYTICAL MODELS. ANALYTICAL MODEL PRESENTS BETTER AGREEMENT WITH NUMERICAL SIMULATION.

Case D—Final Fluid Composition Comparison			
Component	Numerical Simulation %	Semi-Analytical %	Analytical %
CO_2	61.369	60.015	61.584
N_2	6.817	6.667	6.831
C_1	11.670	12.222	11.593
C_2- C_4	2.086	2.185	2.070
C_5- C_6	2.118	2.218	2.102
C_{7+}	15.940	16.694	15.820

In summary, UCSC for given reservoir and injection fluids, reservoir properties, and designed pressures, predicted by the analytical model was 808.91 MMlb-mol, corresponding to 728.02 MMlb-mol of CO_2 and 80.89 MMlb-mol of N_2. This is equivalent to 14.51 Mt of injected CO_2, given the injection fluid composition. This amount corresponds to 13 years of CO_2 emissions from a 200 MW coal-fired power plant.

Table 5.22 displays a summary of the results obtained from reservoir numerical simulation and the analytical model for the 24 study cases. The table summarizes reservoir and injected fluids, temperature, pressures at each stage of the process, produced water, injected moles from numerical simulation and analytical model, and the difference between results. Results from analytical model match those from reservoir simulation with small differences, 1.3% molar basis in average. Slightly larger difference (3.61%) was observed in cases with carbon monoxide in the injected fluid.

Carbon monoxide was not an original component in the fluid models and the equation of state parameters were not calibrated for such component, thus presenting a small inconsistency.

Table 5.22—SUMMARY OF RESULTS. ANALYTICAL MODEL RESULTS MATCH THOSE FROM RESERVOIR NUMERICAL SIMULATION. LARGEST DIFFERENCE PRESENTS IN CASES WITH CARBON MONOXIDE, UNCALIBRATED COMPONENT IN RESERVOIR FLUID.

Summary of Results											
Case	**F_r**	**F_i**	**T,** °F	**p_{init},** psia	**p_{dep},** psia	**p_{target},** psia	**Δp,** psi	**W_p** MM-STB	**Δn^S,** x10^6 lb-mol	**Δn^A,** x10^6 lb-mol	**Diff,** %
1	V-O	1	100	8,846	6,292	8,803	2,510	0	189.1	187.1	1.06
2	V-O	2	100	8,846	3,547	8,788	5,241	0	678.9	684.1	0.78
3*	V-O	3	150	8,847	4,004	8,790	4,786	0	633.6	619.4	2.23
4	V-O	4	150	8,847	6,252	8,000	1,748	0	141.8	142.9	0.80
5	V-O	5	200	7,794	3,188	7,658	4,470	16.6	338.2	339.0	0.22
6	V-O	6	200	6,848	471	5,380	4,909	0	1,451	1,499	3.29
7	V-O	1	250	8,249	7,063	8,179	1,117	0	105.4	104.3	1.07
8	V-O	2	250	6,820	4,943	6,743	1,800	0.3	157.6	156.8	0.54
9	G-C	3	270	5,851	1,019	4,185	3,166	0	907.6	918.8	1.22
10	G-C	4	270	7,250	5,678	7,181	1,503	0	153.8	156.2	1.56
11	G-C	5	270	8,795	528	7,853	7,325	39.7	737.4	753.0	2.12
12*	G-C	6	285	8,849	2,914	6,049	3,135	0	661.8	685.6	3.61
13	G-C	1	285	7,550	5,866	7,286	1,420	0	156.4	155.9	0.34
14	G-C	2	285	7,496	389	7,245	6,856	37.6	738.5	750.4	1.61
15	G-C	3	285	5,852	2,001	4,008	2,007	0	543.4	540.9	0.46
16	G-C	4	285	7,498	4,818	7,313	2,495	3.8	188.5	190.8	1.23
17*	B-O	1	250	6,094	5,821	6,090	269	0	19.8	19.8	0.22
18*	B-O	2	200	6,094	978	6,038	5,059	80.9	809.9	808.9	0.13
19	B-O	3	200	6,094	1,099	4,611	3,512	79.3	647.9	657.2	1.44
20	B-O	4	250	6,092	5,296	5,820	524	0	38.9	39.2	0.91
21	B-O	5	250	6,092	3,803	5,820	2,017	0	243.5	238.6	2.00
22	B-O	6	250	6,092	3,395	4,712	1,317	3.8	237.6	241.6	1.68
23	B-O	1	285	6,090	4,990	5,950	960	0	82.2	83.3	1.39
24	B-O	2	285	6,090	3,232	5,890	2,658	0.3	386.2	388.4	0.56

*Denotes Cases A, B, C, and D, detailed in the previous sections.

Time of computation (CPU time) for all 24 studied cases from numerical simulation and analytical model are presented in **Table 5.23**. Analytical model performs several times faster than numerical simulation. Numerical simulation handles fluid flow appropriately, if correct and detailed input data is provided, increasing computation time when multi-phase fluids and drastic changes in production/injection schemes are present. CO_2 storage involves compositional calculations, multi-phase hydrocarbon fluids, and changes in production/injection strategies once depletion pressure is achieved. The analytical model is more consistent in the computational time, calculating fluid quantities and properties at different conditions analytically.

Fig. 5.18 shows the data presented in Table 5.23 on a graph. The analytical model performs several orders of magnitude faster than numerical simulation in all 24 cases. Average CPU time in the analytical model was 5 seconds.

Table 5.23—CPU TIME. ANALYTICAL MODEL PERFORMS CONSIDERABLY FASTER THAN NUMERICAL SIMULATION.

CPU Time		
Case	Numerical Simulation CPU_{time}, s	Analytical Model CPU_{time}, s
1	520	4
2	754	5
3*	932	4
4	473	4
5	658	9
6	1537	10
7	943	4
8	261	4
9	1378	4
10	652	5
11	2017	8
12*	1044	10
13	627	4
14	2111	4
15	614	4
16	8540	5
17*	376	3
18*	872	3
19	795	4
20	1017	4
21	3159	5
22	3237	6
23	1739	4
24	3750	4

*Denotes Cases A, B, C, and D, detailed in the previous sections.

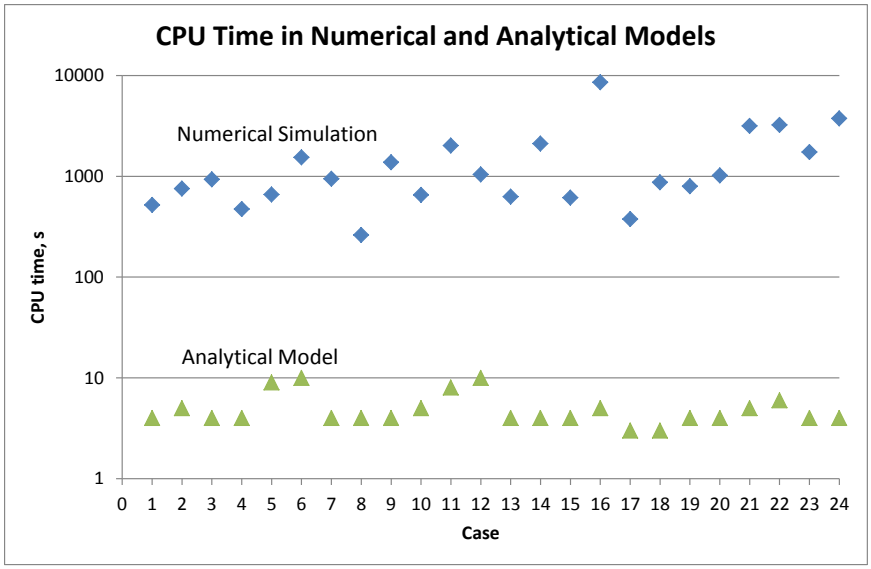

Fig. 5.18—CPU time in numerical and analytical model. Analytical model performs several orders of magnitude faster than numerical simulation in all 24 cases.

5.2 Reservoir Size Effect on UCSC

The effect of reservoir size on UCSC was analyzed using Case D as base scenario. Reservoir size has inherent uncertainty in its estimation from volumetric, seismic, material balance, and other used techniques. Sensitivity analysis is often performed to evaluate pessimistic, most likely, and, optimistic reservoir size scenarios.

In CO_2 storage projects reservoir size, along with other properties, determine the UCSC. Reservoir simulation gridding techniques, equilibrium initialization, and convergence issues during numerical calculations, make reservoir size sensitivity a time consuming task. On the other hand, reservoir size sensitivity with the analytical model, is an easy and fast task performed only by varying the pore volume.

Case D was modified to increase the reservoir pore volume by a factor of 1.5. This involved grid modifications to consider the new reservoir volume and a new production/injection schedule to achieve the same depletion and target pressures.

Results from numerical simulation in **Table 5.24** are presented for Cased D and pore volume of Case D increased 1.5 times. Results show that UCSC also increased by a factor of 1.5, being the ratio of injected moles to total final moles essentially the same in both cases, nearly 68%. CPU time in the numerical simulation model increased from 872 to 941 seconds, in addition of the time required to modify the simulation grid, production/injection schedule, and evaluating correct initialization of the model.

Table 5.24—RESERVOIR SIZE SENSITIVITY ON CASE D FROM NUMERICAL SIMULATION. UCSC INCREASES PROPORTIONALLY WITH PORE VOLUME. CPU TIME INCREASES IN NEW MODIFIED MODEL IN ADDITION TO REQUIRED TIME TO MODIFY GRID AND PRODUCTION/INJECTION SCHEDULE.

Property	Case D	Case D x 1.5 PV
Reservoir fluid	B-O	
Injection fluid	2	
Injection fluid components	90%CO_2 – 10%N_2	
Temperature, °F	200	
Initial pressure, psia	6,094	
Depletion pressure, psia	978	
Target pressure, psia	6,038	
Δp, psi	5,059	
Initial water saturation, %	68.56	
Water production, MMSTB	80.9	121.3
Initial pore volume, MMbbl	546.24	819.35
OOIP, MMSTB	102.36	153.55
n_{dep}, MMlb-mol	378.16	567.24
Δn, MMlb-mol	809.96	1,215.36
$\Delta n/(n_{dep}+\Delta n)$	0.6817	0.6818
CPU time, s	872	941

Similar results were obtained from the analytical model in a fraction of the time by changing the available initial pore volume in two runs that took 3 seconds each.

5.3 Temperature Effect on UCSC

The effect of temperature on UCSC was analyzed using the base case of a gas condensate reservoir. The gas condensate fluid composition was given in Section 4.2.1. Injected fluid used was 80% CO_2 and 20% N_2 (Fluid 3 from Table 4.7). Three different temperatures were used; 100°F, 200°F, and 285°F.

Initial reservoir pressure varied in each case according to temperature, average initial pressure for the three cases was 5,850 psia. The reservoir was produced until reaching 3,000 psia at depletion stage. No water was produced during depletion. After depletion, the CO_2-based stream was injected to repressurize the reservoir to 7,000 psia average pressure. **Table 5.25** displays initial, depletion, and target pressures in each case, as well as initial pore volume and water saturation. Notice that initial pressures and water saturations are different at each temperature, they were calculated from thermodynamic equilibrium performed in the initialization of the reservoir numerical simulator.

Table 5.25—RESERVOIR PROPERTIES. TEMPERATURE EFFECT SENSITIVITY. INITIAL PRESSURE AND WATER SATURATION ARE CALCULATED FROM THERMODYNAMIC EQUILIBRIUM IN EACH CASE.

Property	100°F	200°F	285°F
Initial pressure, psia	5,848	5,850	5,852
Depletion pressure, psia	3,000	3,000	3,000
Target pressure, psia	7,000	7,000	7,000
Initial pore volume, MMbbl	546	546	546
Initial water saturation, %	19.45	18.69	18.32

Table 5.26 shows fluid compositions at depletion stage for each temperature case. Compositions were estimated from reservoir numerical simulation.

Table 5.26—FLUID COMPOSITIONS AT DEPLETION STAGE FROM RESERVOIR SIMULATION. TEMPERATURE EFFECT ON UCSC.

Temperature Effect—Depletion Fluid Compositions			
Component	**100°F**	**200°F**	**285°F**
CO_2, %	4.615	4.530	4.516
N_2, %	0.000	0.000	0.000
C_1, %	58.005	57.910	59.114
C_2- C_3, %	14.474	14.289	14.243
C_4- C_6, %	5.149	5.067	4.934
C_7- C_{10}, %	8.831	8.783	8.273
C_{11+}, %	8.926	9.422	8.920

High temperatures cause fluid volume expansion. **Fig. 5.19** demonstrates that high temperature reservoirs have less capacity to store CO_2 than low temperature reservoirs. For the same amount of fluid injected, high temperature case causes the fluid to occupy more volume and fill the pore space, reducing the UCSC in comparison with a similar reservoir scenario with lower temperature.

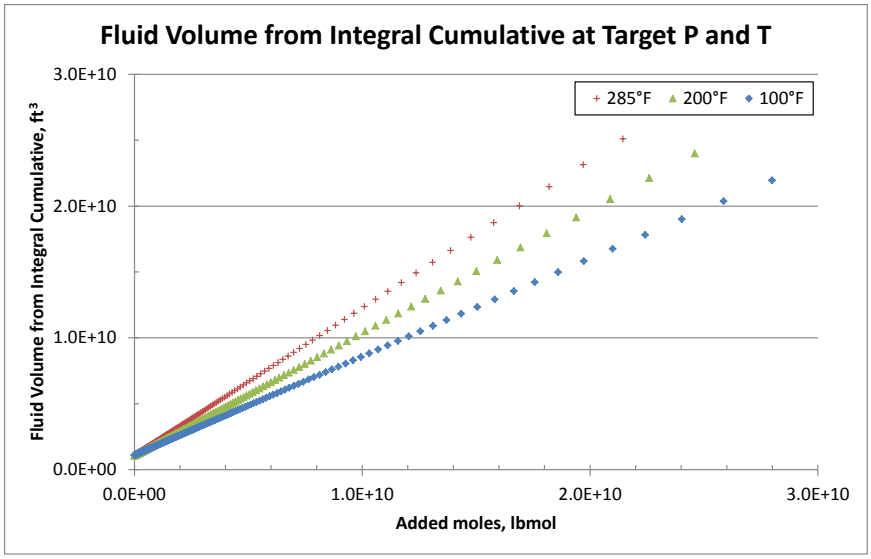

Fig. 5.19—Temperature effect on fluid volume at target pressure. Solubility of CO_2 in hydrocarbon is lower at higher temperatures, in addition to the increased swollen volume, which combined reduce the UCSC.

Fig. 5.19 is the result of the analysis of fluid volume from the analytical model. This plot is constructed at final target pressure, 7,000 psia in these cases, and the corresponding reservoir temperature of 100°F, 200°F, and 285°F. The left-most first point is the fictitious volume occupy by the fluid composition at depletion stage at target pressure. Subsequent data points were calculated with the analytical model methodology.

5.4 CO_2 Dissolution in Brine

Previous studies have suggested that during injection stage, CO_2 dissolution in water is negligible (Sifuentes et al. 2009). This dissolution effect becomes noticeable only after a few hundred years of storage. Additionally, the rate of CO_2 dissolution in brine is

usually appraised, from numerical simulation, using diffusion coefficients, which have to be estimated from laboratory experiments and have high uncertainty.

An additional analysis on Case D, presented previously on Section 5.1.4, was performed to estimate the amount of CO_2 that would dissolved in the brine assuming instantaneous dissolution, implementing an analytical model proposed by Rowe and Chou (1970). This analytical model uses pressure, temperature, and brine salinity as inputs.

CO_2 distribution in the reservoir at the end of injection is presented in **Fig. 5.20.** Active cells show reservoir zones with CO_2 composition higher than 8%, where the injected fluid is in contact with brine. Average water saturation in the zones where CO_2 is present is 27.26% and total volume of water in these zones is 31.99 MMSTB; total water volume in the CO_2 zone was calculated adding the volume of water contained in each cell with CO_2 composition equal or larger than 8%.

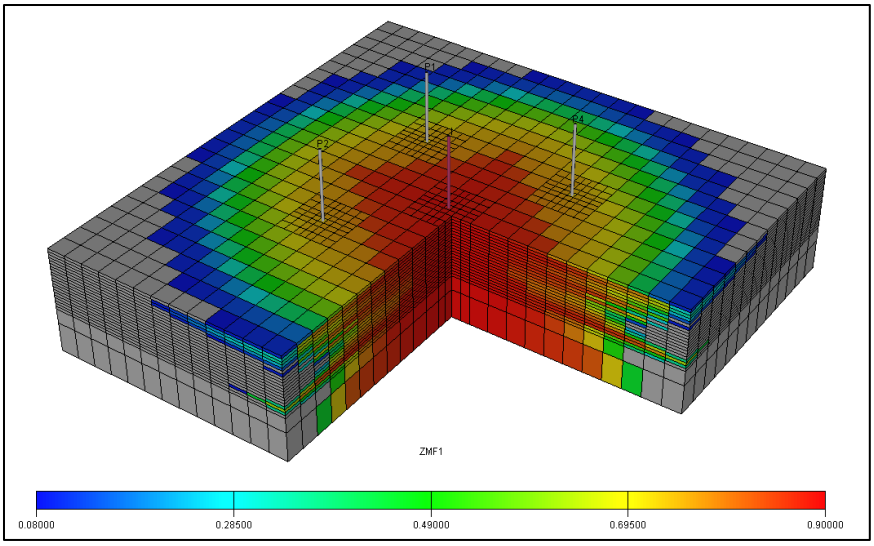

Fig. 5.20—CO_2 composition distribution. Active cells show zones where CO_2 composition is larger than 8%. The total water volume in this zone will be used to estimate maximum CO_2 solubility in brine for this scenario.

Reservoir temperature for Case D was 200°F and final average pressure was 6,038 psia. Entering water volume, pressure and temperature, and assuming different values of brine salinity, the maximum amount of CO_2 that can dissolve into brine was estimated with Rowe and Chou (1970) analytical correlation, detailed in Appendix D.

Table 5.27 displays the maximum amount of CO_2 that can instantaneously dissolve in brine with different salinities and the percentage of the total CO_2 injected that this represents; recall that total CO_2 injected in Case D was 736.41 MMlb-mol. Assuming completely fresh water yields a maximum of 2.25% of dissolved CO_2, which is equivalent to 3 months of CO_2 emissions from a 200 MW coal-fired power plant. More realistic salinities yield to further lower quantities of CO_2 dissolution.

Table 5.27—CO_2 DISSOLVED IN BRINE. PERCENTAGE OF DISSOLVED CO_2 IN BRINE IS NEGLIGIBLE.

Salinity Effect—CO_2 Dissolved in Brine		
Salinity, ppm	**CO_2 dissolved, MMlb-mol**	**Percentage of total CO_2 injected, %**
0	16.59	2.25
5,000	13.99	1.90
10,000	11.79	1.60
25,000	7.07	0.96

Additionally, CO_2 dissolution in brine is not instantaneous and takes long time to occur. CO_2 dissolution in brine does not play an important role in the UCSC of depleted oil and gas reservoirs during injection.

CHAPTER VI

CONCLUSIONS AND RECOMMENDATIONS

The performances of the semi-analytical and analytical models implemented in the algorithm were presented in Chapter V with the discussion of results. Analysis of results indicated the effectiveness, accuracy, and speed of the proposed methods to estimate the ultimate CO_2 storage capacity (UCSC).

6.1 Conclusions

- The proposed analytical method to estimate the UCSC in depleted oil and gas reservoirs is accurate. Difference in UCSC between reservoir simulation and the analytical method was in average 1.3%, with a maximum of 3.6% in all studied cases. Cases involved volatile oil, gas condensate, and black oil reservoir fluids; different injection fluids exhibiting pure CO_2 and several mixtures of CO_2, nitrogen and, carbon monoxide; reservoir temperatures ranging from 100°F to 285°F; single- and multi-phase fluid behavior during depletion and injection; wide range of pressure differentials between depletion and target pressures; and water production while depleting the reservoir.
- Average oil, gas, and water saturations at depletion and at final target conditions can be accurately estimated in the proposed models. Maximum difference in saturations between reservoir simulation and analytical method was 2.35% at

target conditions. This error could be attributed to difference in phase-recognition logics in the models.

- The implementation of analytical method in an algorithm allowed fast estimation of the UCSC in depleted oil and gas reservoirs. The algorithm performs 100 times faster than reservoir simulation in the worst case analyzed, completing the procedure in 5 seconds in average.
- Both proposed models, semi-analytical and analytical, allowed fast and accurate estimations of UCSC in depleted oil and gas reservoirs. Semi-analytical model implementation in an algorithm performs faster than the analytical method and offered accurate results when injected quantities was relatively large or the pressure differential between depletion and target pressures was large. However, the analytical method is more accurate in all the cases.
- The generalized partial molar volume (PMV) derived in this research allowed to complete the calculations required in the analytical method in cases with impure CO_2-based injection streams. The PMV is not constant during injection and its complex behavior is unique for each case, depending on reservoir and injection fluid compositions, pressure, and temperature.
- Depleted oil and gas reservoirs represent a good option for CO_2 storage. Proper selection of target reservoirs and good design of processes allow to store significant amounts of CO_2 emissions. Two of the presented cases were able to store 13 and 18 years of CO_2 emissions from coal-fired power plants of 200 MW and 100 MW capacity.

- Low temperature reservoirs can potentially store more CO_2 that high temperature reservoirs, being the rest of parameters the same. High temperatures cause fluid expansion, increasing the volume occupied by the fluid mixture in the reservoir and reducing the UCSC.
- CO_2 dissolution in brine does not play an important role in the UCSC of depleted oil and gas reservoirs during injection. Even if pure fresh water is present in the reservoir and assuming that the CO_2 will instantaneously saturate the water, only 2.25% of the total CO_2 injected would dissolve. Brines with more realistic salinity dissolved less than 1% of the injected CO_2. For practical purposes, CO_2 dissolution in brine can be neglected during injection in storage projects.

6.2 Recommendations

- Perform further comparisons of UCSC in aquifers and depleted oil and gas reservoirs, both types of formations offer positive and negative features for CO_2 storage. Proper selection of geological formations and correct design of operations can lead to successful projects.
- Implement the estimation of reservoir fluid composition at depletion stage from PVT laboratory experiments and thermodynamic modeling of the fluid. Constant volume depletion and differential liberation with relative permeabilities could offer good estimates of fluid composition at the end of depletion.
- If more rigorous evaluation of CO_2 dissolution in brine is desired, a full three-phase flash calculation can be implemented in the analytical algorithm to

consider interaction between water and injected fluids. This model would have to be combined with an analytical model to estimate CO_2 plume growth and brine-CO_2 interface.

REFERENCES

Barrufet, M.A., Bacquet, A., and Falcone, G. 2010. Analysis of the Storage Capacity for CO_2 Sequestration of a Depleted Gas Condensate Reservoir and a Saline Aquifer. *Journal of Canadian Petroleum Technology* **49** (8). DOI: 10.2118/139771-pa.

Burton, M., Kumar, N., and Bryant, S.L. 2009. CO_2 Injectivity into Brine Aquifers: Why Relative Permeability Matters as Much as Absolute Permeability. *Greenhouse Gas Control Technologies 9* **1** (1): 3091-3098.

Chang, Y.-B., Coats, B.K., and Nolen, J.S. 1998. A Compositional Model for CO_2 Floods Including CO_2 Solubility in Water. *SPE Reservoir Evaluation & Engineering* **1** (2). DOI: 10.2118/35164-pa.

Dake, L.P. 1978. *Fundamentals of Reservoir Engineering*. Amsterdam, The Netherlands: Elsevier. Original edition. ISBN 978-0-444-41830-2.

Dooley, J., Dahowski, R., Davidson, C. et al. 2006. *Carbon Dioxide Capture and Geologic Storage. A Core Element of a Global Energy Technology Strategy to Address Climate Change*. Columbus, OH, USA: Battelle Memorial Institute. Technology Report.

EIA, 2011, U.S. Total Carbon Dioxide Emissions from the Consumption of Energy. U.S. Energy Information Administration. http://tonto.eia.doe.gov/cfapps/ipdbproject/IEDIndex3.cfm?tid=90&pid=44&aid=8. Accessed January 18, 2011.

EPA, 2011, U.S. Geologic Sequestration. U.S. Environmental Protection Agency. http://www.epa.gov/climatechange/emissions/co2_geosequest.html. Accessed March 14, 2011.

Gallo, Y.L., Couillens, P., and Manai, T. 2002. CO_2 Sequestration in Depleted Oil or Gas Reservoirs. Paper SPE 74104-MS presented at the SPE International Conference on Health, Safety and Environment in Oil and Gas Exploration and Production, Kuala Lumpur, Malaysia.

House, N.J., Faulder, D.D., Olson, G.L. et al. 2003. Simulation Study of CO_2 Sequestration in a North Sea Formation. Paper SPE 81202-MS presented at the SPE/EPA/DOE Exploration and Production Environmental Conference, San Antonio, Texas.

Jaramillo, J.M. and Barrufet, M.A. 2001. Effects in the Determination of Oil Reserves Due to Gravitational Compositional Gradients in near-Critical Reservoirs. Paper SPE 71726-MS presented at the SPE Annual Technical Conference and Exhibition, New Orleans, Louisiana.

Koperna, G., Oudinot, A.Y., Mccolpin, G.R. et al. 2009. CO_2-ECBM/Storage Activities at the San Juan Basin's Pump Canyon Test Site. Paper SPE 124002-MS presented at the SPE Annual Technical Conference and Exhibition, New Orleans, Louisiana.

Li, Z., Dong, M., Li, S. et al. 2006. CO_2 Sequestration in Depleted Oil and Gas Reservoirs-Caprock Characterization and Storage Capacity. *Energy Conversion and Management* **47** (11-12): 1372-1382. DOI: 10.1016/j.enconman.2005.08.023.

Metz, B., Davidson, O., Coninck, H.D. et al. 2005. *IPCC Special Report on Carbon Dioxide Capture and Storage*.New York, NY, USA: Cambridge University Press. Original publication. ISBN 13 978-0-521-68551-1

Michelsen, M. and Mollerup, J. 2004. *Thermodynamic Models: Fundamentals & Computational Aspects*. Ed Stenby, E. Denmark: Tie-Line Publications. Original edition. ISBN 87-989961-1-8.

Nguyen, Q.M.R. 2009. Performance of EOR-CO_2 Miscible Process Using a Conceptual Model. M.En. thesis, Texas A&M University, College Station.

Nogueira, M. and Mamora, D.D. 2005. Effect of Flue Gas Impurities on the Process of Injection and Storage of CO_2 in Depleted Gas Reservoirs. Paper SPE 94906-STU presented at the SPE/EPA/DOE Exploration and Production Environmental Conference.

Okwen, R.T., Stewart, M.T., and Cunningham, J.A. 2010. Analytical Solution for Estimating Storage Efficiency of Geologic Sequestration of CO_2. *International Journal Of Greenhouse Gas Control* **4** (1): 102-107.

Oruganti, Y. 2009. Pressure Build-up During CO_2 Storage in Partially Confined Aquifers. *Greenhouse Gas Control Technologies 9* **1** (1): 3315-3322.

Peng, D.-Y. and Robinson, D.B. 1976. A New Two-Constant Equation of State. *Industrial & Engineering Chemistry Fundamentals* **15** (1): 59-64. DOI: 10.1021/i160057a011.

Ramon, J.C. and Fajardo, A. 2006. Sedimentology, Sequence Stratigraphy, and Reservoir Architecture of the Eocene Mirador Formation, Cupiagua Field, Llanos Foothills, Colombia. *AAPG Memoir* (88/SEPM Special Publication): p. 433-469. DOI: 10.1306/1215884M883276.

Rowe, A.M. and Chou, J.C.S. 1970. Pressure-Volume-Temperature-Concentration Relation of Aqueous Nacl Solutions. *Journal Of Chemical And Engineering Data* **15** (1): 61-66.

Schlumberger, 2010a. *Eclipse Technical Description and Reference Manual 2010.1*. Abingdon, UK: Schlumberger.

Schlumberger, 2010b. *Petrel 2010.1*. Oslo, Norway: Schlumberger.

Schlumberger, 2010c. *PVTi Reference Manual 2010.1*. Abingdon, UK: Schlumberger.

Sifuentes, W.F., Giddins, M.A., and Blunt, M.J. 2009. Modeling CO_2 Storage in Aquifers: Assessing the Key Contributors to Uncertainty. Paper SPE 123582-MS presented at the Offshore Europe, Aberdeen, UK.

Snow, N. 2010. CO_2 Injection Under Way in Alabama EOR Pilot Project. *Oil & Gas Journal* **108** (9): 27.

Soave, G. 1972. Equilibrium Constants from a Modified Redlich-Kwong Equation of State. *Chemical Engineering Science* **27** (6): 1197-1203. DOI: 10.1016/0009-2509(72)80096-4.

van der Meer, L.G.H. 1995. The CO_2 Storage Efficiency of Aquifers. *Energy Conversion and Management* **36** (6-9): 513-518. DOI: 10.1016/0196-8904(95)00056-j.

van der Meer, L.G.H. and Ferhat, Y. 2009. CO_2 Storage Capacity Calculations for the Dutch Subsurface. *Energy Procedia* **1** (1): 2615-2622.

van der Waals, J. 1873. Over De Continuiteit Van Den Gas- En Vloeistoftoestand (on the Continuity of the Gas and Liquid State). Ph.D. dissertation, Lieden University, The Netherlands.

Walkenbach, J. 2010. *Excel 2010 Power Programming with VBA*. Hoboken, NJ, USA: Wiley Publishing, Inc. Original edition. ISBN 978-0-470-47535-5.

APPENDIX A

This appendix presents the derivation of the partial molar volume definition, as well as the derivation of the final expression to calculate a generalized form of the partial volume concept with more than one component changing the mole fraction.

Partial Molar Volume

The partial molar volume (PMV) was defined in the Section 2.3 as the change of total volume of a mixture with respect to the change of moles of the component "i" at constant pressure and temperature. Eq. (A.1) shows the equation form of this definition.

$$\bar{V}_i = \left(\frac{\partial V}{\partial n_i}\right)_{p,T,n_j} \quad \text{.....(A.1)}$$

In a system where two of the three variables are related in the form of Eq. (A.2), one of the variables may be selected as the independent variable and the other two as dependent variables (Michelsen and Mollerup 2004).

$$F(x, y, z) = 0 \quad \text{.....(A.2)}$$

If the independent variable is kept constant, working the partial derivative expressions the relationship presented in Eq. (A.3) may be obtained. This relationship is often called as the "minus one rule".

$$\left(\frac{\partial z}{\partial x}\right)_y \left(\frac{\partial x}{\partial y}\right)_z \left(\frac{\partial y}{\partial z}\right)_x = -1 \quad \text{.....(A.3)}$$

Clearly, the function displayed in the right hand side (RHS) of Eq. (A.1) has four variables, and it can be expressed as shown in Eq. (A.4).

$$F(p, V, T, n) = 0 \quad \text{.....(A.4)}$$

Then, at constant n, the minus one rule can be expressed as Eq. (A.5) presents (Michelsen and Mollerup 2004).

$$\left(\frac{\partial p}{\partial V}\right)_{T,n} \left(\frac{\partial V}{\partial T}\right)_{p,n} \left(\frac{\partial T}{\partial p}\right)_{V,n} = -1 \quad \text{.....(A.5)}$$

During the production and CO_2 injection process, the reservoir temperature is assumed constant for all practical purposes. For this case, Eq. (A.6) presents the relationship between the variables.

$$\left(\frac{\partial p}{\partial V}\right)_{T,n} \left(\frac{\partial V}{\partial n_i}\right)_{p,T,n_j} \left(\frac{\partial n_i}{\partial p}\right)_{V,T,n_j} = -1 \quad \text{.....(A.6)}$$

Finally, combining Eqs. (A.1) and (A.6), Eq. (A.7) is obtained.

$$\bar{V}_i = \left(\frac{\partial V}{\partial n_i}\right)_{p,T,n_j} = -\frac{\left(\frac{\partial p}{\partial n_i}\right)_{V,T,n_j}}{\left(\frac{\partial p}{\partial V}\right)_{T,n}} \quad \text{.....(A.7)}$$

Generalization of the Partial Molar Volume Concept

This subsection presents the generalization of the PMV concept with more than one component changing its molar fraction, and the basic concept presented in Eq. (A.7) holds. However, in Eq. (A.8) the sub-index "i", that denotes the change of the component "i" in the mixture, is replaced by "x" to indicate that all the components in the mixture can change their molar fractions in the same proportion.

$$\bar{V}_x = \left(\frac{\partial V}{\partial n_x}\right)_{p,T,n_j} = -\frac{\left(\frac{\partial p}{\partial n_x}\right)_{V,T,n_j}}{\left(\frac{\partial p}{\partial V}\right)_{T,n}} \quad \text{(A.8)}$$

The derivation of the final form of Eq. (A.8) will be performed in 3 sections. The first section corresponds to the partial derivative of p with respect to n_x (numerator of the RHS of the equation) and the second section corresponds to the partial derivative of p with respect to V (denominator of the RHS of the equation). The third section presents the simplifications to reach the final form of the equation. For these sections, recall the PR-EOS presented in Eq. (2.8).

$$p = \frac{RT}{\mathcal{v} - b_m} - \frac{(a\alpha)_m}{\mathcal{v}^2 + 2b_m\mathcal{v} - {b_m}^2} \quad \text{(2.8)}$$

Eq. (A.9) presents the same equation expressed in terms of total volume V and number of moles n.

$$p = \frac{RTn}{V - nb_m} - \frac{n^2(a\alpha)_m}{V^2 + 2nb_mV - n^2{b_m}^2} \quad \text{.....(A.9)}$$

1. Partial derivative of *p* with respect to n_x

This step involves the derivation of Eq. (A.9) with respect to n_x. To simplify the derivation process, the repulsion and attraction terms will be derived separately.

Repulsion Term Derivative

Differentiating the repulsion term with respect to n_x yields:

$$\frac{\partial}{\partial n_x}\left(\frac{RTn}{V - nb_m}\right) = \frac{RT}{(V - nb_m)^2}\left[(V - nb_m) - \frac{\partial}{\partial n_x}(V - nb_m)\right] \quad \text{..... (A.10)}$$

Solving the partial derivative in the brackets, applying the basic definitions presented in Appendix B (Eqs. B.11, B.12 and B.18), the equation can be written as follows:

$$\frac{\partial}{\partial n_x}\left(\frac{RTn}{V - nb_m}\right) = \frac{RT}{(V - nb_m)^2}\left[(V - nb_m) + n\sum_{i=1}^{N_c} f_i b_i\right] \quad \text{..... (A.11)}$$

where f_i represents the mole fraction of the component "i" in the injection stream. Finally, simplifying the terms yields to:

$$\frac{\partial}{\partial n_x}\left(\frac{RTn}{V - nb_m}\right) = \frac{RT}{V - nb_m} + \frac{RTn\sum_{i=1}^{N_c} f_i b_i}{(V - nb_m)^2} \quad \text{..... (A.12)}$$

Attraction Term Derivative

Differentiating the attraction term with respect to n_x yields:

$$\frac{\partial}{\partial n_x}\left(\frac{n^2(a\alpha)_m}{V^2+2nb_m\,V-n^2{b_m}^2}\right)=\frac{1}{D^2}\left\{D\left[n^2\frac{\partial(a\alpha)_m}{\partial n_x}+2n(a\alpha)_m\right]\ldots\right.$$

$$\left.\ldots-(a\alpha)_m n^2\left[2V\left(n\frac{\partial b_m}{\partial n_x}+b_m\frac{\partial n}{\partial n_x}\right)-\left(n^2\frac{\partial b_m^2}{\partial n_x}+b_m^2\frac{\partial n^2}{\partial n_x}\right)\right]\right\} \quad \text{..... (A.13)}$$

where D is the denominator of the attraction term given by Eq. (A.14)

$$D=V^2+2nb_m\,V-n^2{b_m}^2 \quad \text{..... (A.14)}$$

Solving the partial derivative in the brackets, applying the basic definitions presented in Appendix B (Eqs. B.11, B.12, B.18 and B.27), Eq. (A.13) can be written and simplified as follows:

$$\frac{\partial}{\partial n_x}\left(\frac{n^2(a\alpha)_m}{D}\right)=\frac{1}{D^2}\left\{D[2n\Psi]\ldots\right.$$

$$\left.\ldots-(a\alpha)_m n^2\left[2V\sum_{i=1}^{N_c}f_i b_i-2nb_m\sum_{i=1}^{N_c}f_i b_i\right]\right\} \quad \text{..... (A.15)}$$

where Ψ is a part of the partial derivative term of $(a\alpha)_m$ with respect to n_x, showed in Eq. (A.16). The derivative procedure is presented on Appendix B

$$\Psi = \sum_{i=1}^{N_c} \sum_{j \neq i=1}^{N_c} \left[f_i x_j \left(a\alpha_{ij} \right) \right] + \sum_{i=1}^{N_c} [f_i x_i a_i \alpha_i] \quad \text{..... (A.16)}$$

Finally, simplifying Eq. (A.15) yields:

$$\frac{\partial}{\partial n_x} \left(\frac{n^2 (a\alpha)_m}{D} \right) = \frac{2n\Psi}{D} - \frac{2n^2 (a\alpha)_m \, V \sum_{i=1}^{N_c} f_i b_i}{D^2} \dots$$

$$\dots + \frac{2n^3 (a\alpha)_m b \sum_{i=1}^{N_c} f_i b_i}{D^2} \quad \text{..... (A.17)}$$

The final form of the derivative of p with respect to n_x is obtained in Eq. (A.18), by combining Eqs. (A.12) and (A.17).

$$\frac{\partial p}{\partial n_x} = \frac{RT}{V - n b_m} + \frac{RTn \sum_{i=1}^{N_c} f_i b_i}{(V - n b_m)^2} \dots$$

$$\dots - \frac{2n\Psi}{D} + \frac{2n^2 (a\alpha)_m V \sum_{i=1}^{N_c} f_i b_i}{D^2} - \frac{2n^3 (a\alpha)_m b \sum_{i=1}^{N_c} f_i b_i}{D^2} \quad \text{..... (A.18)}$$

2. Partial derivative of *p* with respect to *V*

The derivation of Eq. (A.9) with respect to V can be obtained directly in Eq. (A.19), since the temperature and total number of moles are independent from the total volume of the mixture. Moreover, the parameters $(a\alpha)_m$ and b_m, are also independent from the total volume of the mixture.

$$\frac{\partial p}{\partial V} = -\frac{RT}{(V - nb_m)^2} + \frac{2n^2(a\alpha)_m(V + nb_m)}{\left(V^2 + 2nb_m V - n^2 {b_m}^2\right)^2} \quad \text{..... (A.19)}$$

3. Final Form of the Generalized PMV Expression

Combining Eqs. (A.8), (A.18) and (A.19) and replacing the total volume V and the number of moles n to express the variables terms of molar volume $\mathcal{v}$, yields to:

$$\bar{V}_x = -\frac{R_1 + A_1}{D_1} \quad \text{..... (A.20)}$$

where R_1 and A_1 are the repulsion and attraction terms derivatives with respect to n_x, and D_1 is the partial derivative of p with respect to V, expressed as follows:

$$R_1 = \frac{RT}{\mathcal{v} - b_m} + \frac{RT\sum_{i=1}^{N_c} f_i b_i}{(\mathcal{v} - b_m)^2} \quad \text{..... (A.21)}$$

$$A_1 = -\frac{2\Psi}{(D_{\mathcal{v}})} + \frac{2(a\alpha)_m \mathcal{v}\sum_{i=1}^{N_c} f_i b_i}{(D_{\mathcal{v}})^2} - \frac{2(a\alpha)_m b\sum_{i=1}^{N_c} f_i b_i}{(D_{\mathcal{v}})^2} \quad \text{..... (A.22)}$$

$$D_1 = -\frac{RT}{(\mathcal{v} - b_m)^2} + \frac{2(a\alpha)_m(\mathcal{v} + b_m)}{(D_{\mathcal{v}})^2} \quad \text{..... (A.23)}$$

where $D_{\mathcal{v}}$ is a similar expression of Eq. (A.14) in terms of molar volume, presented in Eq. (A.24).

$$D_{\mathcal{v}} = \mathcal{v}^2 + 2b_m\mathcal{v} - {b_m}^2 \quad \text{..... (A.24)}$$

APPENDIX B

Appendix B presents some basic properties that are necessary to derive the equations presented in this study. The first equations correspond to elemental notions about compositional analysis. Subsequently, slightly more complex expressions present the solution for the derivatives of the mixing rules.

1. Basic Properties

The total number of moles n in a mixture is the summation of the moles in the vapor and liquid phases:

$$n = n^v + n^l \quad \text{.....(B.1)}$$

The number of moles in the vapor, or liquid phase, is the summation of the moles of every component in the corresponding phase:

$$n^v = \sum_{i=1}^{N_c} n^v \text{ and } n^l = \sum_{i=1}^{N_c} n^l \quad \text{.....(B.2)}$$

The mole fraction of the component "i" is the ratio between the total number of moles of the component "i" with respect to the total number of moles of the mixture:

$$z_i = \frac{{n_i}^v + {n_i}^l}{n} \quad \text{.....(B.3)}$$

The liquid mole fraction x_i and the vapor mole fraction y_i of the component "i" is given by the ratio between the number of moles of the component "i", in the liquid or vapor phase, with respect to the number of moles in the liquid or vapor phase correspondingly:

$$x_i = \frac{{n_i}^l}{n^l} \text{ and } y_i = \frac{{n_i}^v}{n^v} \quad \text{.....(B.4)}$$

The molar volume $\mathscr{v}$ of a fluid is an intensive property given by the ratio of the total volume occupied by the fluid and its total number of moles:

$$\mathscr{v} = \frac{V}{n} \quad \text{.....(B.5)}$$

2. Mixing Rules Derivatives

The derivatives of the mixing rules with respect to the number of moles changing in the fluid represent an important part of the derivation of the generalized form of the partial molar volume concept.

The original definition of the partial molar volume (PMV) relates the change of volume of the fluid with respect to the change of moles of one component. The generalized PMV considers that all the components can change their number of moles, thus their molar composition.

The generalization will be presented starting from a 3-components mixture in liquid phase. The three components are allowed to change their mole fraction by adding moles in a certain ratio, as the injection stream has constant composition.

The number of added moles n_x is given by the summation of the added moles of each component:

$$n_x = \Delta n_1 + \Delta n_2 + \Delta n_3 = \sum_{i=1}^{N_c} \Delta n_i \quad \text{.....(B.6)}$$

The added moles of the component "i" is given by the total number of moles added and the injection mole fraction of the corresponding component f_i:

$$\Delta n_i = f_i n_x \quad \text{.....(B.7)}$$

The final number of moles, after the injection, of the component "i" is equal to the summation of the original number of moles, before the injection, of component "i" and the added moles of the same component:

$$n_i = n_i{}^o + \Delta n_i \quad \text{.....(B.8)}$$

The molar composition of the injected fluid must add to unity:

$$\sum_{i=1}^{N_c} \mathrm{f_i} = 1 \quad \text{.....(B.9)}$$

The final number of moles in the fluid is given by the summation of the initial number of moles and the added moles:

$$n = n^o + n_x \quad \text{.....(B.10)}$$

The generalized PMV involves derivatives with respect to the total number of moles n_x changing in the fluid. The derivative of the number of moles of component "i" with respect to n_x is given by Eq. (B.11), combining the basic concepts presented in Eqs. (B.7) and (B.8).

$$\frac{\partial n_i}{\partial n_x} = \frac{\partial}{\partial n_x}(n_i{}^o + f_i n_x) = f_i \quad \text{.....(B.11)}$$

Similarly, using Eq. (B.10) as base, the derivative of the final number of moles with respect to n_x is:

$$\frac{\partial n}{\partial n_x} = \frac{\partial}{\partial n_x}(n^o + n_x) = 1 \quad \text{.....(B.12)}$$

2.1. Linear Mixing Rule Derivative

The linear mixing rule for a 3-component mixture in liquid phase is given as follows:

$$b_m = \sum_{i=1}^{N_c} x_i b_i = x_1 b_1 + x_2 b_2 + x_3 b_3 \quad \text{.....(B.13)}$$

Expressed in terms of moles, Eq. (B.13), becomes:

$$b_m = \frac{{n_1}^l}{n^l} b_1 + \frac{{n_2}^l}{n^l} b_2 + \frac{{n_3}^l}{n^l} b_3 \quad \text{(B.14)}$$

Differentiating Eq. (B.14) with respect to the added moles n_x, assuming that the mixture remains in single phase ($n^l = n$), results:

$$\frac{\partial b_m}{\partial n_x} = \sum_{i=1}^{3} \frac{b_i}{n^2} \left(n \frac{\partial n_i}{\partial n_x} - n_i \frac{\partial n}{\partial n_x} \right) \quad \text{(B.15)}$$

Combining Eqs. (B.11), (B.12) and (B.15) gives:

$$\frac{\partial b_m}{\partial n_x} = \frac{b_1}{n^2}(f_1 n - n_1) + \frac{b_2}{n^2}(f_2 n - n_2) + \frac{b_3}{n^2}(f_3 n - n_3) \quad \text{(B.16)}$$

Simplifying and expressing in terms of liquid mole fraction:

$$\frac{\partial b_m}{\partial n_x} = \frac{b_1 f_1}{n} + \frac{b_2 f_2}{n} + \frac{b_3 f_3}{n} - \frac{1}{n}(b_1 x_1 + b_2 x_2 + b_3 x_3) \quad \text{(B.17)}$$

Finally, rearranging and generalizing the 3-component case for a fluid with N_c components:

$$\frac{\partial b_m}{\partial n_x} = \frac{1}{n} \left(\sum_{i=1}^{N_c} b_i f_i - b_m \right) \quad \text{(B.18)}$$

2.2. Quadratic Mixing Rule Derivative

The quadratic mixing rule for a 3-component mixture in liquid phase is given as follows:

$$(a\alpha)_m = 2x_1x_2(a\alpha_{1,2}) + 2x_2x_3(a\alpha_{2,3}) + 2x_1x_3(a\alpha_{1,3}) \ldots$$

$$\ldots + {x_1}^2 a_1\alpha_1 + {x_2}^2 a_2\alpha_2 + {x_3}^2 a_3\alpha_3 \quad \ldots\ldots \text{(B.19)}$$

where the term $(a\alpha_{i,j})$ is expressed as a function of a and α parameters of the components, and k_{ij} represents the binary interaction coefficient (BIC) between components "i" and "j":

$$(a\alpha_{i,j}) = \sqrt{a_i\alpha_i a_j\alpha_j}(1 - k_{ij}) \quad \ldots\ldots \text{(B.20)}$$

Expressing Eq. (B.19) in terms of number of moles:

$$(a\alpha)_m = \frac{1}{n^2}[2n_1n_2(a\alpha_{1,2}) + 2n_2n_3(a\alpha_{2,3}) + 2n_1n_3(a\alpha_{1,3}) \ldots$$

$$\ldots + {n_1}^2 a_1\alpha_1 + {n_2}^2 a_2\alpha_2 + {n_3}^2 a_3\alpha_3] \quad \ldots\ldots \text{(B.21)}$$

Differentiating Eq. (B.21) with respect to the added moles n_x results:

$$\frac{\partial(a\alpha)_m}{\partial n_x} = \frac{1}{n^4}\left[\frac{\partial\Lambda}{\partial n_x}n^2 - \Lambda\frac{\partial(n^2)}{\partial n_x}\right] = \frac{1}{n^2}\frac{\partial\Lambda}{\partial n_x} - \frac{2}{n^3}\Lambda \quad \ldots\ldots \text{(B.22)}$$

where Λ is the content of the brackets in Eq. (B.21) given by:

$$\Lambda = 2n_1n_2(a\alpha_{1,2}) + 2n_2n_3(a\alpha_{2,3}) + 2n_1n_3(a\alpha_{1,3}) \ldots$$

$$\ldots + {n_1}^2a_1\alpha_1 + {n_2}^2a_2\alpha_2 + {n_3}^2a_3\alpha_3 \quad \text{...(B.23)}$$

The partial derivative in Eq. (B.22) can be solved using the properties shown in Eqs. (B.11) and (B.12) as follows:

$$\frac{\partial \Lambda}{\partial n_x} = 2(a\alpha_{1,2})(f_1n_2 + f_2n_1) + 2(a\alpha_{2,3})(f_2n_3 + f_3n_2) + 2(a\alpha_{1,3})(f_1n_3 + f_3n_1)..$$

$$\ldots + 2f_1n_1a_1\alpha_1 + 2f_2n_2a_2\alpha_2 + 2f_3n_3a_3\alpha_3 \quad \text{...(B.24)}$$

Simplifying the terms:

$$\frac{\partial \Lambda}{\partial n_x} = 2[f_1n_2(a\alpha_{1,2}) + f_2n_1(a\alpha_{1,2}) + f_2n_3(a\alpha_{2,3}) + f_3n_2(a\alpha_{2,3}) \ldots$$

$$\ldots + f_1n_3(a\alpha_{1,3}) + f_3n_1(a\alpha_{1,3}) + \sum_{i=1}^{3} f_in_ia_i\alpha_i \quad \text{.......................................(B.25)}$$

Further simplifying, Eq. (B.25) becomes:

$$\frac{\partial \Lambda}{\partial n_x} = 2\left[\sum_{i=1}^{3}\sum_{j\neq i=1}^{3} f_in_j(a\alpha_{i,j}) + \sum_{i=1}^{3} f_in_ia_i\alpha_i\right] \quad \text{...(B.26)}$$

Finally, combining Eqs. (B.22) and (B.26), and generalizing the 3-component case for a fluid with N_c components:

$$\frac{\partial(a\alpha)_m}{\partial n_x} = \frac{2}{n}[\Psi - (a\alpha)_m] \quad \text{.....(B.27)}$$

where:

$$\Psi = \sum_{i=1}^{N_c} \sum_{j \neq i=1}^{N_c} f_i x_j \left(a\alpha_{i,j}\right) + \sum_{i=1}^{N_c} f_i x_i a_i \alpha_i \quad \text{.....(B.28)}$$

APPENDIX C

Appendix C displays the relative permeability and capillary pressure tables used for the gas condensate and the black oil models. Both sets of relative permeability curves were processed in the similarly in the reservoir simulation model, assuming gas and water complete segregation within each grid cell (Schlumberger 2010a).

Table C.1—THREE-PHASE RELATIVE PERMEABILITY AND CAPILLARY PRESSURE FOR GAS CONDENSATE FLUID MODEL.

Water			Gas			Oil		
S_w	k_{rw}	p_{cow}	S_g	k_{rg}	p_{cog}	S_o	k_{ro}	p_c
0.16	0	50.0	0	0	0	0	0	0
0.18	0	41.0	0.04	0.005	0.1	0.04	0	0
0.20	0.002	32.0	0.08	0.013	0.2	0.08	0	0
0.24	0.010	21.0	0.12	0.026	0.3	0.12	0	0
0.28	0.020	15.5	0.16	0.040	0.4	0.16	0	0
0.32	0.033	12.0	0.20	0.058	0.5	0.20	0	0
0.36	0.049	9.2	0.24	0.078	0.6	0.24	0	0
0.40	0.066	7.0	0.28	0.100	0.7	0.28	0.005	0.01
0.44	0.090	5.3	0.32	0.126	0.8	0.32	0.012	0.01
0.48	0.119	4.2	0.36	0.156	0.9	0.36	0.024	0.02
0.52	0.150	3.4	0.40	0.187	1.0	0.40	0.040	0.04
0.56	0.186	2.7	0.44	0.222	1.1	0.44	0.060	0.06
0.60	0.227	2.1	0.48	0.260	1.2	0.48	0.082	0.08
0.64	0.277	1.7	0.56	0.349	1.4	0.52	0.112	0.11
0.68	0.330	1.3	0.60	0.400	1.5	0.56	0.150	0.15
0.72	0.390	1.0	0.64	0.450	1.6	0.60	0.196	0.20
0.76	0.462	0.7	0.68	0.505	1.7	0.68	0.315	0.32
0.80	0.540	0.5	0.72	0.562	1.8	0.72	0.400	0.40
0.84	0.620	0.4	0.76	0.620	1.9	0.76	0.513	0.51
0.88	0.710	0.3	0.80	0.680	2.0	0.80	0.650	0.65
0.92	0.800	0.2	0.84	0.740	2.1	0.84	0.800	0.80
0.96	0.900	0.1						
1	1	0						

Table C.2—THREE-PHASE RELATIVE PERMEABILITY AND CAPILLARY PRESSURE FOR BLACK OIL FLUID MODEL.

Water			Gas			Oil		
S_w	k_{rw}	p_{cow}	S_g	k_{rg}	p_{cog}	S_o	k_{ro}	p_c
0.20	0	32.0	0	0	0	0	0	0
0.24	0.003	21.0	0.05	0	0.1	0.30	0	0
0.28	0.010	15.5	0.10	0.004	0.2	0.33	0.005	0.01
0.32	0.023	12.0	0.15	0.015	0.3	0.36	0.018	0.02
0.36	0.040	9.2	0.20	0.033	0.4	0.39	0.038	0.04
0.40	0.063	7.0	0.25	0.059	0.5	0.42	0.064	0.06
0.44	0.090	5.3	0.30	0.093	0.6	0.45	0.096	0.10
0.48	0.123	4.2	0.35	0.133	0.7	0.48	0.133	0.13
0.52	0.160	3.4	0.40	0.181	0.8	0.51	0.175	0.18
0.56	0.203	2.7	0.45	0.237	0.9	0.54	0.223	0.22
0.60	0.250	2.1	0.50	0.300	1.0	0.57	0.275	0.28
0.64	0.303	1.7	0.55	0.370	1.1	0.60	0.333	0.33
0.68	0.360	1.3	0.60	0.448	1.2	0.63	0.395	0.40
0.72	0.423	1.0	0.65	0.533	1.3	0.66	0.462	0.46
0.76	0.490	0.7	0.70	0.626	1.4	0.69	0.533	0.53
0.80	0.563	0.5	0.75	0.726	1.5	0.72	0.609	0.61
0.84	0.640	0.4	0.80	0.834	1.6	0.75	0.690	0.61
0.88	0.723	0.3				0.78	0.775	0.78
0.92	0.810	0.2				0.80	0.834	0.83
0.96	0.903	0.1						
1	1	0						

APPENDIX D

Appendix D presents correlations to estimate the maximum CO_2 solubility in brine at given pressure, temperature, and salinity (Chang et al. 1998; Rowe and Chou 1970). Pressure ranges from 0 to 10,000 psia, temperature from 104 to 212 °F and salinity from 0 to 250,000 ppm. Solubility increases with pressure and it decreases as salinity and temperature increase.

CO_2 solubility in distilled water is estimated with Eqs. (D.1) or (D.2) according to the case.

$$R_{sw} = a.p\left[1 - b.sin\left(\frac{\pi}{2}\frac{c.p}{c.p+1}\right)\right] \quad \text{if } p < p^0 \quad \text{..... (D.1)}$$

$$R_{sw} = R_{sw}^0 + m.(p - p^0) \quad \text{if } p \geq p^0 \quad \text{..... (D.2)}$$

where:

$$a = \sum_{i=0}^{4} a_i.10^{-3i}.T^i \quad \text{..... (D.3)}$$

$$b = \sum_{i=0}^{4} b_i.10^{-3i}.T^i \quad 0 < b < 1 \quad \text{..... (D.4)}$$

$$c = 10^{-3} \sum_{i=0}^{4} c_i . 10^{-3i} . T^i \quad \text{..... (D.5)}$$

$$p^0 = \frac{2}{\pi} \frac{sin^{-1}(b^2)}{c\left[1 - \frac{2}{\pi} sin^{-1}(b^2)\right]} \quad \text{..... (D.6)}$$

$$R_{sw}^0 = a . p^0 (1 - b^3) \quad \text{..... (D.7)}$$

$$m = a\left\{1 - b\left[sin\left(\frac{\pi}{2}\frac{c.p^0}{c.p^0 + 1}\right) + \frac{\pi}{2}\frac{c.p^0}{(c.p^0 + 1)^2} cos\left(\frac{\pi}{2}\frac{c.p^0}{c.p^0 + 1}\right)\right]\right\} \quad \text{..... (D.8)}$$

R_{sw} is the CO_2 solubility in SCF of CO_2 per STB of water, T is the temperature in °F, p is pressure in psia, and the coefficients are shown in **Table D.1**.

Table D.1—VALUES OF COEFFICIENTS FOR CO_2 SOLUBILITY IN WATER CORRELATION

	Values of Coefficients				
	i=0	i=1	i=2	i=3	i=4
a_i	1.163	-16.630	111.0730	-376.8590	524.8890
b_i	0.965	-0.272	0.0923	-0.1008	0.0998
c_i	1.280	-10.757	52.6960	-222.3950	462.6720

Solubility of CO_2 in brine can be estimated from Eq. (D.9)

$$log\left(\frac{R_{sb}}{R_{sw}}\right) = -0.028 . S . T^{-0.12} \quad \text{..... (D.9)}$$

where R_{sb} is the CO_2 solubility in SCF of CO_2 per STB of brine and S is the brine salinity in weight percent of solid (1% = 10,000 ppm).

VITA

Ernesto Valbuena Olivares holds a Bachelor of Science in petroleum engineering from La Universidad del Zulia, Venezuela, 2008. He worked in Schlumberger from 2007 to 2009 holding positions as research intern and reservoir engineer for enhanced oil recovery (EOR) processes in heavy oil crudes, and production logging and pressure transient testing analysis.

He joined the Master of Science program at Texas A&M University in 2009. His research interests include fluid phase behavior and thermodynamics, EOR and reservoir-surface integration. He plans to continue graduate studies on the petroleum engineering doctoral program at Texas A&M University. Mr. Valbuena is also actively involved in the Society of Petroleum Engineers (SPE) as the Graduate Representative in the TAMU-SPE Student Chapter, 2011-2012.

Name:	Ernesto Valbuena Olivares
Address:	3116 TAMU Richardson Building. Petroleum Engineering Dept. College Station, TX 77843
Email Address:	eduvfo@gmail.com
Education:	B.S., Petroleum Engineering, La Universidad del Zulia, 2008 M.S., Petroleum Engineering, Texas A&M University, 2011